Exploring Higher-Dimensional Gauge Theory: A Model of Early Dark Energy and A Non-Abelian Gauge Theory with Magnetic Flux Background

大久保, 勇利

https://hdl.handle.net/2324/7182295

出版情報：Kyushu University, 2023, 博士（理学）, 課程博士
バージョン：
権利関係：

Ph.D. Dissertation

Exploring Higher-Dimensional Gauge Theory: A Model of Early Dark Energy and A Non-Abelian Gauge Theory with Magnetic Flux Background

Yuri OKUBO

Department of Physics

Graduate School of Science

Kyushu University

December, 2023

Abstract

The standard model (SM) of particle physics is a successful theory and well describes the world of elementary particles. However, there exist some phenomena that the SM can not explain, and its extensions such as superstring theory, Grand Unified Theory (GUT), and Gauge Higgs Unification (GHU), have been widely discussed. A lot of these theoretical attempts are based on theories defined on higher-dimensional spacetime, which is a promising framework for building theories beyond the standard model.

In this thesis, we focus on gauge theories defined on higher-dimensional spacetime. Extra components of a gauge field in a higher-dimensional gauge theory yield scalar fields in the 4D effective theory. The underlying gauge symmetry constrains some feature of the scalar field. For example, the gauge invariance prohibits it from having a mass term at tree level. In addition, quantum corrections to its mass is also restricted by the gauge symmetry and kept finite.

The scalar field that naturally arises from higher-dimensional gauge theories can help to explain physics beyond the Standard model. In GHUs, this scalar is identified as the Higgs field and the hierarchy problem can be solved by the underlying higher-dimensional gauge symmetry. Furthermore, this scalar field has also been regarded as a cosmological scalar field such as the inflaton or quintessence. In this thesis, based on the framework of higher-dimensional gauge theories, we show two different studies and suggest some further applications.

The first study is motivated by Early Dark Energy (EDE), which has been considered a promising solution to Hubble tension in cosmology. In this scenario, the extra energy component helps to solve the discrepancy in the value of the Hubble constant between local and cosmic microwave background observations. Theoretically, the behavior of the EDE can be explained by a scalar field, but its physical origin must be clarified. Such a scalar field is expected to be explained by BSM.

In the first study, the origin of the EDE scalar is examined from the viewpoint of higher-dimensional gauge theories. We identify the scalar field obtained from the extra component of the gauge field in a 5D $U(1)$ gauge theory as the EDE scalar. The 5D gauge symmetry prohibits the existence of a potential for the extra-dimensional scalar at tree level, but an effective potential is generated by

quantum effects. We show that by choosing appropriate parameters such as the charges and bulk masses of matter fields included in the theory, this effective potential can have the shape and scale necessary to realize the EDE. Furthermore, the time evolution of the equation of state and energy density of this system is analyzed numerically to show that an EDE-like behavior is realized in this model.

In the second study, we construct an $SU(n)$ gauge theory defined on a 6D spacetime whose extra dimensions are compactified into a torus and penetrated by a background magnetic field. It has been shown in specific setups of $U(1)$ and $SU(2)$ that the background magnetic field spontaneously breaks the translational symmetry on the torus and the extra-dimensional component becomes a Nambu-Goldstone boson of the broken translational symmetry, and as a result, quantum corrections to its mass are completely canceled. This feature expands the applicability of higher-dimensional gauge theory, and therefore, higher-dimensional gauge theory with a background magnetic field is an attractive framework.

We extend the gauge groups such as $U(1)$ and $SU(2)$ assumed in previous studies to general $SU(n)$ and calculate the mass spectrum of 4D effective theories mainly aiming to apply to GHUs and GUTs. Not only the gauge group but also the background field are assumed to be general as far as it is consistent with the theory. Furthermore, the gauge parameter in the standard R_ξ gauge fixing is left unfixed. Our result shows the existence of tachyonic modes, which have been pointed out in some previous studies, regardless of the choice of the gauge parameter and direction of the flux background in the representation space. This result suggests that tachyon condensation will occur if the stabilization of the tachyonic modes is not considered. Finally, we discuss the phenomenological implications of the mass spectrum.

This thesis is based on the following published papers:

- K. Kojima and Y. Okubo,
  "Early Dark Energy from a Higher-dimensional Gauge Theory",
  Phys.Rev.D **106** (2022) 6, 063540, arXiv:2205.13777 [astro-ph.CO].

- K. Kojima, Y. Okubo and C. S. Takeda,
  "Mass spectrum in a six-dimensional $SU(n)$ gauge theory on a magnetized torus,"
  JHEP **08** (2023), 083, arXiv:2306.00644 [hep-th].

Contents

List of Figures

List of Tables

Chapter 1

Introduction

The Standard Model (SM) of particle physics is a very successful theory, which well describes the world of elementary particles including quarks, leptons, gauge bosons, and Higgs bosons. Theoretically, the SM is based on the gauge principle and is described by the $SU(3)_c \times SU(2)_L \times U(1)_Y$ gauge theory. The $SU(2)_L \times U(1)_Y$ part corresponds to the electroweak theory, and this symmetry is broken to the electromagnetic $U(1)_{\mathrm{EM}}$ symmetry by the Higgs taking the vacuum expectation value (vev). The remaining part, $SU(3)_c$, describes the strong interaction between quarks and is known as quantum chromodynamics. The SM is in agreement with various observations with very high accuracy.

However, there remain some phenomena that the SM can not explain. For example, the SM does not include gravitational interaction which is not renormalizable in the framework of quantum field theory. The dark sector, *i.e.*, dark matter and dark energy, is also not accounted for in the SM. In addition, there are some theoretical problems such as the hierarchy problem. Since the quantum correction to the mass of the Higgs particle is sensitive to the cutoff scale due to the lack of symmetry in the Higgs sector, an unnatural fine-tuning is needed to obtain the observed Higgs mass, 125 GeV [1]. There are several other things that the SM can not explain, such as the origin of neutrino masses and the quantization of charge.

To solve these problems, various extensions of the SM have been discussed so far. For example, supersymmetry, which is the symmetry under the interchange of bosons and fermions, has widely been discussed [2, 3]. If a theory has this additional symmetry, the quantum corrections to the Higgs mass from bosons and their superpartners, fermions, cancel each other, which leads to the resolution of the hierarchy problem. Another extension of the SM is Grand Unified Theory (GUT) [4, 5]. GUTs unify the three gauge groups of the SM into a single gauge group, such as $SU(5)$, $SO(10)$, and E_6. Due to the unification, the charge quantization can be explained, and the parameters of the theory can be greatly reduced.

In addition to these models, various other extensions of the SM have been widely discussed, such as superstring theory, which can achieve quantization of gravity.

Some of these approaches to the physics beyond the Standard Model (BSM) are based on the framework of higher-dimensional gauge theory that is defined on a spacetime with compact extra dimensions. For instance, GUT models defined in higher dimensional spacetime have been discussed [6, 7]. In these models, part of a gauge symmetry in a higher-dimensional gauge theory is broken by conditions related to the geometry of the compact extra dimensions, such as boundary conditions, and do not appear in the 4D effective theory. Using this feature, we can construct interesting models that might not be possible in a 4D spacetime. For example, it is known that the doublet-triplet splitting problem that requires fine-tuning of parameters in some GUT models can be solved in a 5D gauge theory where the extra dimension is compactified into $S^1/(Z_2 \times Z_2')$ [8]. Therefore, gauge theories defined in higher-dimensional spacetime could lead to the unification of the SM interactions.

Another example of the BSM based on the framework of higher-dimensional gauge theory is the Gauge-Higgs Unification (GHU). In a higher-dimensional spacetime, gauge fields have extra components due to the increase in spacetime dimensions, and they transform as scalars under 4D Lorentz transformations. In GHU, the zero-modes of these scalar fields originating from the extra components of the gauge field are identified as scalars causing gauge symmetry breaking [9–12]. The higher-dimensional gauge symmetry prohibits the scalar field from having a potential, but an effective potential can be generated by quantum effects. The scalar field can have a nontrivial vev in this potential, which gives mass to some gauge fields, and gauge symmetry is partly broken. This symmetry breaking has been widely discussed in the contexts of both the electroweak symmetry breaking and unified gauge symmetry breaking [13–39]. In these scenarios, the features of the Higgs scalar are restricted by the underlying gauge symmetry, and therefore, the quantum correction to its mass is kept finite. Consequently, the hierarchy problem can be solved in GHU models.

As the examples above show, a higher-dimensional gauge theory is a versatile framework with various possibilities for constructing BSMs. In this thesis, we present two studies based on the framework of higher-dimensional gauge theory. They are based on different backgrounds and motivations, which are shown below.

Hubble Tension and Early Dark Energy

Standard cosmology is based on Einstein's gravity and cosmological principle, which assumes that the universe is homogeneous and isotropic. In addition, as the dark sector of the universe, dark energy originating the cosmological constant

Λ and non-relativistic cold dark matter are assumed, and this model is called the ΛCDM model. The ΛCDM has been consistent with most astronomical measurements over the years. However, in recent years, a problem has arisen in the standard cosmology. The value of the Hubble constant, which represents the cosmic expansion rate at present, is not consistent between the two different types of observations.

One way to estimate the value of the Hubble constant H_0 is by observing nearby astronomical objects. The determination of H_0 through this method is based on the cosmic distance ladder, where the value of H_0 is obtained by combining observations at various distance scales. For instance, the Supernova H_0 for the Equation of State (SH0ES) project obtained $H_0 = 74.03 \pm 1.42$ km s^{-1} Mpc^{-1} using the Cepheid calibrated Type Ia supernovae [40]. From the local observation, the H_0 value has been determined with very high accuracy.

Another way used for the H_0 determination is by observing the cosmic microwave background (CMB), which is a footprint of the Big Bang and contains information on the structure and history of the universe. The Hubble constant H_0 can also be determined from CMB measurements by assuming a cosmological model, and the *Planck* collaboration obtained $H_0 = 67.4 \pm 0.5$ km s^{-1} Mpc^{-1} by assuming the ΛCDM model in 2018 [41]. The H_0 value obtained from the CMB measurement is smaller than the local value. A recent analysis shows a 5σ difference between them [42]. This discrepancy between the two types of observations is called *Hubble tension*. Since the ΛCDM model is assumed for estimating the value of H_0 in the CMB measurements, this tension potentially suggests that the successful model of cosmology may need modification.

Motivated by this problem, extensions of the ΛCDM have been studied [43–45]. For example, models involving extra relativistic degrees of freedom [46–52], extra interactions [53–56], and modified gravity [57–61] have been proposed. In addition, there exist modifications of late-time dark energy properties [62–70]. Besides these approaches, various other modifications have been discussed.

Early dark energy (EDE) is also one of the promising scenarios [71–77]. EDE is an additional source of energy and behaves as dark energy until a certain time before recombination. The EDE accounts for a few percent of the total energy of the universe at this time and then dilutes faster than the energy density of the non-relativistic matter. The existence of EDE slightly modifies the cosmic expansion before the recombination with little effect on the late-time physics, which leads to a larger value of the Hubble constant obtained from the CMB data. Recently, many models and analyses related to EDE have been studied [78–89].

If EDE really exists in this universe, we have to clarify its physical origin. In some models of EDE, the behavior of the EDE is explained by a scalar field. For example, a canonical scalar field with an extended pseudo Nambu-Goldstone boson (PNGB) potential has been discussed [73]. As we will discuss in Chap. 3, the shape and mass parameters of the potential are constrained by the condition for the energy density of the scalar field to behave as EDE. Such scalar field giving EDE is not included in the SM, so it is expected that BSM can naturally explain the origin of the EDE scalar field.

In this thesis, we propose an EDE model based on a 5D $U(1)$ gauge theory. As mentioned above, the extra-component of the gauge field behaves as a scalar field in the 4D effective theory. This scalar field can play some cosmological role and was already considered as an inflaton [90] or quintessence [91]. We regard it as the EDE scalar field. The potential for the scalar is flat at tree level due to the 5D gauge symmetry, but an effective potential is generated by quantum effects. The properties of the potential are constrained by the underlying gauge symmetry, and we will see that it can have an ideal feature for the realization of EDE.

Flux Compactification

In higher-dimensional gauge theories with more than two compact extra dimensions, a background gauge field that gives a magnetic field penetrating the extra dimensions can be assumed, and this compactification is known as *flux compactification* or *magnetic compactification*. It was originally discussed extensively in the context of moduli stabilization in string theory [92–95], but it has been widely discussed also in the context of field theory. Higher-dimensional gauge theories with background magnetic flux have a lot of interesting features. For example, flux background with toroidal or orbifold compactifications yields chiral fermions having a generation structure [96–104]. In addition, the flavor structure of quarks and leptons, such as masses and mixing angles, has been widely examined in this setup [105–112]. This magnetic flux can also be a source of supersymmetry breaking [113].

In addition to the above, higher-dimensional gauge theories with background flux have a remarkable feature. The scalar field originating from a higher-dimensional gauge field is massless at tree level due to the higher-dimensional gauge symmetry. In the without flux case, quantum corrections to the mass arise, and their order is typically the compactification scale, which is the scale of the compact extra dimension. However, remarkably, in setups with non-vanishing flux, it was showed that the corrections are completely canceled out. This property was first demonstrated in an abelian gauge theory with $\mathcal{N} = 1$ supersymmetry [114], and later confirmed also in a non-supersymmetric abelian theory without supersymmetry [115]. It was also shown that the cancellation of the one-loop corrections are caused by the spontaneously symmetry breaking of the translational symmetry on the torus. The existence of the flux background breaks the translational symmetry on the torus. The extra-dimensional scalar is regarded as the NG boson related to the spontaneously broken translational symmetry, and it remains massless even under quantum corrections. A similar discussion has been carried out in a non-abelian $SU(2)$ gauge theory [116]. In addition, it has been shown that this cancellation holds even when considering higher-order loop corrections [117] and higher-dimensional operators [118].

This property enlarges the possibilities of higher-dimensional gauge theory. As mentioned, we obtain a finite correction to the mass, proportional to the compactification scale (2.63) in cases of vanishing flux. In GHUs, the zero-mode of the extra-dimensional component of a gauge field is regarded as the Higgs field, so the dynamically generated mass should be the observed Higgs mass 125 GeV, which means that the compactification scale can not be much larger than the weak scale. On the other hand, in non-vanishing flux cases, the extra dimensional gauge field corresponds to the NG boson of the broken translational symmetry, and it is kept massless even under quantum corrections. In addition, adding a term that explicitly breaks the translational symmetry to such theories leads to a finite correction to the mass [119]. If the breaking term is small, the finite correction is suppressed in comparison to the compactification scale. Therefore, the observed Higgs mass can be realized even when the compactification scale is much larger than the weak scale, which enlarges the possibilities for model building in GHU. A model of inflation based on this setup was also proposed [120], and a higher-dimensional gauge theory with background flux is an attractive setup from a phenomenological point of view.

Many of the previous studies have assumed specific gauge groups and background configurations. For further phenomenological applications, more comprehensive and general studies are needed to explore viable models based on the flux background. Therefore, in this work, we consider the extension of these discussions to an $SU(n)$ gauge group. In Chap. 5, we examine an $SU(n)$ pure Yang-Mills theory with a general background, including continuous Wilson lines in addition to a magnetic flux. We derive the mass spectrum of the theory, keeping the R_ξ gauge fixing parameter, and discuss its phenomenological implications. Our result shows the existence of tachyonic modes, which should be appropriately treated when considering applications of this model. Based on this study, we can consider various phenomenological applications of non-abelian gauge theories with magnetic flux background.

Organization of this Thesis

This thesis is organized as follows. In Chap. 2, we review the fundamentals of higher-dimensional gauge theory. Basic concepts of high-dimensional gauge theory, which will be required in later chapters, will be introduced. In Chap. 3, we also review the Early Dark Energy. We illustrate how the existence of EDE can solve the Hubble tension and that the behavior of EDE can be explained by a canonical scalar field with a suitable potential. Chap. 4 shows a model of EDE based on a 5D abelian gauge theory. In Chap. 5, we present another study on a 6D non-abelian gauge theory with a background magnetic flux. Finally, we conclude this thesis in Chap. 6.

Chapter 2

Basics of Higher-dimensional Gauge Theory

In this chapter, we review fundamentals of higher-dimensional gauge theories. In the first two sections, the quantum electrodynamics (QED) defined on $\mathcal{M}_4 \times S^1$ spacetime is introduced. In Sec. 2.3, we show the 4D low energy effective theory obtained from the 5D QED. After discussing some topics related to gauge transformation in Sec. 2.4 and Sec. 2.5, Sec 2.6 treats the effective potential generated for the zero-mode of the extra-dimensional component of the gauge field, which is regarded as a scalar field in the 4D effective theory. In Sec. 2.7, we comment on S^1/Z_2 orbifold compactification. Finally, in Sec 2.8, we review the quantum mechanics of a charged particle in a constant magnetic field as a preparation for Chap. 5.

2.1 Compact Extra-dimension: S^1

In this chapter, we consider a 5D spacetime with a compact extra dimension. We denote the spacetime coordinates by x^M $(M = 0, 1, 2, 3, 5)$, and we also use x^μ $(\mu = 0, 1, 2, 3)$ and $y = x^5$. A function of x^μ and y is simply expressed as $f(x, y)$. We often omit x in the argument when the x^μ-dependence is obvious or unimportant.

We mainly consider $\mathcal{M}_4 \times S^1$ spacetime where a compact extra-dimension S^1 exists at each point on the 4D Minkowski spacetime $\mathcal{M}_4$ (Fig. 2.1(a)). Let R be the radius of the extra-dimension S^1. The extra-dimension can be constructed by the identification

$$y \sim y + 2\pi R m \quad (m \in \mathbb{Z}), \tag{2.1}$$

as shown in Fig. 2.1(b). Since S^1 is flat, the metric of the 5D spacetime is given by $\eta^{MN} = \mathrm{diag}(- + + + +)$. The *compactification scale* $M_c = (2\pi R)^{-1}$ is the typical scale of a theory defined on this spacetime.

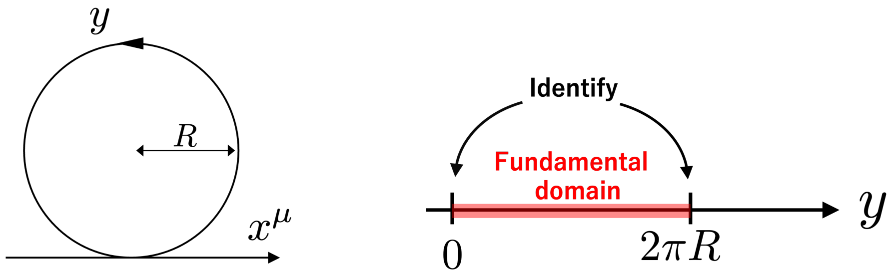

(a) 5D spacetime $\mathcal{M}_4 \times S^1$ **(b)** Identification $y \sim y + 2\pi R$

Figure 2.1: (a) 5D spacetime with a compact extra-dimension S^1 and (b) the identification to obtain S^1

The action of a theory defined on $\mathcal{M}_4 \times S^1$ spacetime is expressed using the corresponding 5D Lagrangian $\mathcal{L}_{5D}(x, y)$ as

$$S = \int d^4x \int_0^{2\pi R} dy\, \mathcal{L}_{5D}(x, y). \tag{2.2}$$

The 5D Lagrangian has to be single-valued on S^1, *i.e.*, the condition

$$\mathcal{L}_{5D}(x, y + 2\pi R) = \mathcal{L}_{5D}(x, y), \tag{2.3}$$

must be satisfied [121]. As discussed later, fields must satisfy some boundary conditions such that the Lagrangian satisfies this condition.

In Chap. 3, we also consider the orbifold S^1/Z_2 as an extra-dimension. This compact space is explained in Sec. 2.7 after finishing the introduction of all the fundamental concepts in the S^1 case. Chap. 5 discusses a non-abelian gauge theory defined on a 6D spacetime whose extra-dimensions are compactified to a torus, which is a straightforward generalization of the following discussion in the S^1 case.

2.2 5D QED

As a simple example of a higher-dimensional gauge theory, let us consider the 5D $U(1)$ gauge theory defined on $\mathcal{M}_4 \times S^1$ spacetime. Let $A_M(x, y)$ and $\psi(x, y)$ be a $U(1)$ gauge field and a Dirac field charged under the $U(1)$. The action of the 5D

QED is given by

$$S = \int_0^{2\pi R} dy \int d^4x \; \mathcal{L}_{5D,\mathrm{QED}}(x,y), \tag{2.4}$$

$$\mathcal{L}_{5D,\mathrm{QED}} = \bar{\psi}(x,y)(i\Gamma^M D_M - M_\psi)\psi(x,y) - \frac{1}{4}F^{MN}F_{MN}, \tag{2.5}$$

$$D_M = \partial_M - ig_5 q_\psi A_M(x,y), \tag{2.6}$$

$$F_{MN}(x,y) = \partial_M A_N(x,y) - \partial_N A_M(x,y), \tag{2.7}$$

where g_5 is the gauge coupling constant and $q_\psi(\in \mathbb{Z})$ is a $U(1)$ charge of the Dirac field. In what follows, we set $q_\psi = 1$ for simplicity. The parameter M_ψ, called *bulk mass*, represents the mass of the fermion in the 5D spacetime. The matrix Γ^M satisfies the 5D Clifford algebra

$$\{\Gamma^M, \Gamma^N\} = -2\eta^{MN}, \tag{2.8}$$

and is the 5D version of the gamma matrices. The Dirac conjugate of the fermionic field is defined by $\bar{\psi}(x,y) = \psi^\dagger(x,y)\Gamma^0$. By using the 4D gamma matrices γ^μ and $\gamma^5 = i\gamma^0\gamma^1\gamma^2\gamma^3$, we can express the 5D gamma matrices as $\Gamma^M = (\gamma^\mu, -i\gamma^5)$. Note that the mass dimensions of the fields and the gauge coupling constant included in the Lagrangian differ from those of the 4D theory. The Dirac field ψ, the gauge field A_M and the gauge coupling g_5 have the mass dimensions 2, 3/2 and $-1/2$, respectively. The Lagrangian density is invariant under the $U(1)$ gauge transformation

$$\begin{aligned} \psi(x,y) &\to \psi^{\mathrm{gt}}(x,y) = e^{i\Lambda(x,y)}\psi(x,y), \\ A_M(x,y) &\to A_M^{\mathrm{gt}} = A_M(x,y) + \frac{1}{g_5}\partial_M\Lambda(x,y). \end{aligned} \tag{2.9}$$

To define a gauge theory in higher-dimensional spacetime with compact extra-dimensions, we have to specify boundary conditions for fields in addition to writing down a Lagrangian. As discussed in Sec. 2.1, the Lagrangian in Eq. (2.5) has to satisfy the single-valued condition (2.3), which yields the boundary conditions

$$\psi(x, y+2\pi R) = e^{i2\pi\eta_\psi}\psi(x,y) \quad (\eta_\psi \in \mathbb{R}), \tag{2.10}$$

$$A_M(x, y+2\pi R) = A_M(x,y)\ , \tag{2.11}$$

on the 5D fields. Since ψ is included in the form of $\bar{\psi}\psi$ in the Lagrangian, the existence of the twist $e^{i2\pi\eta_\psi}$ is allowed.

A 5D field satisfying a boundary condition can be expanded by 4D fields. In the 5D example, the fields ψ and A_M satisfy the boundary conditions (2.10) and (2.11). For such fields, we can perform Fourier series expansions as

$$\psi(x,y) = \frac{1}{\sqrt{2\pi R}} \sum_{n=-\infty}^{\infty} \psi^{(n)}(x)\xi_n^{\psi}(y), \tag{2.12}$$

$$A_M(x,y) = \frac{1}{\sqrt{2\pi R}} \sum_{n=-\infty}^{\infty} A_M^{(n)}(x)\xi_n^{A_M}(y), \tag{2.13}$$

where the mode functions $\xi_n^{\psi}(y)$ and $\xi_n^{A_M}(y)$ can be chosen as

$$\xi_n^{\psi}(y) = e^{-i\frac{n+\eta_\psi}{R}y}, \quad \text{and} \quad \xi_n^{A_M}(y) = e^{-i\frac{n}{R}y}. \tag{2.14}$$

One can easily check that the mode functions satisfy the boundary conditions (2.10) and (2.11) and the orthogonal condition

$$\int_0^{2\pi R} \bar{\xi}_n^{\psi}\xi_m^{\psi} = \int_0^{2\pi R} \bar{\xi}_n^{A_M}\xi_m^{A_M} = 2\pi R\delta_{nm}, \tag{2.15}$$

where $\bar{\xi}_n^{\psi}$ and $\bar{\xi}_n^{A_M}$ are the complex conjugates of ξ_n^{ψ} and $\xi_n^{A_M}$, respectively. In this context, the mode expansion is especially called *Kaluza-Klein (KK) expansion*. Since $A_M(x,y)$ is a real valued field, the coefficient $A_M^{(n)}$ satisfies $A_M^{(-n)} = A_M^{(n)*}$. In the next section, we will see that the 4D fields $\psi^{(n)}(x)$ and $A_M^{(n)}(x)$ appear in the 4D effective theory obtained from the 5D QED.

2.3 4D Effective Theory

Performing the integral

$$\mathcal{L}_{4D,\text{QED}} = \int_0^{2\pi R} dy\ \mathcal{L}_{5D,\text{QED}}\ , \tag{2.16}$$

we obtain a 4D effective theory $\mathcal{L}_{4D,\text{QED}}$ that describes physics at energy scales lower than the compactification scale M_c. Here, we explicitly perform the extra-dimensional integration by substituting the Lagrangian (2.5) and the KK expansions (2.12) and (2.13). To do this, we divide $\mathcal{L}_{5D,\text{QED}}$ into the gauge sector and fermionic sector and discuss them separately.

2.3.1 Gauge Field

First, we calculate the gauge sector

$$\mathcal{L}_g = -\frac{1}{4}F_{MN}F^{MN} = -\frac{1}{4}F_{\mu\nu}F^{\mu\nu} - \frac{1}{2}F_{\mu y}F^{\mu y}\ , \tag{2.17}$$

$$F_{\mu\nu} = \partial_\mu A_\nu - \partial_\nu A_\mu\ , \tag{2.18}$$

$$F_{\mu y} = \partial_\mu A_y - \partial_y A_\mu\ . \tag{2.19}$$

For later discussion, we add the gauge fixing term

$$\mathcal{L}_\xi = -\frac{1}{2\xi}(\partial_\mu A^\mu + \xi \partial_y A_y)^2, \tag{2.20}$$

and consider the gauge-fixed Lagrangian

$$\begin{aligned}\mathcal{L}_g^{\mathrm{gf}} &= -\frac{1}{4}F_{MN}F^{MN} - \frac{1}{2\xi}(\partial_\mu A^\mu + \xi \partial_y A_y)^2 \\ &= \frac{1}{2}A_\mu\left[\eta^{\mu\nu}(\Box + \partial_y^2) + (1-\xi^{-1}\partial^\mu\partial^\nu)\right]A_\nu + \frac{1}{2}A_y[\Box + \xi\partial_y^2]A_y,\end{aligned} \tag{2.21}$$

where we performed an integral by parts, and $\Box = \partial^\mu\partial_\mu$ is the 4D d'Alembertian. Substituting the KK expansion (2.13) and using the orthogonal condition (2.15), we obtain

$$\begin{aligned}\mathcal{L}_{4D,g}^{\mathrm{gf}} = \sum_{n=-\infty}^{+\infty}\Bigg\{&\frac{1}{2}A_\mu^{(n)*}\left[\eta^{\mu\nu}\left(\Box + \frac{n^2}{R^2}\right) + (1-\xi^{-1})\partial^\mu\partial^\nu\right]A_\nu^{(n)} \\ &+ \frac{1}{2}A_y^{(n)*}\left(\Box + \xi\frac{n^2}{R^2}\right)A_y^{(n)}\Bigg\}\end{aligned} \tag{2.22}$$

$$\begin{aligned}= &\frac{1}{2}A_\mu^{(0)}\left[\eta^{\mu\nu}\Box + (1-\xi^{-1})\partial^\mu\partial^\nu\right]A_\nu^{(0)} + \frac{1}{2}A_y^{(0)}\Box A_y^{(0)} \\ &+ \sum_{n\neq 0}\Bigg\{\frac{1}{2}A_\mu^{(n)*}\left[\eta^{\mu\nu}\left(\Box + \frac{n^2}{R^2}\right) + \left(1-\xi^{-1}\right)\partial^\mu\partial^\nu\right]A_\nu^{(n)} \\ &+ \frac{1}{2}A_y^{(n)*}\left(\Box + \xi\frac{n^2}{R^2}\right)A_y^{(n)}\Bigg\}.\end{aligned} \tag{2.23}$$

The third and fourth terms in the last line, which contain mixing terms between real part and imaginary part of $A_M^{(n)}$, can be diagonalized by taking the linear combinations $(A_M^{(n)} + A_M^{(-n)})/2$ and $-i(A_M^{(n)} - A_M^{(-n)})/2$ without changing the Klein-Gordon-like operator. This Lagrangian contains an infinite number of the 4D gauge fields $A_\mu^{(n)}$ and $A_y^{(n)}$.

From the 4D Lagrangian, one finds that the 4D mass of $A_\mu^{(n)}$ is given as

$$M^2(A_\mu^{(n)}) = \frac{n^2}{R^2}, \tag{2.24}$$

and the nonzero KK modes $A_\mu^{(n)}$ $(n \neq 0)$ are massive. This result is independent of the introduction of a gauge-fixed term, and the existence of the mass term means that the 4D Lagrangian is not invariant under $A_\mu^{(n)}(x) \to A_\mu^{(n)}(x) + \frac{1}{\tilde{g}_4}\partial_\mu\Lambda(x)$ for $n \neq 0$. This implies that part of the symmetry that the 5D theory had is broken. Only the zero-mode part is invariant under such gauge transformations. The 5D

$U(1)$ gauge symmetry is broken to the 4D $U(1)$ gauge symmetry that acts only on the zero-mode of the 4D gauge field. In Sec. 2.5, we discuss symmetries in the 4D effective theory in more detail.

The masses of the nonzero-modes $M(A_\mu^{(n)})$ $(n \neq 0)$ are proportional to the compactification scale M_c. Therefore, the nonzero-modes decouple from the 4D effective theory, which describes physics below the compactification scale. The nonzero-modes of $A_y^{(n)}$ are also massive, and their masses depend on the gauge parameter ξ. This means that $A_y^{(n)}$ corresponds to a would-be Nambu-Goldstone mode giving a longitudinal mode to the massive gauge field $A_\mu^{(n)}$. Ignoring all the massive modes, we obtain

$$\mathcal{L}_{4D,g}^{\rm gf} \simeq \frac{1}{2} A_\mu^{(0)} \left[\eta^{\mu\nu} \Box + (1-\xi^{-1}) \partial^\mu \partial^\nu \right] A_\nu^{(0)} + \frac{1}{2} A_y^{(0)} \Box A_y^{(0)}, \tag{2.25}$$

as the 4D effective theory. From the 5D gauge sector, we have obtained a 4D gauge field $A_\mu^{(0)}$ and a 4D scalar field $A_y^{(0)}$. The 5D gauge invariance constrains the features of the scalar field $A_y^{(0)}$. For example, we can not write down the potential including mass terms for the gauge field in the 5D action, so there is no potential for $A_y^{(0)}$ in the 4D effective theory. As we will see later, the underlying gauge invariance also restricts properties of $A_y^{(0)}$ at the quantum level.

2.3.2 Dirac Field

Next, let us discuss the fermionic sector

$$\begin{aligned} \mathcal{L}_f &= \bar{\psi}(i\Gamma^M D_M - M_\psi)\psi \\ &= \bar{\psi} \left[i\Gamma^\mu (\partial_\mu - i g_5 A_\mu) + i\Gamma^5 (\partial_y - i g_5 A_y) - M_\psi \right] \psi. \end{aligned} \tag{2.26}$$

Here, we mainly focus on the mass spectrum of $\psi^{(n)}$. The integration of the first term and the third term is almost trivial because the operator in the square bracket does not act on the mode function in the KK expansion. Ignoring the nonzero-modes of A_M, the y integration of these terms yields

$$\mathcal{L}_{4D,f} \ni \sum_{n=-\infty}^{+\infty} \bar{\psi}^{(n)} \left[i\gamma^\mu \left(\partial_\mu - i \frac{g_5}{\sqrt{2\pi R}} A_\mu^{(0)} \right) - M_\psi \right] \psi^{(n)}, \tag{2.27}$$

from which we see that the 4D gauge coupling is given by

$$\tilde{g}_4 = \frac{g_5}{\sqrt{2\pi R}}. \tag{2.28}$$

This coupling $\tilde{g}_4$ has no mass dimension. In addition to the interaction between $\psi^{(n)}$ and $A_\mu^{(0)}$, there are also interactions between the fermionic modes and the higher KK modes of $A_\mu^{(n)}$ that are not relevant to our discussion now. We show the complete effective Lagrangian including the interaction terms in Sec. 2.5. The remaining term $i\Gamma^5(\partial_y - ig_5 A_y)$ gives an additional contribution to the $\psi^{(n)}$ mass and interactions between $\psi^{(n)}$ and $A_y^{(0)}$. Combining this contribution with Eq. (2.27), the term we are interested in is

$$\mathcal{L}_{4D,f} \ni \sum_{n=-\infty}^{+\infty} \bar{\psi}^{(n)} \left[i\gamma^\mu D_\mu^{(0)} - M_\psi - i\gamma^5 \left(\frac{n+\eta_\psi}{R} + \tilde{g}_4 A_y^{(0)} \right) \right] \psi^{(n)}, \tag{2.29}$$

where we introduced $D_\mu^{(0)} = \partial_\mu - iq_\psi \tilde{g}_4 A_\mu^{(0)}$ ($q_\psi = 1$ for now).

To derive the mass spectrum, let us consider the equation of motion (EoM) for $\psi^{(n)}$. A homogeneous background $\langle A_y \rangle = (2\pi R)^{-1/2} \langle A_y^{(0)} \rangle$ can be introduced without contradicting the 4D Lorentz invariance. On the other hand, the 4D Lorentz invariance prohibits A_μ from having a background value. By neglecting the fluctuations of $A_M^{(n)}$, we obtain the EoM

$$\left[i\gamma^\mu \partial_\mu - M_\psi - i\gamma^5 \left(\frac{n+\eta_\psi}{R} + \tilde{g}_4 \langle A_y^{(0)} \rangle \right) \right] \psi^{(n)} = 0, \tag{2.30}$$

for $\psi^{(n)}$ interacting only with the background field. Further acting an operator $(i\gamma^\mu\partial_\mu + M_\psi + i\gamma^5(\frac{n+\eta_\psi}{R} + \tilde{g}_4\langle A_y^{(0)}\rangle))$ on this equation yields

$$\left[\Box - M_\psi^2 - \left(\frac{n+\eta_\psi}{R} + \tilde{g}_4 \langle A_y^{(0)} \rangle \right)^2 \right] \psi^{(n)} = 0, \tag{2.31}$$

which means that the mass of $\psi^{(n)}$ is given by

$$M^2(\psi^{(n)}) = M_\psi^2 + \left(\frac{n}{R} + \frac{\eta_\psi}{R} + \tilde{g}_4 \langle A_y^{(0)} \rangle \right)^2. \tag{2.32}$$

We can recover the $U(1)$ charge by replacing $\tilde{g}_4$ by $q_\psi \tilde{g}_4$.

Let us first consider the $\langle A_y^{(0)} \rangle = 0$ and $\eta_\psi = 0$ case, where the 5D fermion satisfies a periodic boundary condition $\psi(y + 2\pi R) = \psi(y)$. In this case, the zero-mode $\psi^{(0)}$ has a mass M_ψ and remains in the 4D effective theory if the bulk mass is much smaller than the compactification scale. When $M_\psi = 0$, the mass spectrum (2.32) is equivalent to the one for the gauge field (2.24), and we obtain a massless Dirac fermion $\psi^{(0)}$ in the 4D effective theory. Next, we discuss the case with a nontrivial background $\langle A_y^{(0)} \rangle \neq 0$. There is an additional contribution from the interaction between the background, and the zero-mode mass is nonzero even when $M_\psi = 0$. This is similar to the way fermions acquire mass through coupling with the vev of a Higgs scalar in the Higgs mechanism; indeed, in GHU, $A_y^{(0)}$ is identified with the Higgs field. The background value $\langle A_y^{(0)} \rangle$ is not determined at tree-level because there is no potential for $A_y^{(0)}$ due to the 5D gauge symmetry. However, we will see that an effective potential is dynamically generated at loop-level. Finally, we turn to the case with a nontrivial phase ($\eta_\psi \neq 0$) in the boundary condition. In this case, the zero-mode has a large mass $\propto M_c$ and decouples from the 4D effective theory. Since η_ψ is the phase of the boundary condition, we can say that different boundary conditions yield different 4D effective theories. Therefore, theories with different boundary conditions describe different physics. More precisely, the theory has a 5D gauge symmetry, so there exists a gauge-equivalent class of boundary conditions. Roughly speaking, theories with boundary conditions belonging to the same class describe the same 4D physics in different ways. We will discuss this point in detail in Sec. 2.4.

2.3.3 Scalar Field

So far, we have discussed the mass spectra of the gauge and fermionic fields. We can also consider a charged scalar field $\phi(x, y)$, whose Lagrangian is given by

$$\mathcal{L}_{5D,b} = -|D_M \phi|^2 - M_\phi^2 |\phi|^2, \qquad D_M = \partial_M - i q_\phi g_5 A_M. \tag{2.33}$$

Here, M_ϕ is the bulk mass of ϕ, and $q_\phi (\in \mathbb{Z})$ is a $U(1)$ charge. The scalar has to satisfy the boundary condition

$$\phi(y + 2\pi R) = e^{i\eta_\phi} \phi(y), \tag{2.34}$$

and the KK expansion consistent with this boundary condition is

$$\phi(x, y) = \frac{1}{\sqrt{2\pi R}} \sum_{n=-\infty}^{+\infty} \phi^{(n)}(x) \xi_n^\phi(y), \tag{2.35}$$

$$\xi_n^\phi = e^{-i\frac{n+\eta_\phi}{R} y}. \tag{2.36}$$

We can derive the mass spectrum for $\phi^{(n)}$ in the same way as we did for $\psi^{(n)}$, and obtain

$$M^2(\phi^{(n)}) = M_\phi^2 + \left(\frac{n}{R} + \frac{\eta_\phi}{R} + q_\psi \tilde{g}_4 \langle A_y^{(0)} \rangle \right)^2. \tag{2.37}$$

In chapter 3, we consider the 5D scalar field in addition to the fermionic field.

2.3.4 Non-Abelian Gauge Field and Symmetry Breaking

Here, we comment on non-abelian gauge theories, which are discussed in Chap. 5. Let $\boldsymbol{A}_M$ be a non-abelian gauge field. In non-abelian gauge theories, the gauge field has self-interaction through the commutator $[\boldsymbol{A}_M, \boldsymbol{A}_N]$. Therefore, $\boldsymbol{A}_\mu$ can couple with the extra-dimensional background $\langle \boldsymbol{A}_y \rangle$, which makes some components of the 4D gauge field $\boldsymbol{A}_\mu^{(0)}$ massive. To be more concrete, let us consider the $SU(2)$ gauge theory where the gauge field is expanded by the Pauli matrices σ^i $(i = 1, 2, 3)$ as

$$\boldsymbol{A}_M = A_M^1 \frac{\sigma^1}{2} + A_M^2 \frac{\sigma^2}{2} + A_M^3 \frac{\sigma^3}{2}, \tag{2.38}$$

and assume a homogeneous background

$$\langle \boldsymbol{A}_y \rangle = v_y \sigma^3 = v_y \begin{pmatrix} 1 & 0 \\ 0 & -1 \end{pmatrix}, \tag{2.39}$$

where v_y is a real parameter. The term proportional to $([\langle \boldsymbol{A}_y \rangle, \boldsymbol{A}_\mu])^2$ in the kinetic term for the 5D gauge field yields mass terms for KK modes of $\boldsymbol{A}_\mu$. Since the last term in Eq. (2.38) commutes with this background, $\langle \boldsymbol{A}_y \rangle$ has no interaction with A_μ^3 and does not affect its mass spectrum. Therefore, the zero-mode of A_μ^3 remains massless in the 4D effective theory. On the other hand, A_μ^1 and A_μ^2 couple to the background, which gives nonzero mass to their zero-modes. Thus, the background breaks the gauge symmetry in the higher-dimensional theory, and the 5D $SU(2)$ gauge symmetry is broken to $U(1)$ in the 4D effective theory in this example. We will treat this kind of symmetry breaking in Chap. 5.

2.4 Boundary Condition and Gauge Transformation

As shown above, the boundary condition affects physical quantities like the mass spectrum in the 4D effective theory, which means that 5D theories with different boundary conditions yield different 4D effective theories. However, since the Lagrangian has a $U(1)$ gauge invariance, there are gauge equivalent classes of 4D effective theories. The boundary conditions (2.10) and (2.11) are gauge-dependent, and after the gauge transformation (2.9), the boundary conditions become

$$\psi^{\rm gt}(y + 2\pi R) = e^{i\eta_\psi} e^{i(\Lambda(y+2\pi R) - \Lambda(y))} \psi^{\rm gt}(y), \tag{2.40}$$

$$A_M^{\rm gt}(y + 2\pi R) = A_M^{\rm gt}(y) - \frac{1}{g_5}(\partial_M \Lambda(y + 2\pi R) - \partial_M \Lambda(y)). \tag{2.41}$$

In general, while the gauge transformation keeps the action unchanged, it changes the boundary conditions and the resulting effective theory. The gauge invariance ensures that different effective theories related to each other through gauge transformations describe the same physics.

To illustrate it, let us consider the 5D QED where the boundary condition for ψ is

$$\psi(y + 2\pi R) = e^{i\eta_\psi}\psi(y) \quad (\eta_\psi \neq 0), \tag{2.42}$$

and A_y has no background value, i,e., $\langle A_y \rangle = 0$. In this setup, the mass spectrum of $\psi^{(n)}$ is given by

$$M^2(\psi^{(n)}) = M_\psi^2 + \left(\frac{n + \eta_\psi}{R}\right)^2, \tag{2.43}$$

and $\psi^{(0)}$ decouples from the effective theory due to the twist η_ψ in the boundary condition. Before performing the integration over the extra dimensions to obtain the effective theory, we can perform a 5D gauge transformation by

$$\Lambda(y) = \frac{\eta_\psi}{R} y. \tag{2.44}$$

The gauge transformation changes the boundary condition for ψ to

$$\psi^{\mathrm{gt}}(y + 2\pi R) = \psi^{\mathrm{gt}}(y). \tag{2.45}$$

In this gauge, the boundary condition for the Dirac field is periodic, and there is no twist contributing to the mass spectrum. Instead, A_y shifts as

$$A_y(x, y) \to A_y^{\mathrm{gt}}(x, y) = A_y(x, y) + \frac{\eta_\psi}{g_5 R}, \tag{2.46}$$

which means that $A_y^{(0)}$ has a nonzero background value $\langle A_y^{\mathrm{gt}(0)} \rangle = \frac{\eta_\psi}{\tilde{g}_4 R}$ in this gauge. The mass spectrum of the fermion is

$$M^2(\psi^{\mathrm{gt}(n)}) = M_\psi^2 + \left(\frac{n}{R} + \tilde{g}_4 \langle A_y^{\mathrm{gt}(0)} \rangle\right)^2. \tag{2.47}$$

In this gauge, instead of having no contribution from the twist phase η_ψ, $A_y^{\mathrm{gt}(0)}$ has a nontrivial background value, resulting in the same mass spectrum. Although the origin of the mass contribution is different in the two gauges, 5D theories with different but gauge-equivalent boundary conditions describe the same 4D physics.

2.5 Symmetry in the 4D Effective Theory and Wilson Line

Let us discuss the symmetry in the 4D effective theory obtained from the 5D QED (2.5) in more detail. Without the R_ξ gauge fixing, we obtain the following

Lagrangians for the gauge and fermionic sectors.

$$\begin{aligned}\mathcal{L}_{4D,g} = &-\frac{1}{4}F^{(0)}_{\mu\nu}F^{\mu\nu(0)} - \frac{1}{2}(\partial_\mu A^{(0)}_y)^2 \\ &+\sum_{n\neq 0}\Bigg[-\frac{1}{4}F^{(n)*}_{\mu\nu}F^{\mu\nu(n)} + \frac{n^2}{R^2}A^{(n)*}_\mu A^{\mu(n)} - \frac{1}{2}|\partial_\mu A^{(n)}_y|^2 \\ &\qquad\qquad - i\frac{n}{2R}\left\{(\partial^\mu A^{(n)}_y)A^{(n)*}_\mu - A^{(n)}_\mu(\partial^\mu A^{(n)}_y)^*\right\}\Bigg],\end{aligned} \tag{2.48}$$

$$\begin{aligned}\mathcal{L}_{4D,f} = &\sum_{n=-\infty}^{+\infty}\bar{\psi}^{(n)}\left[i\gamma^\mu D^{(0)}_\mu - M_\psi - i\gamma^5\left(\frac{n+\eta_\psi}{R}+\tilde{g}_4 A^{(0)}_y\right)\right]\psi^{(n)} \\ &+\tilde{g}_4\sum_{n=-\infty}^{+\infty}\sum_{n'\neq 0}\bar{\psi}^{(n+n')}\left[\gamma^\mu A^{(n')}_\mu - i\gamma^5 A^{(n')}_y\right]\psi^{(n)}.\end{aligned} \tag{2.49}$$

Here, we have introduced the field strength of the n–th mode of the gauge field

$$F^{(n)}_{\mu\nu} = \partial_\mu A^{(n)}_\nu - \partial_\nu A^{(n)}_\mu. \tag{2.50}$$

In the gauge sector without gauge fixing (2.48), the last line, which contains the mixing between $A^{(n)}_\mu$ and $A^{(n)}_y$, implies that the nonzero-modes of $A^{(n)}_y$ correspond to the would-be Nambu-Goldstone modes. The last line in the fermionic sector (2.49) represents the interactions between the fermions and nonzero-modes of $A^{(n)}_M$, which are ignored in Eq. (2.29). To derive this part from the 5D QED Lagrangian, we used

$$\int_0^{2\pi R} dy\ \bar{\xi}^\psi_{n_1}\xi^{A_M}_{n_2}\xi^\psi_{n_3} = 2\pi R\delta_{n_1,n_2+n_3}. \tag{2.51}$$

Let us discuss the symmetry in the 4D effective Lagrangian given by the sum of Eqs. (2.48) and (2.49). The 4D effective theory is invariant under the following transformations:

$$\begin{gathered}A^{(0)}_\mu(x) \to A^{(0)}_\mu(x) + \frac{1}{\tilde{g}_4}\partial_\mu\tilde{\Lambda}(x), \quad A^{(0)}_y \to A^{(0)}_y + \frac{m}{\tilde{g}_4 R}, \\ A^{(n)}_\mu(x) \to A^{(n)}_\mu(x), \quad A^{(n)}_y(x) \to A^{(n)}_y(x) \quad (n\neq 0), \\ \psi^{(n)}(x) \to \psi^{\mathrm{gt}(n)}(x) = e^{i\tilde{\Lambda}(x)}\psi^{(n+m)}(x).\end{gathered} \tag{2.52}$$

The transformations related to $\tilde{\Lambda}(x)$ correspond to the 4D $U(1)$ gauge symmetry that remains in the 4D effective theory. On the other hand, since $A^{(n)}_\mu$ $(n \neq 0)$ are massive, they have no gauge symmetry. In addition to the 4D gauge symmetry, the

Lagrangians are invariant under the constant shift related to the integer m. The constant shift of $A_y^{(0)}$ effectively changes n/R to $(n+m)/R$ in the parentheses in Eq. (2.49), but $\psi^{(n)}$ transforms to $\psi^{(n+m)}$ at the same time, and therefore, the first term in $\mathcal{L}_{4D,f}$ is kept unchanged under the transformation. The second term in $\mathcal{L}_{4D,f}$ and the gauge sector $\mathcal{L}_{4D,g}$ are trivially invariant under the transformation. Therefore, the transformations in Eq. (2.52) keep the 4D effective theory obtained from the 5D QED invariant.

There is a 5D gauge transformation related to the above 4D transformation, and it is given by the 5D gauge transformation function

$$\Lambda(x,y) = \tilde{\Lambda}(x) + \frac{m}{R}y \qquad (m \in \mathbb{Z}). \tag{2.53}$$

The transformations of the 5D fields A_M and ψ are given by

$$A_\mu^{\rm gt}(x,y) = A_\mu(x,y) + \frac{1}{g_5}\partial_\mu \tilde{\Lambda}(x), \quad A_y^{\rm gt}(x,y) = A_y(x,y) + \frac{m}{g_5 R}, \tag{2.54}$$

$$\psi^{\rm gt}(x,y) = e^{i\tilde{\Lambda}(x)} e^{i\frac{m}{R}y}\psi(x,y). \tag{2.55}$$

As shown in Appx. 2, this gauge transformation acts the KK modes of the fields as Eq. (2.52). From this transformation function and Eqs. (2.40) and (2.41), we find that this gauge transformation does not change not only the 5D QED Lagrangian but also the boundary conditions. In other words, the 5D gauge transformation (2.53) does not change the 5D theory at all, and this invariance appears in the 4D effective theory as the symmetry under the 4D transformation (2.52).

There exists an operator that contains the information of the symmetry in the 4D effective theory. In our 5D theory, the extra-dimension S^1 is not simply connected, and we can introduce a non-contractive loop operator

$$\langle W \rangle = e^{ig_5 \int_0^{2\pi R} dy\ \langle A_y \rangle} = e^{2\pi i R \tilde{g}_4 \langle A_y^{(0)} \rangle} = e^{i\theta_5}, \tag{2.56}$$

called the *Wilson line*. Here, we defined the Wilson line phase

$$\theta_5 = 2\pi R \tilde{g}_4 \langle A_y^{(0)} \rangle. \tag{2.57}$$

The Wilson line is not invariant under general 5D gauge transformations but is invariant under the transformation (2.52). Indeed, under the gauge transformation (2.52), the Wilson line phase shifts as $\theta_5 \to \theta_5 + 2\pi m$, and the Wilson line itself remains unchanged. The mass spectrum of a matter φ $(= \psi,\ \phi)$ can be expressed as

$$M(\varphi^{(n)}) = M_\varphi^2 + \left(\frac{n+\eta_\varphi}{R} + \frac{q_\varphi \theta_5}{2\pi R}\right)^2, \tag{2.58}$$

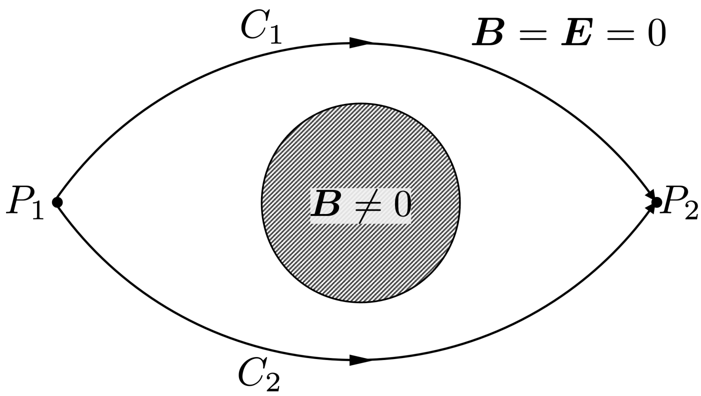

Figure 2.2: Aharonov-Bohm effect

by using the Wilson line phase. The whole tower of the KK masses is invariant under $\theta_5 \to \theta_5 + 2\pi R$ as mentioned. We will see that the effective potential for $A_y^{(0)}$ is generated as a function of the Wilson line.

The above discussion can be understood by an analogy with the Aharonov-Bohm effect in quantum mechanics [122]. Aharonov and Bohm examined the quantum mechanics of a charged particle around a solenoid in which the magnetic field exists only inside (Fig. 2.2). When a beam of charged particles is injected from the point P_1, the waves passing above (C_1) and below (C_2) the solenoid interfere with each other at point P_2. This interference can be observed in a screen at P_2 as interference fringes. The magnitude of the interference is determined by the difference in phases of the wave functions

$$\theta_{\mathrm{AB}} = e \oint_{C_1 - C_2} d\boldsymbol{x} \cdot \boldsymbol{A} = e\boldsymbol{\Phi}, \tag{2.59}$$

where e is the charge of the particle, $\boldsymbol{A}$ is the gauge field, and Φ is the magnetic flux penetrating the solenoid. The interference is caused by the fact that the space is not simply connected due to the magnetic field. The phase difference θ_{AB} is called the Aharanov-Bohm (AB) phase. Since θ_{AB} is a phase, the shift $\theta_{\mathrm{AB}} \to \theta_{\mathrm{AB}} + 2\pi m$ ($m \in \mathbb{Z}$) does not affect the interference fringes on the screen.

In our 5D theory, the screen at P_2 and the closed loop $C_1 - C_2$ correspond to the 4D spacetime $\mathcal{M}_4$ and the extra-dimension S^1, respectively. As the shift of the AB phase by 2π does not change the interference fringes on the screen, the shift of the Wilson line phase does not affect the 4D theory.

2.6 Effective Potential

In Sec. 2.3, we derived the 4D effective Lagrangian from the 5D QED Lagrangian (2.4). At least at classical level, the WL scalar $A_y^{(0)}$ has no potential including the mass term because we can not write the mass term $A_M A^M$ in the 5D QED Lagrangian, which conflicts with the local gauge symmetry. As mentioned above, however, the effective potential is generated as a function of the Wilson line $\langle W \rangle = e^{i\theta_5}$, which is a non-local operator, through interactions with $\psi^{(n)}$ and $\phi^{(n)}$. In this section, we derive the effective potential.

As shown in Sec. 2.3, $A_y^{(0)}$ interacts with $\psi^{(n)}$ and $\phi^{(n)}$. Using the vertices, we can consider one-loop diagrams as shown in Fig. 2.3. The effective potential is generated through the interactions shown in Fig. 2.3. Integrating out all of the KK modes of matter field φ we obtain

$$\Delta V_\varphi(\theta_5) = i\frac{n_\varphi}{2} \sum_{n=-\infty}^{\infty} \int \frac{d^4p}{(2\pi)^4} \ln\left[-p^2 + M^2(\varphi^{(n)})\right], \tag{2.60}$$

as the contribution from the field. Here, n_φ is the degrees of freedom of φ, where $n_\psi = 4$ for the fermion ψ and $n_\phi = -2$ for the scalar ϕ. The difference in the sign comes from the fermion loop factor. Although the higher-order KK modes of $\psi^{(n)}$ and $\phi^{(n)}$ decouples from the low-energy effective theory, we must sum over all KK modes to obtain finite corrections when evaluating the effective potential [13]. Otherwise, gauge symmetry can not be preserved. This can be understood as follows. The mode $\varphi^{(n)}$, whose corresponding mode function is given by $\exp(-i\frac{n+\eta_\varphi}{R}y)$, has a momentum $\propto n/R$ in the y direction. Therefore, introducing a cutoff in the KK mode is essentially equivalent to performing the cutoff regularization, which is well known to be incompatible with gauge symmetry. To respect the gauge invariance, all KK modes must be added up.

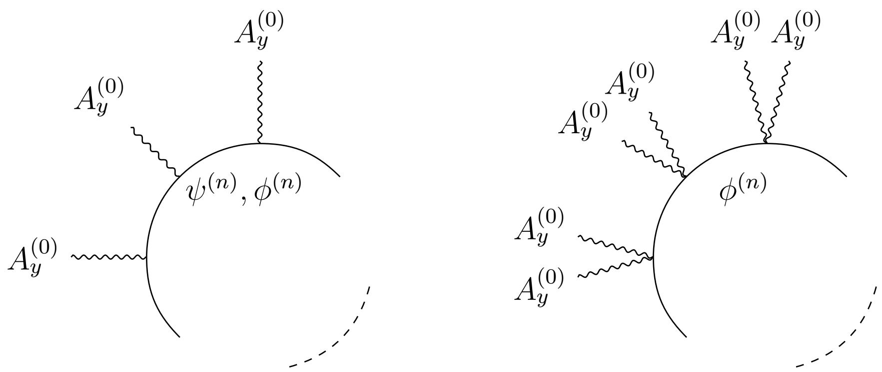

Figure 2.3: one-loop interactions contributing to the effective potential for $A_y^{(0)}$.

We can perform the momentum integral in Eq. (2.60) and finally obtain the following expression [123, 124]:

$$\Delta V_\varphi(\theta_5) = \frac{3n_\varphi M_c^4}{4\pi^2}\sum_{\ell=1}^{\infty} e^{-\ell M_\varphi/M_c}\left[\frac{1}{\ell^5} + \frac{1}{\ell^4}\frac{M_\varphi}{M_c} + \frac{1}{3\ell^3}\frac{M_\varphi^2}{M_c^2}\right]\cos[\ell(q_\varphi\theta_5 - 2\pi\eta_\varphi)]. \tag{2.61}$$

Since $\cos[\ell(q_\psi\theta + \eta_\varphi)] = \mathrm{Re}(\langle W\rangle^{q_\varphi \ell} e^{-i\ell\eta_\varphi})$, the effective potential is a function of the Wilson line and consistent with gauge invariance remaining in the 4D effective theory. The derivation of this expression is shown in Appx. A.2. The summation over the KK modes n is converted to a summation of the *winding number* that represents how many times the matter loop winds around the extra dimension. The $\ell = 0$ contribution is divergent, but we ignored it because it is constant and does not depend on θ_5. The θ_5-dependent part is generated by the non-local interactions where the matter field wraps around S^1 at least once, which is why we obtain the finite potential for the 4D scalar field $\langle A_y^{(0)}\rangle$. The potential is periodic under the shift $\theta \to \theta + 2\pi$. The total potential $V_{\text{eff}}(\theta_5)$ is obtained by adding up the contributions from all matter fields, which are ψ and ϕ in this case.

When the bulk mass is zero, the potential is reduced to

$$\Delta V_\varphi(\theta_5) = \frac{3n_\varphi M_c^4}{4\pi^2}\sum_{\ell=1}^{\infty}\frac{1}{\ell^5}\cos[\ell(q_\varphi\theta_5 - 2\pi\eta_\varphi)], \tag{2.62}$$

from which we find that the scale of the potential is M_c^4. In the 5D QED with $n_\psi = 4$, $q_\psi = 1$, and $\eta_\psi = 0$, the potential has minima at $\theta_5 \sim m\pi$ ($m \in \mathbb{Z}$), and the mass spectrum of $\psi^{(n)}$ contains the contribution from $\langle A_y^{(0)}\rangle \neq 0$. The mass correction around the minima can be calculated from the effective potential as

$$m^2_{A_y^{(0)}} = \left.\frac{\partial^2\Delta V_\psi(\theta_5)}{\partial A_y^{(0)2}}\right|_{\theta_5 = m\pi} = \frac{\tilde{g}_4^2}{M_c^2}\left.\frac{\partial^2\Delta V_\psi(\theta_5)}{\partial\theta_5^2}\right|_{\theta_5 = m\pi} = \frac{3\tilde{g}_4^2\zeta(3)}{\pi^2}M_c^2, \tag{2.63}$$

where

$$\zeta(z) = \sum_{\ell=1}^{\infty}\frac{1}{\ell^3}, \tag{2.64}$$

is the Riemann zeta function, and $\zeta(3) \simeq 1.202$. The field $A_y^{(0)}$ acquires a finite mass $\propto M_c$ through the quantum interaction.

In the nonzero bulk mass case $M_\varphi \neq 0$, we have the factor $e^{-\ell M_\varphi/M_c}$ in the summation. This factor represents that the existence of the bulk mass suppresses the propagation in the S^1 direction. This bulk mass suppression plays an important role in chapter 3, where we apply a 5D gauge theory with matter fields to EDE.

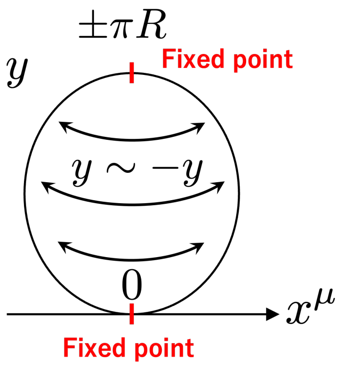

Figure 2.4: S^1/Z_2 orbifold. The points $y = 0$ and $y = \pm\pi R$ that are identified with themselves are called the fixed points.

2.7 S^1/Z_2 Orbifold

So far, we have assumed S^1 as the extra-dimension. In Chap. 3, we also consider S^1/Z_2 that can be obtained by further imposing the identification

$$y \sim -y, \tag{2.65}$$

on S_1 (Fig. 2.4). Due to this identification, the length of the extra-dimension is halved, and its integration interval becomes $[0, \pi R]$. On S^1/Z_2, a 5D Lagrangian has to satisfy

$$\mathcal{L}_{5D}(x, -y) = \mathcal{L}_{5D}(x, y), \tag{2.66}$$

in addition to Eq. (2.3), and this condition results in additional conditions for the field in the 5D QED. As a result, the 4D Lagrangian obtained from the 5D one also changes.

Before discussing the conditions and the 4D effective theory, we briefly explain why a geometry such as S^1/Z_2 is considered. In 5D theories, the chirality operator γ^5 does not commute with the generator of the 5D Lorentz transformation $\Sigma^{MN} = \frac{i}{4}[\Gamma^M, \Gamma^N]$ as $[\gamma^5, \Sigma^{\mu y}] \neq 0$. This fact means that right- and left-handed Weyl fermions mix with each other under 5D Lorentz transformations and we have to include both of them in a 5D Lagrangian to keep the 5D Lorentz invariance. In other words, fermions must be included in the form of Dirac fermion $\psi(x, y) = (\psi_R(x, y), \psi_L(x, y))^{\mathrm{T}}$. Therefore, it is difficult to realize a chiral theory such as the SM. However, the 5D Lorentz invariance is not fully preserved when the extra dimension is compact, and a chiral effective theory can be realized by choosing an appropriate geometry of the extra-dimension. In a 5D spacetime, S_1/Z_2 is one of such good choices to realize a chiral Lagrangian as a 4D effective theory.

To illustrate it, let us again consider the 5D QED (2.5) with $M_\psi = 0$ and $\eta_\psi = 0$. If the 5D fields satisfy the conditions

$$\psi(-y) = \pm i\Gamma^5\psi(y) = \pm\gamma^5\psi(y), \tag{2.67}$$

$$A_\mu(-y) = A_\mu(y), \quad A_y(-y) = -A_y(y), \tag{2.68}$$

the condition (2.66) can be satisfied. The sign in Eq. (2.67) is arbitrary, and we choose the minus, here. Then, in the chiral basis of the gamma matrices, the condition (2.67) yields

$$\psi_R(-y) = -\psi_R(y), \quad \psi_L(-y) = +\psi_L(y). \tag{2.69}$$

Now, A_M and $\psi_{R,L}$ satisfy the periodic boundary condition, and their KK expansions are given by

$$\tilde{\varphi}(x,y) = \frac{1}{\sqrt{2\pi R}}\tilde{\varphi}^{(0)}_{\text{even}} + \frac{1}{\sqrt{2\pi R}}\sum_{n=1}^{+\infty}\left[\tilde{\varphi}^{(n)}_{\text{even}}(x)\cos\left(\frac{n}{R}y\right) + \tilde{\varphi}^{(n)}_{\text{odd}}(x)\sin\left(\frac{n}{R}y\right)\right], \tag{2.70}$$

where $\tilde{\varphi} = A_M, \psi_L, \psi_R$, and a different basis of the mode function was chosen than before. The conditions (2.68) and (2.69) further constrain the KK expansion. For the fields that are even under $y \to -y$, *i.e.*, A_μ and ψ_L, $\tilde{\varphi}^{(n)}_{\text{odd}}$ must be zero to satisfy the parity condition. On the other hand, A_y and ψ_R, which are odd under the parity transformation, can not have even KK modes. The lack of even modes also means that there is no zero-mode for the field. Therefore, only ψ_L has a zero-mode and the 4D effective theory becomes chiral in this case.

In the example above, A_y can not have the zero-mode, which is not good because the zero-mode is identified as a cosmological scalar in Chap. 4. Fortunately, however, Eq. (2.68) is not the only possible choice. To obtain an zero-mode of A_y, we can consider the different boundary conditions as $A_\mu(x,-y) = -A_\mu(x,y)$ and $A_y(x,-y) = A_y(x,y)$ instead of Eq. (2.68). These boundary conditions are related to the outer automorphism, which is the complex conjugation of the representation of $U(1)$, and are called the conjugate boundary condition [125–127]. In this case, only A_y has a zero-mode, and A_μ has no massless mode. Therefore, the $U(1)$ gauge symmetry is broken. In chap. 4, we consider this setup as well as the S^1 compactification.

There is another subtle point in the S^1/Z_2 case. Under the parity transformation (2.67), the 5D fermion bilinear transforms as $\bar{\psi}\psi \to -\bar{\psi}\psi$, so the bulk mass term $M_\psi\bar{\psi}\psi$ is not invariant. This is why we set $M_\psi = 0$ in the above discussion. Instead, however, we can introduce a modified mass term $\epsilon(y)M_\psi\bar{\psi}\psi$, where $\epsilon(y) = 1$ for $y \geq 0$ and $\epsilon(y) = -1$ for $y < 0$ [124]. This bulk mass gives exactly the same contribution to the mass spectrum as in Eq. (2.32) for the S^1 case.

In the setup where A_y has a zero-mode, we can calculate the effective potential as done in Sec. 2.6. Since the mass spectra of the matter fields $\psi^{(n)}$ and $\psi^{(n)}$ do not change from those of the S^1 case, we obtain almost the same effective potential as in Eq. (2.61). The difference appears only in the degrees of freedom n_φ. On S^1/Z_2, the scalar $\phi(y)$ must satisfy the condition (2.67), and $\phi(y)$ also has to satisfy $\phi(-y) = +\phi(y)$ or $\phi(-y) = -\phi(y)$. As discussed for the fermion, the condition removes half of the KK mode. Therefore, the contribution to the effective potential is also halved, and $n_\psi = 2$ for a fermion and $n_\phi = -1$ for a complex scalar.

2.8 Quantum Mechanics of a Charged Particle in a Magnetic Field

In Chap. 5, we consider a 6D gauge theory with a magnetic flux background. Since the extra dimension is a 2D spacetime in this setup, it is helpful to review the quantum mechanical system of a charged particle in a 2D spacetime with a constant magnetic field, whose energy spectrum is known as the *Landau level* [128]. In Chap. 5, we will consider a 2D extra space compactified into a torus, but here we instead impose the periodic boundary conditions on the wave function.

In this setup, the Hamiltonian of a charged particle with mass m and charge e is given by

$$\hat{H} = \frac{1}{2m}(\hat{\Pi}_x^2 + \hat{\Pi}_y^2), \tag{2.71}$$

$$\hat{\Pi}_x = \hat{p}_x - eA_x, \quad \hat{\Pi}_y = \hat{p}_y - eA_y, \tag{2.72}$$

where $\hat{p}_x$ and $\hat{p}_y$ are the momenta of the particle, and the gauge field A_i $(i = x, y)$ giving the background magnetic field is

$$A_x(x, y) = -\frac{1}{2}(1-\gamma)B_0 y, \quad A_y(x, y) = \frac{1}{2}(1+\gamma)B_0 x. \tag{2.73}$$

We can freely choose the gauge parameter γ, but the physical consequences are independent of it. Substituting this background configuration, the Hamiltonian (2.71) becomes

$$\hat{H} = \frac{1}{2m}\left[\left(\hat{p}_x + \frac{1}{2}(1-\gamma)B_0 y\right)^2 + \left(\hat{p}_x - \frac{1}{2}(1+\gamma)B_0 y\right)^2\right]. \tag{2.74}$$

In what follows, for simplicity, we choose the *Landau gauge* $\gamma = 1$, where the Hamiltonian is reduced to

$$\hat{H} = \frac{1}{2m}\left[\hat{p}_x^2 + (\hat{p}_y - eB_0\hat{x})^2\right]. \tag{2.75}$$

The energy spectrum of the charged particle is determined by the time-independent Schrödinger equation

$$\hat{H}\psi(x,y) = E\psi(x,y), \tag{2.76}$$

where $\psi(x,y)$ is the wave function of the charged particle.

As mentioned above, we impose periodic boundary conditions on the wave function as

$$\psi(x+L_x, y) = \psi(x,y), \quad \psi(x, y+L_y) = \psi(x,y), \tag{2.77}$$

where L_x and L_y are unit length in the x- and y-directions, respectively. In this case, the strength of the background magnetic field B_0 is quantized. To illustrate it, let us consider the boundary conditions of the background gauge field. In the Landau gauge, we obtain the following relations from the background (2.73).

$$\begin{aligned} A_i(x+L_x, y) &= A_i(x,y) + \frac{1}{e}\partial_i T_x(x,y), \\ A_i(x, y+L_y) &= A_i(x,y) + \frac{1}{e}\partial_i T_y(x,y). \end{aligned} \tag{2.78}$$

Here, the functions T_i are defined as

$$T_x(x,y) = eB_0 L_x y, \quad T_y(x,y) = 0. \tag{2.79}$$

The relations in Eq. (2.78) mean that $A_i(L_x, y)$ and $A_i(x, L_y)$ differ from $A_i(0,y)$ and $A_i(x,0)$, respectively, but their difference in each direction can be represented by a gauge transformation. This is almost trivial since we are assuming the uniform background field B_0. In the Landau gauge, $T_x(x,y)$ is zero and the first relation is trivial, but it can be a nontrivial function in other gauges.

The gauge covariance of the Schödinger equation requires that the wave function $\psi(x,y)$ satisfies

$$\begin{aligned} \psi(x+L_x, y) &= e^{iT_x(x,y)}\psi(x,y), \\ \psi(x, y+L_y) &= e^{iT_y(x,y)}\psi(x,y). \end{aligned} \tag{2.80}$$

The wave function also has to satisfy the periodic boundary condition (2.77), which yields

$$eB_0 L_x L_y = 2\pi N \quad (N \in \mathbb{Z}). \tag{2.81}$$

This relation means that the magnetic flux $\Phi = B_0 L_x L_y$ is expressed as

$$\Phi = \phi_0 N, \qquad \phi_0 = \frac{2\pi}{e}, \tag{2.82}$$

where the integer N must be positive when $B_0 > 0$. In the system where the periodic boundary condition on the wave function is imposed, the magnetic flux is quantized in units of ϕ_0.

Next, we discuss the energy spectrum of the system. One finds that $\hat{p}_y$ and $\hat{H}$ are simultaneously diagonalizable since $[\hat{p}_y, \hat{H}] = 0$. Thus, we can expand the wave function as $\psi(x,y) = e^{ip_y y}\tilde{\psi}(x)$ and obtain the Hamiltonian for $\tilde{\psi}(x)$

$$\hat{H}_x = \frac{1}{2m}\hat{p}_x^2 + \frac{m\omega_c^2}{2}(\hat{x} - x_0)^2, \tag{2.83}$$

where

$$\omega_c = \frac{|e|B_0}{m}, \quad x_0 = \frac{p_y}{eB_0}, \tag{2.84}$$

and p_y is the eigenvalue of $\hat{p}_y$. Eq. (2.83) is equivalent to the Hamiltonian of the harmonic oscillator centered at x_0, and ω_c is called the *cyclotron frequency*. In a finite system, the value of p_y is quantized as $p_y = 2\pi\ell/L_y$ ($\ell \in \mathbb{Z}$), and the requirement that the center x_0 must lie in the range $0 \leq x_0 < L_x$ limits the possible values of the integer ℓ as

$$0 \leq \ell \leq N - 1, \tag{2.85}$$

where we used Eq. (2.82). The energy eigenvalue of this system is given by

$$E_{n,\ell} = \omega_c\left(n + \frac{1}{2}\right) \qquad (n = 0, 1, 2, \ldots;\ \ell = 0, 1, \ldots, N-1), \tag{2.86}$$

and the exited states in the x-direction are referred to as *Landau levels*. The energy is independent of the center of the harmonic oscillator labeled by ℓ, and each landau level is degenerate. The number of the degenerated states is proportional to the strength of Φ.

The energy spectrum can be obtained in another way. When the gauge field is given by Eq. (2.73), the operators

$$a^\dagger = \frac{\Pi_x - i\Pi_y}{\sqrt{2eB_0}}, \quad a = \frac{\Pi_x + i\Pi_y}{\sqrt{2eB_0}}, \tag{2.87}$$

satisfy $[a, a^\dagger] = 1$ independent of the gauge parameter γ. Namely, they are creation and annihilation operators, and the Hamiltonian is expressed by

$$\hat{H} = \omega_c\left(a^\dagger a + \frac{1}{2}\right). \tag{2.88}$$

Therefore, we obtain a Landau-level energy spectrum regardless of the choice of the gauge.

Chapter 3

Hubble Tension and Early Dark Energy

In this chapter, we review the EDE solution to the Hubble tension. Sec. 3.1 shows why the EDE makes the value of the Hubble constant obtained from the CMB data larger. In Sec. 3.2, we review the EDE model by a canonical scalar field. We use the extended PNGB potential as an example and discuss how the potential should be for the scalar giving EDE.

3.1 Early Dark Energy

This section reviews the EDE resolution to the Hubble tension. In the following, we assume a homogeneous, isotropic, and flat universe, described by the Friedmann-Lemaître-Robertson-Walker (FLRW) metric.

The scale of the universe at t is expressed by the scale factor $a(t)$, and the Hubble parameter $H(t) = \dot{a}(t)/a(t)$ represents the cosmic expansion rate at t. The Hubble constant H_0 is the present value of the Hubble parameter, *i.e.*, $H_0 = H(t_0)$, where t_0 represents the present time. The redshift $z(t) = a(t_0)/a(t) - 1$ is often used instead of t to represent time. In terms of the redshift, $z = 0$ corresponds to t_0 and $z = \infty$ is at the beginning of the universe.

The time evolution of the Hubble parameter is determined by the energy density of the universe $\rho(z)$, which also depends on time. In the standard ΛCDM model, the non-relativistic matter $\rho_m(z)$, radiation $\rho_r(z)$, and cosmological constant $\rho_{\Lambda,0}$ contribute to the total energy density. Here, in addition to these ΛCDM contributions, we suppose the existence of a scalar field corresponding to the EDE scalar, which gives a non-negligible contribution $\rho_\phi(z)$ to the total energy density for later discussion. Then, the total energy density is given by

$$\rho(z) = \rho_m(z) + \rho_r(z) + \rho_{\Lambda,0} + \rho_\phi(z), \tag{3.1}$$

where $\rho_\phi(z) = 0$ in the ΛCDM.

The time evolution of the energy density of each element x $(= m, r, \Lambda)$ in ΛCDM is determined by a parameter called the equation of state (EoS) w_x. The equation of state is given by the ratio of the pressure and energy density of the element, and $w_m = 0$, $w_r = 1/3$, and $w_\Lambda = -1$ for the non-relativistic matter, radiation, and cosmological constant, respectively. The time-evolution of x

$$\rho_x(z) = \rho_{x,0}(1+z)^{-3(1+w_x)}, \tag{3.2}$$

where we defined $\rho_{m,0} \equiv \rho_m(0)$ and $\rho_{r,0} \equiv \rho_r(0)$. The energy densities of matter and radiation dilute with the cosmic expansion, and $\rho_r(z)$ dilutes faster than $\rho_m(z)$. On the other hand, the energy density of the cosmological constant does not depend on time and does not decay.

The Friedmann equation

$$3M_\mathrm{P}^2 H^2 = \rho(z) = \rho_{m,0}(1+z)^3 + \rho_{r,0}(1+z)^4 + \rho_{\Lambda,0} + \rho_\phi(z), \tag{3.3}$$

determines the time evolution of $a(t)$. Here $M_\mathrm{P} = (8\pi G)^{-1/2} \simeq 2.4 \times 10^{18}$ GeV is the reduced Planck mass, and G is the gravitational constant. We define the energy density parameters $\Omega_{x,0} \equiv \rho_{x,0}/\rho(0)$ and a parameter h that represents H_0 in units of $\bar{H}_0 = 100$ km s^{-1} Mpc^{-1} to rewrite Eq. (3.3) as

$$H = \bar{H}_0\sqrt{\Omega_{m,0}h^2(1+z)^3 + \Omega_{r,0}h^2(1+z)^4 + \Omega_{\Lambda,0}h^2}, \tag{3.4}$$

for the ΛCDM model ($\rho_\phi = 0$). The density parameters $\Omega_{x,0}$ represent the fraction of the energy of x out of the total energy at the present time and satisfy

$$\Omega_{m,0} + \Omega_{r,0} + \Omega_{\Lambda,0} = 1, \qquad 0 \le \Omega_{x,0} \le 1, \quad (x = m, r, \Lambda), \tag{3.5}$$

by definition. The parameters $\Omega_{x,0}$ and h determine the time evolution of the universe in the ΛCDM model.

These cosmological parameters are determined observationally. Here, we see how they are determined from the CMB observations. The CMB average temperature T_0 determines the energy density parameter of the photon $\Omega_{\gamma,0}$, and $\Omega_{\gamma,0}h^2 = 2.47 \times 10^{-5}$ is obtained for $T_0 = 2.725$ K [129]. In addition to the photon, the neutrinos also contribute to the energy density of the radiation. The neutrino contribution can be included by using the relation $\Omega_{r,0} = (1 + 0.227N_\mathrm{eff})\Omega_{\gamma,0}$, where N_eff is the relativistic degrees of freedom of neutrinos [130]. The SM predicts $N_\mathrm{eff} = 3.044$ [131], so we obtain $\Omega_{r,0}h^2 = 4.18 \times 10^{-5}$. The energy density of the baryonic matter $\Omega_{b,0}$ and the total energy density of matter including DM $\Omega_{m,0}$ can be determined from the CMB power spectrum. The ratio of even-numbered to odd-numbered peak amplitudes determines $\Omega_{b,0}h^2$, and the ratio of the first peak to the other peaks determines $\Omega_{m,0}h^2$. The *Planck* collaboration obtained $\Omega_{b,0}h^2 = 0.0224 \pm 0.0001$ and $\Omega_{m,0}h^2 = 0.143 \pm 0.001$ [41]. By using these values, we find that the matter-radiation equality, where $\Omega_{r,0}h^2(1+z)^4$ and $\Omega_{m,0}h^2(1+z)^3$ coincides, occur at $z_{\rm eq} \simeq 3400$.

The Hubble parameter H_0 is determined by the angular size of the sound horizon θ_* at the CMB last-scattering. The value of θ_* can be derived from the location of the first peak in the CMB power spectra. The observable θ_* is related with the comoving distance $D(z_*)$ and the sound horizon $r_{s,*}$ that can be evaluated assuming a cosmological model as

$$\theta_* \equiv \frac{r_{s,*}}{D(z_*)}, \tag{3.6}$$

where $z_* \simeq 1090$ is the redshift at the last-scattering surface. The quantities $r_{s,*}$ and $D(z_*)$ are determined by the physics before and after the recombination, respectively, and given by

$$r_{s,*} = \int_{z_*}^{\infty} dz \frac{c_s(z)}{H}, \qquad D(z_*) = \int_0^{z_*} dz \frac{1}{H}, \tag{3.7}$$

where

$$c_s(z) = \left(1 + \frac{3\Omega_{b,0}h^2}{4\Omega_{\gamma,0}h^2(1+z)}\right)^{-1/2}, \tag{3.8}$$

is the sound speed in the baryon-photon fluid. The sound horizon $r_{s,*}$ hardly depends on the dark energy parameter $\Omega_{\Lambda,0}$ since the contribution in Eq. (3.4) is much smaller for $z \geq z_*$. Thus, using the values of $\Omega_{m,0}h^2$ and $\Omega_{r,0}h^2$ given in the previous paragraph, we can calculate the value of the sound horizon and obtain $r_{s,*} = 0.481\bar{H}_0^{-1} \approx 144$ Mpc. On the other hand, the value of $D(z_*)$ is sensitive to the dark energy density parameter. For $z \leq z_*$, the dark energy density parameter can not be ignored in Eq. (3.4), and it affects the integral for $D(z_*)$. Instead, in Eq. (3.7), we can eliminate $\Omega_{\Lambda,0}$ using Eq. (3.5). Substituting the values of $\Omega_{m,0}h^2$ and $\Omega_{r,0}h^2$ into $D(z_*)$ in Eq. (3.7), the comoving distance becomes a function of only h. Performing the integration numerically, we obtain $D(z_*) \simeq 3.2/H_0$, and thus Eq. (3.6) yields

$$H_0 \approx \frac{3.2\theta_*}{r_{s,*}}. \tag{3.9}$$

Therefore, for given θ_* and $r_{s,*}$, we can estimate H_0. A more precise analysis using Markov Chain Monte Carlo simulations gives $H_0 = 67.4 \pm 0.5$ km s^{-1} Mpc^{-1} [41], but this is much smaller than values obtained from various local observations.

The relation (3.9) implies that if the value of $r_{s,*}$ is smaller than the one calculated by assuming the ΛCDM, the value of H_0 obtained from the CMB observations gets larger. More precisely, if $r_{s,*}$ can be reduced without reducing the numerator 3.2 $\propto D(z_*)$, H_0 becomes larger. Eq. (3.7) tells us that we need a modification that makes $H(z)$ larger only in the pre-recombination era ($z_* < z$). In the EDE scenario, this modification is realized by the additional contribution $\rho_\phi(z)$ that is not negligible only for $z_* < z$ and hardly affects the total energy density after the recombination, *i.e.*, $\rho_\phi(z)/\rho(z) \ll 1$ for $z < z_*$.

More concretely, EDE behaves as dark energy before a certain time $z_{\rm EDE}(> z_*)$ and its energy density decays faster than the background non-relativistic matter in $z < z_{\rm EDE}$ (Fig. 3.1). In Fig. 3.1, the blue, red, and magenta lines correspond to the energy fractions of the radiation, non-relativistic matter, and cosmological constant, respectively. As in the ΛCDM model, there are three periods in which each of these elements dominates the universe. For $z > z_{\rm EDE}$, the energy density of EDE is constant while those of the background radiation and non-relativistic matter decay as $(1+z)^{-4}$ and $(1+z)^{-3}$, respectively. Therefore, the energy fraction of EDE increases and reaches a maximum ($\sim \mathcal{O}(1)\%$) at time $z_{\rm EDE}$. On the other hand, in the epoch $z < z_{\rm EDE}$, the energy fraction decreases since the energy density of EDE decays faster than $\rho_m(z)$. Therefore, EDE can reduce the value of $r_{*,s}$ while having little effect on the cosmic expansion after recombination, *i.e.*, hardly changing the comoving distance $D(z_*)$.

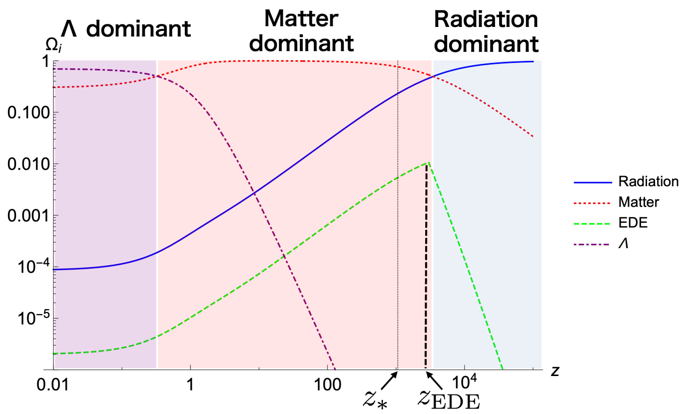

Figure 3.1: Cosmic history with EDE. The vertical axis represents the energy fraction. The colored regions correspond to the radiation, non-relativistic matter, and cosmological constant dominant epochs, respectively. z_* is the redshift at the recombination. For $z > z_{\rm EDE}$, EDE (green dashed line) behaves as dark energy. After accounting for a few percent of the total energy density at $z = z_{\rm EDE}$, the EDE energy density decays faster than the background non-relativistic matter (in this example, as fast as radiation).

3.2 Scalar Field EDE

Several possibilities and models of EDE have recently been studied [43]. Here, we mainly consider the cases where the EDE is given by a canonical and homogeneous scalar field $\phi(t)$ whose action is

$$S = \int d^4x \sqrt{-g} \left[\frac{1}{2}\dot{\phi}^2 - V(\phi) \right]. \tag{3.10}$$

Here, g is the determinant of the FLRW metric, and $V(\phi)$ is a potential for the scalar. The energy density ρ_ϕ and pressure p_ϕ of this scalar are given by

$$\rho_\phi = \frac{1}{2}\dot{\phi}^2 + V(\phi), \quad p_\phi = \frac{1}{2}\dot{\phi}^2 - V(\phi). \tag{3.11}$$

The EoS of this scalar field is

$$w_\phi = \frac{p_\phi}{\rho_\phi} = \frac{\frac{1}{2}\dot{\phi}^2 - V(\phi)}{\frac{1}{2}\dot{\phi}^2 + V(\phi)}, \tag{3.12}$$

from which one finds that w_ϕ varies with the dynamics of ϕ. The time evolution of the scalar field in the FLRW spacetime is determined by the EoM

$$\ddot{\phi}(t) + 3H(t)\dot{\phi}(t) + V_{,\phi} = 0, \tag{3.13}$$

where $V_{,\phi} = \partial V/\partial\phi$. The EoM is equivalent to the one of a particle with a time-dependent friction, called *Hubble friction*, and in the potential $V(\phi)$.

From Eqs. (3.12) and (3.13), we can understand intuitively how the scalar gives EDE. Since the Hubble parameter behaves as $\sim 1/t$ in the matter-dominated and the radiation-dominated periods, the friction is very large in the early universe. As a result, the scalar rolls very slowly in the potential, and the EoS behaves as $w_\phi \sim -1$ since the potential term is much larger than the kinetic term. The friction decreases and eventually the scalar begins to roll quickly along the potential. The redshift where the scalar starts to roll down corresponds to $z_{\rm EDE}$ in the previous section.The value of $z_{\rm EDE}$ that can alleviate the Hubble tension and is consistent with the late time measurement is model-dependent, and it is typically $z_* < z_{\rm EDE} \leq 10^6$ [79]. The EoS starts deviating from -1 at this time, and the time evolution thereafter depends on the shape of the potential. Therefore, if the potential has an appropriate shape, the transition of EoS from $w_\phi \sim -1$ to $w_\phi > 0$ is realized.

To discuss the realization of EDE by a scalar field in detail, let us assume the extended pseudo Nambu-Goldstone boson (PNGB) potential

$$V^{(n)}(\phi) = \Lambda^4_{(n)} \left(1 + \cos\frac{\phi}{f} \right)^n \qquad (n \in \mathbb{Z},\ n \geq 1), \tag{3.14}$$

which is discussed in Ref. [73]. The parameters $\Lambda_{(n)}$ and f have mass dimension 1. The PNGB potential is considered to be generated by non-perturbative effects such as instanton expansion and interpreted as the result of the spontaneous breakdown of approximate global symmetries. The parameter f corresponds to the symmetry breaking scale. The energy scale $\Lambda_{(1)}$ corresponds to the dynamical scale of the non-perturbative effects, and the $n \geq 2$ contributions are generated through higher-order instanton effects. In general, the potential for ϕ can be expressed as $V(\phi) = \sum_n V^{(n)}(\phi)$. Since $\Lambda_{(n)}/\Lambda_{(1)} \ll 1$ is naturally expected if $\Lambda_{(1)}$ is more suppressed than some ultra-violet cutoff scale [132, 133], the $n = 1$ contribution is usually dominant, *i.e.*, $V(\phi) \simeq V^{(1)}$. However, if there is some mechanism by which the $n = 1$ potential cancels, it is possible that the $n = 2$ is the leading contribution. Similarly, there is a possibility that $V^{(n)}$ is dominant for some reason, so we consider here the general case $V(\phi) \simeq V^{(n)}$.

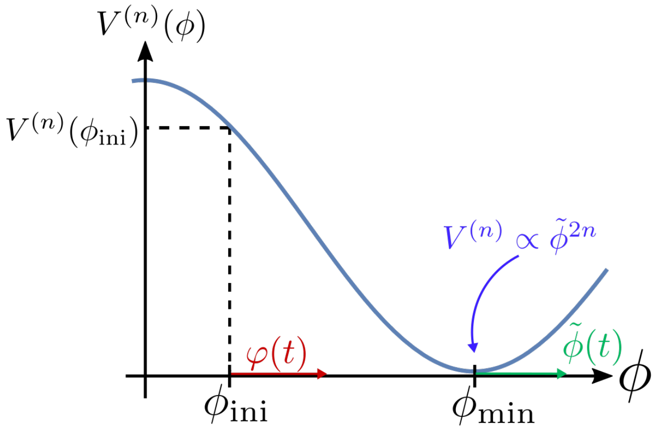

Figure 3.2: The PNGB type potential $V^{(n)}(\phi)$ in Eq. (3.14). $\phi_{\rm ini}$ is the initial value of the EDE scalar and $\varphi(t)$ represents the deviation from $\phi_{\rm ini}$. After the scalar rolls down the potential, it oscillates around $\phi_{\rm min}$. $\tilde{\phi}(t)$ is the deviation from this minimum.

Now, we discuss the conditions that must be satisfied for the scalar with the PNGB potential to give an EDE. Let $\phi_{\rm ini}$ be a initial value of $\phi(t)$ (Fig. 3.2). In the epoch $z \gg z_{\rm EDE}$, the scalar is almost frozen in the potential due to the Hubble friction. In the slow-roll phase, the energy density of the field is approximately given by $\rho_\phi \simeq V \simeq \Lambda_{(n)}^4$, which has to account for a few percent of the total energy density of the universe at $z_{\rm EDE}$. Since the typical scale of energy density at that period is $\rho(z_{\rm EDE}) \sim (1\ {\rm eV})^4$, the scale of the PNGB potential must be

$$\Lambda_{(n)} \sim 1\ {\rm eV}. \tag{3.15}$$

Next, we obtain another constraint on the potential from the condition for the transition to the fast-roll phase to occur at the appropriate timing. Let φ be the deviation from the initial value $\phi_{\rm ini}$ and write $\phi = \phi_{\rm ini} + \varphi$. We assume $\phi_{\rm ini}/f \ll 1$ just for simplicity and derive the EoM for the fluctuation. In the slow-roll phase, the first term in Eq. (3.13) can be ignored, and the EoM can be expressed as

$$\frac{1}{t}\dot{\varphi} = \frac{\Lambda_{(n)}^4}{f^2}\varphi, \tag{3.16}$$

in the lowest order of φ. We used $H(t) \sim 1/t$ and ignored an unimportant $\mathcal{O}(1)$ factor. The solution of this equation is

$$\varphi = \phi_{\rm ini} \exp\left(\frac{\Lambda_{(n)}^4}{2f^2}t^2\right) \sim \phi_{\rm ini} \exp\left(\frac{\Lambda_{(n)}^4}{f^2 H^2(t)}\right), \tag{3.17}$$

from which one finds that φ begins to deviate from $\phi_{\rm ini}$ rapidly when $\Lambda_{(n)}^4/f^2 = H^2$. The fast-roll has to start at $z_{\rm EDE}$, so using $H(z_{\rm EDE}) = \sqrt{\rho(z_{\rm EDE})/(3M_{\rm P}^2)} \sim 10^{-28}$ eV and Eq. (3.15) yields a constraint on f as

$$f \sim 10^{28}\ \text{eV} \sim M_{\rm P}. \tag{3.18}$$

Finally, we discuss the condition for $w_\phi > 0$ in $z \leq z_{\rm EDE}$. The scalar falls down to a minimum $\phi_{\rm min}$ and oscillates around this point. The EoS also oscillates with the oscillation of the field, and its time-averaged value depends on the shape of the potential. Around a minimum (*e.g.*, $\phi = \pi$), the extended PNGB potential (3.14) is expanded as

$$V^{(n)}(\tilde{\phi}) \simeq \frac{\Lambda_{(n)}^4}{2^n}\tilde{\phi}^{2n}, \tag{3.19}$$

where $\tilde{\phi}$ is the deviation from the minimum. For large values of n, the potential becomes flat, the period when the kinetic term becomes dominant in the EoS is extended, and the mean value of w_ϕ approaches 1. It is known that the time-averaged value is approximately given by

$$\langle w_\phi \rangle = \frac{n-1}{n+1}, \tag{3.20}$$

in the oscillating phase [134]. Therefore, for the energy density ρ_ϕ to decrease faster than ρ_m, $n \geq 2$ is required [79]. In the $n = 2$ case, $\langle w_\phi \rangle \sim 1/3$ holds during the oscillation, and ρ_ϕ behaves like ρ_r. Thus, the EDE scenario with the $n = 2$ potential and models with extra radiation components, which modify $N_{\rm eff}$ [41,135–137], are partly degenerate in their predictions. A novel and minimal setting occurs in the $n = 3$ case, which is suggested to be the most effective in addressing the Hubble tension in the analysis presented in [73].

We have obtained three conditions: (1) on the scale of the potential $\Lambda_{(n)} \sim 1$ eV, (2) on the symmetry breaking scale $f \sim M_{\mathrm{P}}$, and (3) on the shape of the potential, requiring $n \geq 2$ for oscillating scenarios. Similar arguments can also be made for other potentials, and we get restrictions on their parameters. The EDE scalar with such properties is expected to be naturally explained from a theoretical particle physics point of view. However, the potential looks challenging to realize from models of particle physics. First, the potential scale ~ 1 eV is very small, and it seems difficult to derive this tiny scale from typical BSMs. In addition, there is a vast hierarchy between $\Lambda_{(n)} \sim 1$ eV and $f \sim M_{\mathrm{P}}$, which implies an underlying mechanism that controls the potential. Ultralight axions can have potentials with hierarchical mass scales [132], and they have been proposed as possible candidates for the EDE scalar [73, 74, 79]. However, the PNGB potential usually has the $n = 1$ contribution and does not satisfy the third condition $n \geq 2$, and therefore, can not realize the dilution of the EDE energy density. Thus, if an axion-like particle is identified as the EDE scalar, an unknown mechanism, which ensures that $n \geq 2$ contributions dominate in the potential, is required. Natural scenarios should account for the suppression of the $n = 1$ contribution without fine-tuning. It does not appear to be easy to construct a model that satisfies all three conditions.

In the next chapter, as an alternative to the axion case, we point out that the scalar potential suitable to the EDE scenario appears in models incorporating a compact extra dimension. An extra-dimensional component of gauge fields naturally has a potential adequate to realize the EDE.

Chapter 4

Early Dark Energy from a 5D Abelian Gauge Theory

In this chapter, we propose a model of EDE based on a higher-dimensional gauge theory. We identify the zero-mode of the extra component of the gauge field in a 5D $U(1)$ gauge theory defined on a $\mathcal{M}_4 \times S^1$ spacetime as the EDE scalar and examine the possibility that the dynamically generated effective potential has the suitable properties discussed in the previous chapter. In Sec. 4.1, we present a setup of a higher-dimensional gauge theory that we consider as the origin of EDE in this study. Then, based on the discussion in Chap. 3, we discuss the conditions that the parameters in our model must satisfy in order to explain EDE. In Sec. 4.3, we show concrete examples that realize the EDE potential and check the behavior of the system numerically. Finally, in Sec. 4.4, we briefly summarize the study and provide some discussions.

4.1 EDE Model Based on a 5D $U(1)$ Gauge Theory with Matter Fields

This paper considers a 5D $U(1)_D$ gauge theory, the simplest higher-dimensional gauge theory, and examines the possibilities that A_y gives EDE. The extra-dimension is assumed to be compactified to S^1 or S^1/Z_2. In addition to the gauge field, we introduce N_f flavors of 5D Dirac fields ψ_m ($m = 1, \ldots, N_f$) and N_b flavors of 5D scalar fields ϕ_m ($m = 1, \ldots, N_b$). All the fields are independent of the SM sector and neutral under the SM gauge symmetry, and all the SM fields are singlets under the $U(1)_D$ gauge symmetry. That is, we consider the action

$$S = \int d^4x \int_0^{2\pi R} dy(\mathcal{L}_g + \mathcal{L}_\varphi), \tag{4.1}$$

$$\mathcal{L}_g = -\frac{1}{4}F_{MN}F^{MN}, \quad F_{MN} = \partial_M A_N - \partial_N A_M, \tag{4.2}$$

$$\mathcal{L}_\varphi = \sum_{m=1}^{N_f} \bar{\psi}_m(i\Gamma^M D_M - M_{\psi_m})\psi_m + \sum_{m=1}^{N_b} \left[|D_M\phi_m|^2 - M_{\phi_m}^2|\phi_m|^2\right], \tag{4.3}$$

as a dark sector. The covariant derivative for $\varphi = (\psi_1, \ldots, \psi_{N_f}, \phi_1, \ldots, \phi_{N_b})$ is defined by $D_M = \partial_M - iq_\varphi g_D A_M$, where g_D is the 5D gauge coupling and $q_\varphi(\in \mathbb{Z})$ is the $U(1)_D$ charge of φ. In the S^1/Z_2 case, as mentioned in Sec. 2.7, the bulk mass for the fermion M_{ψ_m} must be replaced by $\epsilon(y)M_{\psi_m}\bar{\psi}\psi$ for the Z_2 parity. In general, the bulk mass M_φ can be different for each field, but we assume that all matter fields have the same bulk mass M for simplicity. We will discuss the different mass case in the end of Sec. 4.3.

We must specify the boundary conditions for the gauge, Dirac, and scalar fields. The boundary condition for the gauge field is chosen so that the zero mode of A_y remains in the 4D effective theory. Namely, we assume the periodic boundary for the S^1 case and the conjugate boundary condition for the S^1/Z_2 case. Only in the the S^1 case, A_μ has a zero mode and the $U(1)_D$ gauge field remains in the 4D effective theory. For the Dirac and scalar fields, the boundary conditions for those fields are assumed to be periodic ,*i.e.*,

$$\varphi(y + 2\pi R) = \varphi(y). \tag{4.4}$$

Thus, the mass spectra of the matter fields take the form of (2.58) with $\eta_\varphi = 0$.

4.2 Effective Potential and EDE conditions

As explained in Chap. 2, $A_y^{(0)}$ has no potential at tree-level, but an effective potential is generated through quantum interactions between the matter fields. The contribution from φ is given by Eq. (2.61). In this study, we assume that the bulk mass M is larger than the compactification scale M_c, *i.e.*, $M > M_c$. In this case, the potential contribution is approximately written as

$$\Delta V_\varphi(\theta_5) \simeq \frac{n_\varphi M^2 M_c^2}{4\pi^2} e^{-M/M_c} \cos(q_\varphi \theta_5). \tag{4.5}$$

The factor n_φ takes 4 (-2) if φ is a 5D fermion (complex scalar) for the S^1 case, whereas n_φ takes 2 (-1) for the S^1/Z_2 case. The exponential factor e^{-M/M_c}, which represents the suppression of nonlocal interactions due to the bulk mass, plays an important role in this scenario. As mentioned in Chap. 2, the scale of the effective potential is M_c^4 for $M = 0$. Thus, it is difficult for the effective potential to be a suitable EDE potential for $M_c \gg 1$ eV. However, for $M \neq 0$, the factor e^{-M/M_c} lowers the scale of the effective potential and allows it to be the EDE scale. In our model, it is possible to obtain the EDE potential from the BSM scale naturally.

While not discussed in Chap. 2, additional contributions to the effective potential can arise through 5D gravitational interactions, which may change the potential structure in Eq. (2.61). However, since the effective potential for $A_y^{(0)}$ is generated by non-local interactions, such quantum gravity correction is expected to be suppressed by the factor e^{-M_5/M_c}, where M_5 is the 5D Planck mass parameter and related to the 4D Planck mass $M_{\rm P}$ as $M_5^3 = M_c M_{\rm P}^2$. Thus, if $M_5 > M$, the contribution from gravity is more suppressed compared to that from the matter field, which is suppressed by e^{-M/M_c}. In this case, the matter contributions are dominant, and the one-loop effective potential for θ_5 is given by $V(\theta_5) = \sum_\varphi \Delta V_\varphi(\theta_5)$.

Based on the above discussions, we study the constraints for the mass parameters in this scenario. To obtain the potential (4.5) as the dominant contribution, the condition

$$M_c < M_\varphi < M_5, \tag{4.6}$$

has to be satisfied. Using $M_5^3 = M_c M_{\rm P}^2$, it can be rewritten as

$$1 < \frac{M_\varphi}{M_c} < \left(\frac{M_{\rm P}}{M_c}\right)^{2/3}. \tag{4.7}$$

For a given value of the M_c, which is a free parameter in this model, this condition determines the allowed range of the bulk mass M. We show the allowed region in Fig. 4.1. The horizontal and vertical axes represent M_c/M_P and M_φ/M_c, and the white area corresponds to the region where the condition (4.7) is satisfied. On the other hand, the blue (red) shaded region is not consistent with the first (second) inequality in Eq. (4.7).

Let us examine the typical value of the parameters that give the required energy scale for EDE discussed in Sec. 3.2. When the potential is given by Eq. (3.14), the typical values of the mass parameters must be $\Lambda_{(n)} \sim 1$ eV and $f \sim M_{\rm P}$ for the scalar to give EDE. Our potential is equivalent to the PNGB type potential with $n = 1$, and, if we ignore $\mathcal{O}(1)$ factors such as n_φ and q_φ,

$$V_0 = \frac{M^2 M_c^2}{4\pi^2} e^{-M/M_c}, \tag{4.8}$$

and $\tilde{g}_D/M_c$ correspond to $\Lambda_{(n)}^4$ and f^{-1}, respectively. Therefore, we obtain the

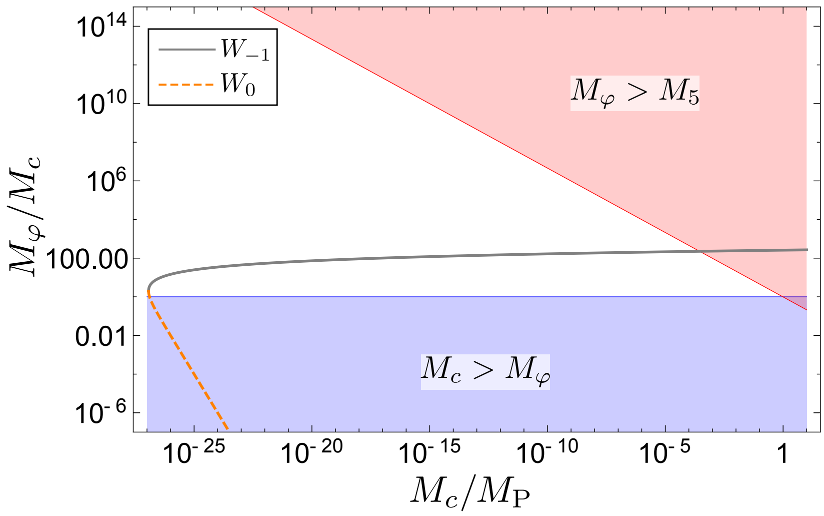

Figure 4.1: The allowed range of the mass parameters in the scenario where the extra-dimensional gauge field is identified as the EDE scalar. The blue shaded region is inconsistent with the first inequality in Eq. (4.7), where a PNGB-like potential (4.5) with a suppressed energy scale suitable for the EDE scalar potential can not be obtained. The red shaded region is inconsistent with the second inequality in Eq. (4.7), where the gravitational corrections to the potential are not safely neglected. The solid (black) and dashed (red) lines correspond to the solution of Eq. (4.10) for a given $M_c/M_{\rm P}$.

following constraints:

$$\frac{M_\varphi^2 M_c^2}{4\pi^2} e^{-M_\varphi/M_c} \sim (1\ \text{eV})^4, \qquad \tilde{g}_D \sim \frac{M_c}{M_{\rm P}}. \tag{4.9}$$

The first condition can be solved for M_φ/M_c, and the solution is given by

$$\frac{M_\varphi}{M_c} = -2W_k\left(-\frac{10^{-54}}{2}\left(\frac{M_c}{M_{\rm P}}\right)^{-2}\right), \tag{4.10}$$

where W_k $(k=-1,0)$ is the Lambert W function. This equation gives a typical scale of M for a given M_c. We show the solution (4.10) in Fig. 4.1. As the figure shows, only the $k=-1$ solution is consistent with the constraint in Eq. (4.6). From Fig. 4.1, one finds that a wide range of the compactification scale is allowed for the present scenario with $M_c/M_{\rm P} \lesssim 10^{-3}$. In most of the allowed regions, the ratio of the bulk mass to the compactification scale is $M_\varphi/M_c \sim \mathcal{O}(100)$. This result is consistent with the approximation made to obtain the expression (4.5), which neglects the $\ell \geq 2$ contributions.

The second relation in Eq. (4.9) implies another advantage of our scenario. The PNGB potential has the problem that the symmetry breaking scale f must be the 4D Planck scale. On the other hand, in our model, it is replaced by the condition for the 4D gauge coupling $\tilde{g}_D$, and therefore, the unnatural mass scale problem does not arise in our model. The 4D gauge coupling constant $\tilde{g}_D$ is determined by $M_c/M_{\rm P}$and $\tilde{g}_D \lesssim 10^{-3}$ in the allowed region. Such a small value of $\tilde{g}_D$ is consistent with the perturbative evaluation and the one-loop approximation of the effective potential in Eq. (2.61).

As discussed in Chap. 3.2, for the energy density of the EDE scalar to dilute faster than that of the background non-relativistic matter, the EDE potential must be expanded as $\tilde{\phi}^{2n}$ $(n \geq 2)$ around the minimum where the scalar eventually oscillates. This condition yields constraints on the $U(1)_D$ charges and numbers of the scalar and Dirac fields in the 5D theory. To illustrate this, let us express the full effective potential for θ_5 as

$$V_{\rm eff}(\theta_5) = -\, V_0 \sum_{\varphi} n_\varphi \left[1 - \cos(q_\varphi \theta_5)\right], \tag{4.11}$$

where we have introduced a constant contribution to the potential in order to set the minimum value of the potential zero. The phase of the Wilson line θ_5 is hereafter referred to as the EDE phase. This potential has an extremum at $\theta_5 = 0$, so let us expand $V_{\rm eff}(\theta_5)$ around this point as

$$V_{\rm eff}(\theta_5) \simeq V_0 \sum_{k=1}^{\infty} \frac{(-1)^k}{2k!} \left(\sum_{\varphi} n_\varphi q_\varphi^{2k} \right) \theta_5^{2k}. \tag{4.12}$$

For the expansion to start from the term $\propto \theta_5^{2n}$, the condition

$$\sum_{\varphi} n_\varphi q_\varphi^{2k} = 0, \tag{4.13}$$

must be satisfied for $k = 1, \ldots, n-1$. In addition, the coefficient of the leading term must be positive for the point to be a local minimum, so

$$\sum_{\varphi} n_\varphi q_\varphi^{2k} > 0, \tag{4.14}$$

also has to be satisfied. For a given set of fields φ with charge q_φ, these conditions give constraints for n_φ. If there exist solutions to the $(n-1)$ simultaneous algebraic equations (4.13) that satisfy the condition (4.14), then the potential $\propto \theta_5^{2n}$ can be realized. The value of n_φ in the solution must also be consistent with the fact that n_φ represents the degrees of freedom of φ.

The simultaneous equations (4.13) are solvable in general. Let us denote the bulk scalars or fermions whose charges are q_i by φ_i ($i = 1, \ldots, n$), where $|q_i| \neq |q_j|$ for $i \neq j$. In addition, let $|d_i|$ be the sum of the degrees of freedom of φ_i, where $d_i < 0$ ($d_i > 0$) for scalars (fermions). If there exist n different bulk fields with different charges, the set of equations (4.13) has the solution given by

$$\frac{d_i}{d_j} = -\frac{q_j^2}{q_i^2} \prod_{\substack{k=1 \\ k \neq i,j}}^{n} \frac{q_j^2 - q_k^2}{q_i^2 - q_k^2} \qquad (i \neq j), \tag{4.15}$$

as shown in Appendix B.1. The charges q_i must be chosen such that Eq. (4.14) is satisfied and d_i is an appropriate value for the sum of the degrees of freedom. Specific setups that satisfy all of these conditions are given in the next section. In such setups, the effective potential around $\theta_5 = 0$ is approximately written as

$$V_{\text{eff}}(\theta_5) \simeq V_{\text{eff}}^{(n)}(\theta_5) = -\frac{V_0}{(2n)!} d_j q_j^2 \left(\prod_{\substack{k=1 \\ k \neq j}}^{n} (q_k^2 - q_j^2) \right) \theta_5^{2n} + \mathcal{O}(\theta_5^{2n+2}), \tag{4.16}$$

which holds for any j.

In our scenario, the third condition $n \geq 2$ for the EDE potential, which is necessary to realize the energy density dilution faster than that of the non-relativistic matter, can be satisfied by appropriately assuming bulk matter contents that satisfy the conditions (4.13) and (4.14). This model can explain the origin of the flatness of the EDE potential around its minimum. In addition, since the constrained parameters are the degrees of freedom n_φ and the charge φ, this scenario does not need any fine-tuning for the cancellation of lower-order terms. This point is also an advantage of our model.

So far, we have assumed the periodic boundary conditions (4.4) for the bulk matter fields. If we assume the anti-periodic boundary condition $\eta_\varphi = 1/2$ for φ, the cosine in the effective potential (4.5) changes as $\cos(q_\varphi \theta_5) \to \cos(q_\varphi \theta_5 - \pi) = -\cos(q_\varphi \theta_5)$, which effectively corresponds to exchanging the sign of the fermionic and bosonic contributions, *i.e.*, $n_\varphi \to -n_\varphi$. Thus, if we change the boundary conditions of all fields from periodic to anti-periodic, the sign of the left-handed side of Eq. (4.14) flips. Therefore, bulk matter contents with periodic boundary conditions that satisfies Eq. (4.13) but not Eq. (4.14) can satisfy both of them with anti-periodic conditions.

In this section, we have considered the 5D $U(1)$ gauge theory (4.1) as the origin of the EDE scalar. The 5D component of the gauge field A_y in the 5D dark sector is identified as the EDE scalar. The effective potential for $A_y^{(0)}$ can be a suitable EDE potential without the unnatural mass scale problems discussed in Sec. 3.2. In our model, the compactification scale of the extra dimension M_c must be smaller than $\mathcal{O}(10^{-3}M_{\rm P})$. The conditions for the potential to be an appropriate EDE potential determine the order of the 4D gauge coupling $\tilde{g}_D$ and the bulk mass M. For $\tilde{g}_D \sim M_c/M_{\rm P}$ and $M_\varphi/M_c \sim \mathcal{O}(100)$, $A_y^{(0)}$ begins to roll down in the potential at $z_{\rm EDE}$ and its energy accounts for $\mathcal{O}(1)\%$ of the total energy in the universe at that time. In addition, the energy density of $A_y^{(0)}$ should decrease faster than that of the matter in the late universe. This behavior can be realized when the charges and degrees of freedom satisfy Eqs. (4.13) and (4.14). Therefore, we can conclude that this model can naturally realize the EDE potential.

4.3 Explicit Examples and Numerical Results

In this section, we provide two specific models where $n = 2$ and $n = 3$ effective potentials are realized and examine the behavior of these systems numerically. The $n = 2$ potential $\propto \theta_5^4$ is realized by the bulk matter content consisting of eight complex scalars with charge q_1 and a 5D fermion with $q_2 = 2q_1$ or $-2q_1$. We refer to the above case as the $n = 2$ model hereafter. The bulk matter content consisting of 15 complex scalars with charge q_1, a complex scalar with charge $q_2 = 3q_1$ or $-3q_1$, and three 5D fermions with charge $q_3 = 2q_1$ or $-2q_1$ realizes the $n = 3$ effective potential. We call this setup the $n = 3$ model.

Let us discuss the time evolution of the EDE phase θ_5 and its energy density ρ_{θ_5} in the above setups. In a 4D low-energy effective theory, $\langle A_y^{(0)}\rangle$ is a canonically normalized scalar field and obeys the same equation of motion as Eq. (3.13). It can be rewritten as the equation of motion for $\theta_5 = 2\pi R\tilde{g}_D\langle A_y^{(0)}\rangle$:

$$\ddot{\theta}_5 + 3H(t)\dot{\theta}_5 + (2\pi R)^2\tilde{g}_D^2\frac{dV_{\rm eff}(\theta_5)}{d\theta_5} = 0. \tag{4.17}$$

For given $V_{\rm eff}(\theta_5)$ and initial conditions for θ_5 and $\dot{\theta}_5$, the time evolution of the EDE phase is determined by this equation. We denote the EoS by w_{θ_5} and the energy density parameter by $\Omega_{\theta_5}(z) = \rho_{\theta_5}(z)/\rho(z)$. The total energy density $\rho(z)$ is given by Eq. (3.3), and $\rho_\phi(z)$ is now replaced by $\rho_{\theta_5}(z)$. If the potential behaves as $V_{\rm eff}(\theta_5) \propto \theta_5^{2n}$ around its minimum, the time average of w_{θ_5} during the oscillation phase is well approximated by the right-hand side in Eq. (3.20).

For a given compactification scale and matter content, the time evolution of the EDE phase depends on $\tilde{g}_D$ and M. From Eq. (4.8), one finds that the bulk mass determines the energy scale of $V_{\rm eff}(\theta_5)$. On the other hand, $\tilde{g}_D$ is irrelevant to the potential but affects the time evolution of the system through the equation of motion (4.17). As discussed in Sec. 3.2, θ_5 is initially frozen in its potential due to the Hubble friction and starts to roll down the potential when the friction gets weak enough. From the equation of motion (4.17), one finds that $\tilde{g}_D$ affects the magnitude of the contribution of the potential term. If $\tilde{g}_D$ is increased, the effect of the Hubble friction term is relatively diminished, and vice versa. Thus, the value of $\tilde{g}_D$ controls the time when the fast roll starts. We will discuss later the parameter dependence in detail.

To examine dynamics of the EDE phase, we numerically solve the EoM (4.17) in the $n = 2$ and 3 models. We set $q_1 = 1$ and initialize the system at $t = t_0$, where $z(t_0) = 10^{42}$. The EDE accounts for only a few percent of the total energy of the universe at most, so we assume that the expansion of the universe is determined by the other energy elements. In the following analysis, we consider a matter-dominated universe where the Hubble parameter scales as $H(t) = 2/(3t)$ to simplify the analysis. For $z \leq z_{\rm eq} \simeq 3400$, our universe is well approximated by this treatment. In the radiation-dominated era, the Hubble parameter scales as $H(t) = 1/(2t)$, and the difference from the scale in the matter-dominated era is just the $\mathcal{O}(1)$ factor. Therefore, our approximation is sufficient to understand the qualitative behavior of the EDE phase in both the matter-dominant and radiation-dominant eras.

As discussed in Sec. 4.2, the orders of the gauge coupling $\tilde{g}_D$ and bulk mass M are determined for a given M_c. The precise values of these parameters are chosen so that the start of the fast-roll and the values of Ω_{θ_5} at that moment match between the $n = 2$ and $n = 3$ models to facilitate a comparison. We show the parameters and initial conditions for the EDE phase used in the following analysis in Table 4.1.

Table 4.1: The parameters and initial conditions for the EDE phase used in the numerical analysis.

model	$M_c/M_{\rm P}$	M/M_c	$\tilde{g}_D$	$\theta_5(t_0)$	$\dot{\theta}_5(t_0)$
$n = 2$	1.0×10^{-6}	212.5	6.95×10^{-6}	$\pi/2$	0
$n = 3$	1.0×10^{-6}	213.1	5.00×10^{-6}	$\pi/2$	0

In Fig. 4.2, we show the effective potential $\bar{V}_{\rm eff}(\theta_5)$ normalized so that its maximal value is one. The dashed (solid) line represents the potential in the $n = 2$ ($n = 3$) model. Around $\theta_5 = 0$, the potential is almost flat and approximately written as the polynomial form $V_{\rm eff}(\theta_5) \propto \theta_5^{2n}$. The $n = 3$ potential is flatter than the $n = 2$ one in this region. The time-evolution of θ_5 in the potential is shown in Fig. 4.3. In both the $n = 2$ (dashed line) and $n = 3$ (solid line) cases, for $z \gtrsim 4000$, θ_5 is frozen due to the Hubble friction. At $z \sim 4000$, θ_5 starts to roll down and then oscillates around $\theta_5 = 0$.

We show the EoS w_ϕ in Fig. 4.4 and the energy density parameter Ω_{θ_5} in Fig. 4.5. From Fig. 4.4, we see that the EoS is constant $w_{\theta_5} \simeq -1$ for $z \gtrsim 4000$ in both cases. The EoS deviates from -1 around $z \sim 4000$ and begins to oscillate

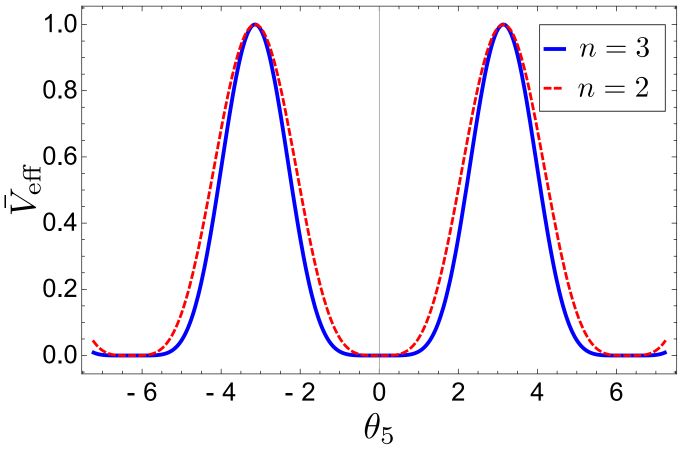

Figure 4.2: The effective potential for θ_5. The potential is normalized as $\bar{V}_{\rm eff}(\theta_5) = V_{\rm eff}(\theta_5)/V_{\rm eff}(\pi)$. The dashed (solid) line corresponds to the $n = 2$ ($n = 3$) case. It shows that the potential is flat around $\theta_5 = 0$, where the potential is approximately written as $V_{\rm eff}(\theta_5) \simeq V_{\rm eff}^{(n)}(\theta_5) \propto \theta_5^{2n}$

due to the oscillation of θ_5 around the minimum of the potential. For the $n = 3$ case, the EoS takes $w_{\theta_5} \simeq 1$ relatively longer than in the $n = 2$ case, as expected from Eq. (3.20). It can be seen from Fig. 4.5 that the energy of θ_5 gives a few percent contribution to the total energy of the universe around $z = 4000$. Before $z \sim 4000$, ρ_{θ_5} decays more slowly than the background matter and radiation energy densities since $w_{\theta_5} < w_m < w_r$ in this phase. Then, around $z = 4000$, the EDE begins to dilute due to the transition of the EoS from $w_{\theta_5} \simeq -1$ to $\langle w_{\theta_5} \rangle > 0$. The dilution of Ω_{θ_5} is faster in the $n = 3$ case than in the $n = 2$ case, as expected from the behavior of the EoS.

Let us discuss the parameter dependence of the time evolution of the system in detail. As discussed above, changing the gauge coupling $\tilde{g}_D$ does not affect the scale of the potential. Therefore, the energy density parameter in the slow-roll phase given by the ratio of $\rho_{\theta_5} \simeq V_0$ to the total energy density is irrelevant to the value of $\tilde{g}_D$. On the other hand, $\tilde{g}_D$ affects the value of $z_{\rm max}$ when the energy density parameter takes maximum and the fast-roll starts, and therefore, the value of the energy density parameter at this moment $\Omega_{\rm max}$ changes. To see how $\Omega_{\rm max}$ depends on $\tilde{g}_D$, the discussion in Sec. 3.2 is helpful. The beginning of the fast-roll $z_{\rm max}$ corresponds to the time when the exponent in Eq. (3.17) reaches ~ 1. Since $\Lambda_{(n)}^4$ and f correspond to V_0 and $M_c/\tilde{g}_D$ in our model, the relation $V_0 \sim (M_c/\tilde{g}_D)^2 H^2(z_{\rm max})$ holds. Using $V_0 \simeq \rho_{\theta_5}(z_{\rm max})$ and the fact that the Hubble parameter is related to the total energy density of the universe as $3M_{\rm P}^2 H^2(z_{\rm max}) = \rho(z_{\rm max})$, we find that $\Omega_{\rm max} \propto 1/\tilde{g}_D^2$ and $\Omega_{\rm max}$ do not depend on

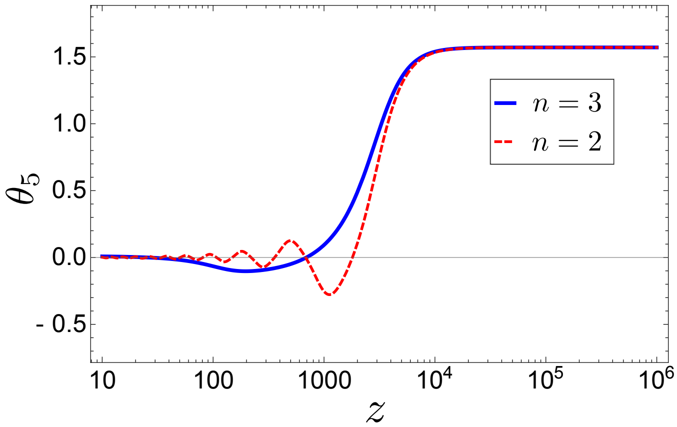

Figure 4.3: The time evolution of θ_5 as a function of the redshift. The dashed (solid) line represents the $n = 2$ ($n = 3$) case. For $z \gtrsim 4000$, θ_5 is frozen in the potential due to the Hubble friction. For $z \sim 4000$, θ_5 begins fast-roll in its potential and finally oscillates around the potential minimum $\theta_5 = 0$.

V_0. This result indicates that the parameter $\tilde{g}_D$ specifies at what value of Ω_{θ_5} the fast-roll occurs. If the value of $\tilde{g}_D$ is large, the fast-roll occurs early, and the value of $\Omega_{\max}$ becomes small.

The bulk mass M, which determines the scale of the effective potential, affect both the energy density parameter at the slow-roll phase $\rho_{\theta_5} \simeq V_0$ and the time when the fast-roll occurs. A larger value of M results in a smaller value of ρ_{θ_5} during the slow-roll phase and a later start of the fast-roll , *i.e.*, a smaller value of $z$max. However, since $\Omega_{\max}$ is independent of V_0, changing the value of M while keeping $\tilde{g}_{\rm D}$ fixed does not change $\Omega_{\max}$.

To check the parameter dependence, we numerically study the $n = 3$ model in more detail. First, we vary the value of $\tilde{g}_D$ while keeping the bulk mass M unchanged. The upper graph in Fig. 4.6 shows the time evolution of ρ_{θ_5} for $\tilde{g}_D = 2.5 \times 10^{-6}$ (blue line), 5.0×10^{-6} (red dashed line) and 10×10^{-6} (green dotted line). As explained, the energy density before $z \sim 4000$ is independent of $\tilde{g}_D$ and does not change if we vary $\tilde{g}_D$. On the other hand, $z_{\max}$ depends on $\tilde{g}_D$. If $\tilde{g}_D$ increases, $z_{\max}$ also increases, in other words, the fast-roll of θ_5 starts earlier. The lower graph in Fig. 4.6 shows how the energy density parameter Ω_{θ_5} depends on the coupling constant $\tilde{g}_D$. The smaller $\tilde{g}_D$ and the later the fast-roll begins, the larger the maximum value of the density parameter $\Omega_{\max}$ becomes. This behavior is consistent with the above discussion.

Next, we vary the value of M while keeping the value of $\tilde{g}_D$ unchanged. The upper and lower graphs in Fig. 4.7 show the bulk mass dependence of ρ_{θ_5} and Ω_{θ_5} respectively. From Eq. (4.11), we see that a larger M suppresses the energy

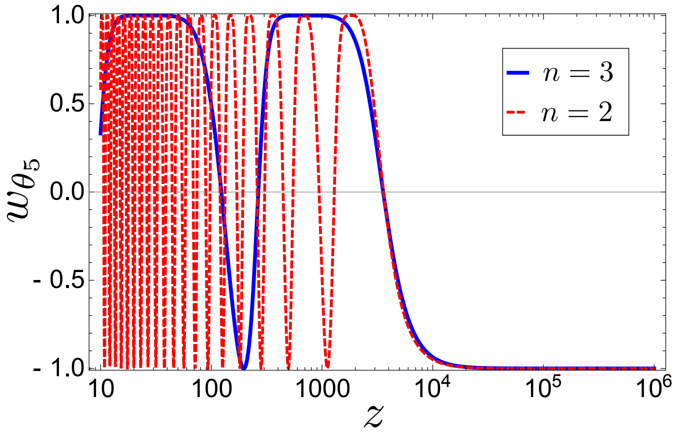

Figure 4.4: The time evolution of the EoS w_{θ_5} as a function of the redshift. The $n = 2$ and $n = 3$ cases correspond to the dashed and solid lines, respectively. For $z \gtrsim 4000$, θ_5 has $w_{\theta_5} \simeq -1$ and gives dark energy. When θ_5 starts to oscillate, w_{θ_5} also begins to oscillate. One finds that the $w_{\theta_5} > 0$ period is longer than the $w_{\theta_5} < 0$ one. Thus, the time-averaged value of w_{θ_5} satisfies $\langle w_{\theta_5} \rangle > 0$.

density in the dark energy phase. On the other hand, the maximum value of the energy density parameter $\Omega_{\rm max}$ is independent of the bulk mass. This is also consistent with the above discussion.

Finally, the relation between the value of $(\tilde{g}_D, M)$ and the value of $(z_{\rm max}, \Omega_{\rm max})$ is shown in Fig. 4.8. Smaller values of the coupling constant and bulk mass increase both $z_{\rm max}$ and $\Omega_{\rm max}$. If precise constraints on $z_{\rm max}$ and $\Omega_{\rm max}$ are obtained from future measurements, we may find implications for the fundamental parameters $\tilde{g}_D$ and M/M_c in our model by using the relation shown in Fig. 4.8. Note that, in a region where $\Omega_{\rm max}$ takes a relatively large value, the approximation by the matter-dominated universe may be worse because ρ_{θ_5} affects the expansion of the universe in such region. To obtain a more accurate result, a complete treatment of the Friedmann equation is required, which is left for future work.

It is possible to roughly estimate the H_0 value predicted in this scenario by evaluating the sound horizon. Ignoring the tiny difference in the value of $D(z_*)$ between ΛCDM and the EDE model, the ratio of the Hubble constants of these models is given by

$$\frac{H_0^{\rm EDE}}{H_0^{\Lambda{\rm CDM}}} = \frac{r_{s,*}^{\Lambda{\rm CDM}}}{r_{s,*}^{\rm EDE}}, \tag{4.18}$$

where H_0^x and $r_{s,*}^x$ ($x = \Lambda{\rm CDM}, {\rm EDE}$) denote the Hubble constant and the sound horizon in each model. As shown in Sec. 3.1, the value of the sound horizon is

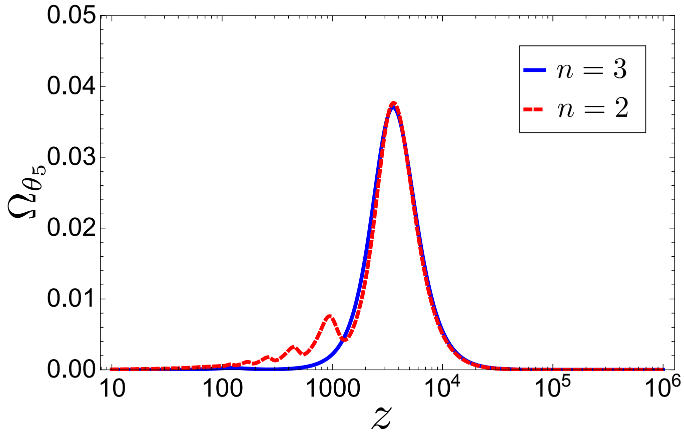

Figure 4.5: The time evolution of the energy density parameter Ω_{θ_5}. The horizontal axis corresponds to the redshift. The dashed and solid lines represent the $n = 2$ and $n = 3$ models, respectively. In the slowly-rolling phase $z \gtrsim 4000$, and the energy density of ρ_ϕ is constant while those of the background non-relativistic matter and radiation dilutes. Thus, the energy density parameter increases in this phase. For $z < 4000$, since the EoS becomes $\langle w_{\theta_5} \rangle > 0$, Ω_{θ_5} dilutes. The dilution is more efficient for the $n = 3$ case.

$r_{s,*}^{\Lambda\mathrm{CDM}} = 144$ Mpc for the ΛCDM. We can evaluate $r_{s,*}^{\mathrm{EDE}}$ by adding ρ_{θ_5} to the energy density in Eq. (3.4). To include the effects of the relativistic matter, we use the relation

$$\begin{aligned} t(z) = \frac{2}{3\bar{H}_0}\frac{1}{\Omega_{m,0}h^2}\Bigg[&\frac{1}{1+z}\sqrt{\Omega_{r,0}h^2 + \frac{\Omega_{m,0}h^2}{1+z}} \\ &- \frac{2\Omega_{r,0}h^2}{\Omega_{m,0}h^2}\left(\sqrt{\Omega_{r,0}h^2 + \frac{\Omega_{m,0}h^2}{1+z}} - \sqrt{\Omega_{r,0}h^2}\right)\Bigg], \end{aligned} \tag{4.19}$$

that holds in the matter- and radiation-dominant universe to rewrite ρ_θ as a function of z. The effect of Ω_{θ_5} is neglected in this relation. For $\Omega_{m,0}$ and $\Omega_{r,0}$, we use the values shown in Sec. 3.1. We need $\rho_{\theta_5}h^2$ to evaluate the sound horizon for the EDE case, so we assume $h = 0.7$ for this term. Under these approximations, we evaluate the right-hand side of (4.18). For the $n = 3$ model with $\tilde{g}_4 = 2.95 \times 10^{-6}$ and $M/M_c = 213.1$, giving $(z_{\max}, \Omega_{\max}) \sim (2500, 0.10)$, we obtain

$$\frac{H_0^{\mathrm{EDE}}}{H_0^{\Lambda\mathrm{CDM}}} \approx 1.05. \tag{4.20}$$

Using the value $H_0^{\Lambda\mathrm{CDM}} = 67.4$ km s^{-1}Mpc^{-1} yields $H_0^{\mathrm{EDE}} = 70.8$ km s^{-1}Mpc^{-1}. We need a detailed analysis including cosmological perturbations without the

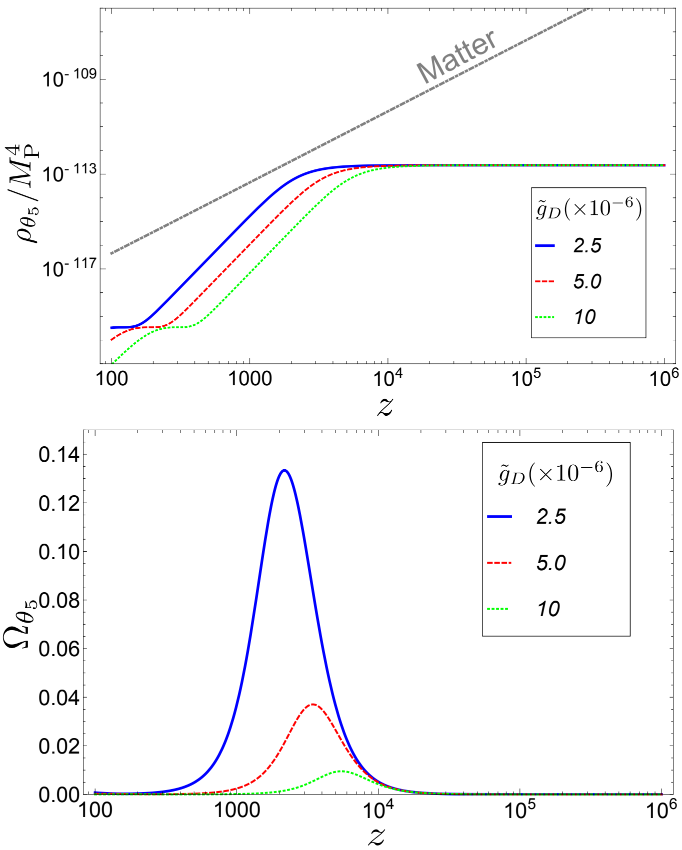

Figure 4.6: The upper and lower graphs show the $\tilde{g}_D$ dependence of the energy density ρ_{θ_5} and the density parameter Ω_{θ_5}, respectively. The other parameters are chosen as the $n = 3$ case in Table 4.1. The 4D gauge coupling $\tilde{g}_D$ determines when the fast-roll of θ_5 starts. The larger the value of $\tilde{g}_D$, the earlier the fast-roll begins, and the peak value of the energy density, $\Omega_{\rm max}$, is suppressed.

approximations used so far to obtain a more accurate value for H_0 and also discuss the consistency with measurements. Such analysis could distinguish our model from other solutions to the Hubble tension, which is left for future studies.

We have analyzed the time evolution of the EDE phase by using the leading effective potential in Eq. (4.11). To obtain the potential, we have ignored the $\ell \geq 2$ terms in Eq. (2.61), which are suppressed by $e^{-\ell M/M_c}$. These terms could contain the lower order terms in θ_5 canceled by the condition (4.13) and could change the behavior of the system. In addition, the potential (2.61) itself is obtained in the one-loop approximation. There are two-loop effects to the leading potential as subleading corrections. For completeness, we need to discuss these higher-order corrections.

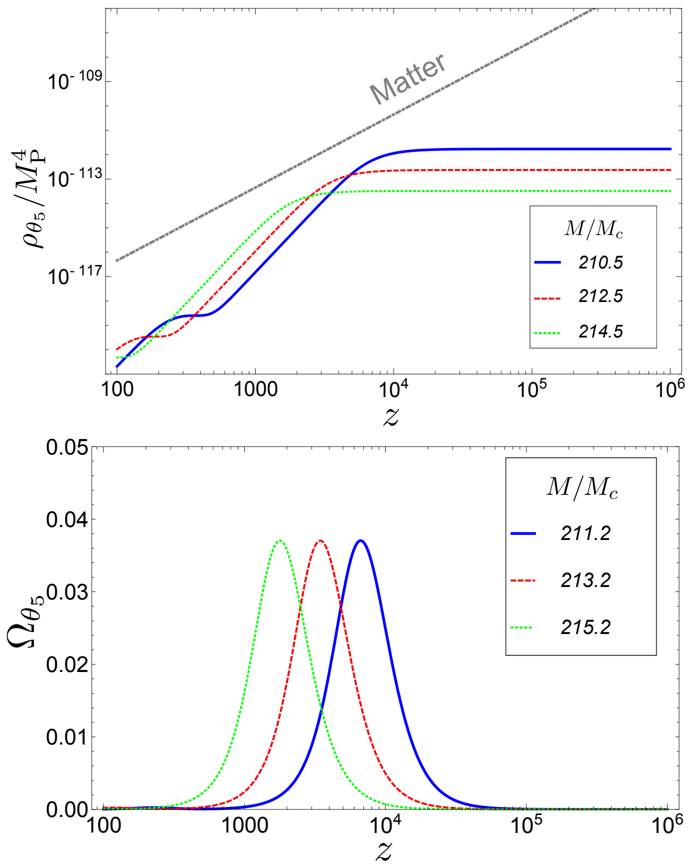

Figure 4.7: The bulk mass M dependence of the energy density ρ_{θ_5} (upper panel) and the energy density parameter Ω_{θ_5} (lower panel). The other parameters are chosen as the $n = 3$ case in Table 4.1. The larger the value of M, the later the dilution of the energy density occurs, while $\Omega_{\max}$ remains unchanged.

In our model, the behavior of ρ_{θ_5} for $z > z_{\mathrm{EDE}}$ is mainly determined by the scale of the effective potential for the EDE phase. Thus, the higher-order corrections hardly affect the time evolution for the system for $z > z_{\mathrm{EDE}}$. On the other hand, for $z < z_{\mathrm{EDE}}$ where θ_5 is oscillating around the potential minimum, the time evolution of the EDE phase is sensitive to the shape of the potential. For example, in the $n = 2$ model, the leading potential is expanded as $V_{\mathrm{eff}}(\theta_5) \propto \theta_5^4$ around the minimum, which realizes $\langle w_{\theta_5} \rangle = 1/3$ in the oscillation phase. If the higher-order corrections include θ_5^2-proportional terms, the potential structure around the minimum changes.

To discuss the effect of the corrections in more detail, we consider the case where the leading potential $V_{\mathrm{eff}}(\theta_5) \propto \theta_5^{2n}$ receives a higher-order correction $\delta V^{(m)} \sim \mathcal{O}(\theta^{2m})$ $(n > m \geq 0)$. The potential including this correction can be parametrized

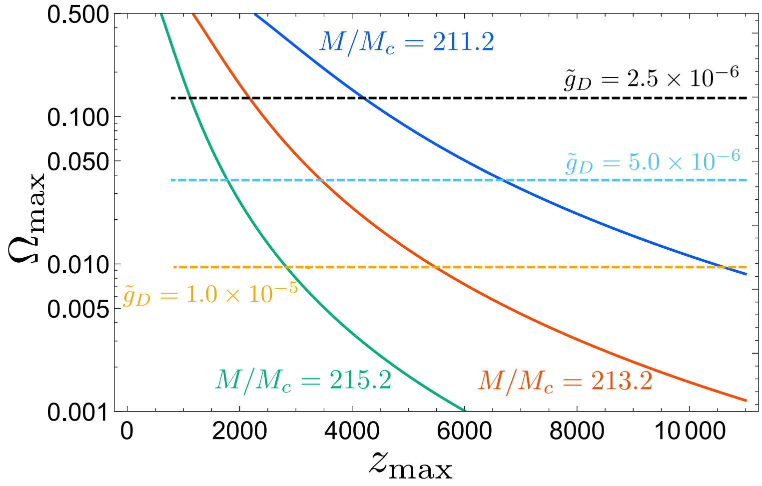

Figure 4.8: The predicted values of $z_{\rm max}$ and $\Omega_{\rm max}$ as functions of $\tilde{g}_D$ and M/M_c. The solid vertical lines represent the case with fixed bulk mass and the dashed horizontal lines represent the case with fixed coupling constants. The fixed values are shown next to each line. The three intersections of the cyan dashed line and solid lines correspond to the peaks that appeared on the right in Fig. 4.7, and the three intersections of the red solid line and dashed lines correspond to the peaks that appeared on the right in Fig. 4.6.

as

$$V_{\rm eff}(\theta_5) + \delta V^{(m)} \propto \theta_5^{2n} + \epsilon\theta_5^{2m} = \theta_5^{2n}\left[1 + \left(\frac{\theta_C}{\theta_5}\right)^{2(n-m)}\right], \tag{4.21}$$

where ϵ is the relative size of the correction to the leading contribution, and we defined the critical value $\theta_C = \epsilon^{1/[2(n-m)]}$. The second term, which represents the contribution of the correction, significantly affects the potential only in the $|\theta_5| \leq \theta_C$ region. In the $|\theta_5| \geq \theta_C$ region, this contribution is negligible, and the potential behaves as $V_{\rm eff}(\theta_5) \propto \theta_5^{2n}$. Therefore, if θ_C is small enough, the potential takes the form of θ_5^{2n} over a wide range, and the time evolution is expected not to change significantly. Indeed, we have numerically checked that the corrections with $\theta_C \lesssim 10^{-2}$ hardly change the results of our numerical analysis.

Let us estimate the typical value of θ_C in our model. The two-loop effect is expected to be suppressed by the factor $|\epsilon| \sim \tilde{g}_D^2/(4\pi^2)$ compared to the one-loop contribution. The value of ϵ is conservatively smaller than 10^{-10} in our numerical calculations with $\tilde{g}_D \sim 10^{-6}$. Thus, we obtain $\theta_C \sim [\tilde{g}_D^2/(4\pi^2)]^{1/[2(n-m)]} \lesssim 10^{-10/[2(n-m)]}$ for this setup, and $10/[2(n-m)] > 2$ has to be satisfied to obtain $\theta_C \lesssim 10^{-2}$. This condition is naturally satisfied for the $n = 2$ and 3 cases, even for

$m = 1$. On the other hand, for $n \geq 4$, our scenario may be disturbed by the two-loop effects. Since the order of the gauge coupling is determined as $\tilde{g}_D \sim M_c/M_{\rm P}$, assuming smaller values for the compactification scale would justify models with larger n. The $\ell \geq 2$ contributions in the effective potential are strongly suppressed by $|\epsilon| \sim e^{-M_\varphi/M_c} \sim e^{-100} \sim 10^{-44}$, therefore they barely affect the time evolution of the system.

Finally, we comment on the effects of non-degenerate bulk masses. In the above analysis, we have assumed that all of the bulk matter fields have the same bulk mass M. However, in general, they can have different bulk masses if there are no underlying symmetries restricting the bulk mass. If such non-degeneracy exists, the bulk mass of a field φ can be expressed by $M + \Delta M_\varphi$, where M is the typical bulk mass scale. If bulk masses of some fields are much larger than those of other fields, contributions from the heavy fields are much more suppressed and can be ignored. Therefore, we consider the case where the difference in the bulk masses is small, *i.e.*, $|\Delta M_\varphi/M| \ll 1$ is satisfied for all fields. In this case, the effective potential (4.11) is modified to

$$V_{\rm eff}(\theta_5) = -V_0 \sum_\varphi \tilde{n}_\varphi [1 - \cos(q_\varphi \theta_5)], \tag{4.22}$$

where we defined the effective degrees of freedom of φ by

$$\tilde{n}_\varphi = e^{-\ell \Delta M_\varphi / M_c} n_\varphi. \tag{4.23}$$

Therefore, in this case, the condition (4.13) constrains the values of $\tilde{n}_\varphi$. Since the bulk mass is a continuous parameter and greatly affects the value of $\tilde{n}_\varphi$, fine-tuning is necessary to realize the cancellation of the lower order terms in the effective potential for θ_5. Except for this unnaturalness problem, our model also works in the non-degenerated bulk mass case.

4.4 Discussion and Summary

In this chapter, we have shown that the extra-dimensional component of the gauge field in a 5D $U(1)_D$ gauge theory can be the EDE scalar, whose energy density can alleviate the Hubble tension. The Wilson line phase associated with the zero mode of the extra component A_y has a dynamically generated PNGB type potential. The effective potential is able to satisfy all conditions for the EDE potential discussed in Chap. 4 by properly choosing the parameters of the theory. In our scenario, M_c, the compactification scale of the extra dimension, is smaller than $\mathcal{O}(10^{-3} M_{\rm P})$. The scale of the mass parameters in the EDE potential, which was constrained by the first two conditions obtained in Chap. 4, can be accounted for by setting the gauge coupling constant and the bulk mass of the matter field included in the theory appropriately for a given value of M_c. In addition, by properly choosing the type, number, and charge of matter fields included in the theory, we can realize the $2n$–th ($n \geq 2$) polynomial potential around its minima. We have shown two concrete setups of realizing $n = 2$ and $n = 3$ potentials and demonstrated numerical calculations to check their time evolution. The results show that EDE can be naturally explained by our model based on higher-dimensional gauge theories.

More specific 5D gauge theory models may have additional implications for both cosmological and particle physics models. Our scenario works with models of S^1 or S^1/Z_2 compactification. Only in the S^1 case, the zero mode of the 4D $U(1)_D$ gauge field $A_\mu^{(0)}$ remains massless in the low energy effective theory. This 4D gauge field can play some kind of cosmological role as a dark photon. For example, if the massless dark photon does not have any interaction with the SM sector, it gives additional contribution to N_{eff}, which also has been considered as the solution to the Hubble tension [136, 137]. Alternatively, the dark photon can be massive through an additional mechanism such as the Stueckelberg mechanism. If the massive dark photon has some interaction with the SM sector, *e.g.*, a kinetic mixing to the SM photon, it can be a candidate of dark matter, and the interactions with the SM sector can predict phenomenologically and experimentally interesting features [138].

In our scenario, the fundamental parameters in the 5D $U(1)_D$ gauge theory, such as the gauge coupling constant, the bulk mass parameters, and the compactification scale, determine the behavior of the system. Thus, the future progress of cosmological measurements may give constraints and insights into particle physics models based on higher-dimensional gauge theories. To reveal the validity of our scenario, further investigations, such as a complete treatment of the Friedmann equation and analyses of cosmological perturbations, are required. We leave them as future work.

Chapter 5

Mass Spectrum of a 6D $SU(n)$ Gauge Theory with Flux Background

This chapter treats another study based on the framework of higher-dimensional gauge theory. As mentioned in Chap. 1, higher-dimensional gauge theories with a magnetic flux background have a lot of attractive features and have been widely discussed. In this study, we generalize this setup aiming to further apply it to phenomenology. In Sec. 5.1, we explain the purpose of this study more clearly. From Sec. 5.2 to Sec. 5.5, we introduce a pure Yang-Mills theory with a flux background defined on a $\mathcal{M}_4 \times T^2$ spacetime. In the following three sections 5.6, 5.7 and 5.8, we calculate quadratic terms of the fluctuation around the background. After deriving the tree-level mass spectrum of the theory in Sec. 5.9, we discuss its phenomenological implication in Sec. 5.10 and summarize this study in the final section.

5.1 Objectives and Motivations

As mentioned in Chap. 1, higher-dimensional gauge theories with a magnetic flux background have a lot of attractive features, which have been widely discussed and various interesting properties have been revealed. There have been studies that examine non-abelian gauge theories, such as $SU(2)$ or $SU(3)$, with a background flux [105, 114, 116, 139, 140]. The background flux taking a direction in the space of a simply-connected gauge group can make some of the 4D gauge fields massive and induce a spontaneous gauge symmetry breaking. In addition, some of those studies have discussed that the background flux yields tachyonic excitations at a low-energy regime, related to the Nielsen-Olsen instabilities [141]. These tachyonic modes can condensate, which seems to have an impact on vacuum structure as examined in superstring models [142, 143]. It may give rich phenomena such as further symmetry breaking in a more general field theoretical setup. For further phenomenological applications of the higher-dimensional gauge theory with a background flux, comprehensive studies in non-abelian gauge theory are necessary.

In this chapter, for future applications to GUT and GHU, we examine a general $SU(n)$ gauge theory with a background flux keeping as much generality as possible. As a first step to consider such a generalization, this work considers a 6D pure Yang-Mills theory with a background flux and mainly focuses on clarifying the complete tree-level mass spectra in low-energy effective theories. We assume a background that satisfies the classical equation of motion and gives a magnetic field in a 2D extra space compactified into T^2. In addition, we explicitly perform a standard R_ξ gauge fixing and derive the mass spectra depending on the gauge parameter ξ, which helps to discuss about physical degrees of freedom at the low-energy regime.

We also aim to confirm the existence of tachyonic modes and clarify how they depend on the choice of the background magnetic field. If tachyons exist, their condensation or stabilization would have to be discussed. Clarifying the properties of the tachyonic modes is necessary to consider the application of this setup.

5.2 Background Spacetime $\mathcal{M}_4 \times T^2$ and Notation

In this chapter, we consider a 6D gauge theory. The spacetime is assumed to be $\mathcal{M}_4 \times T^2$, where $\mathcal{M}_4$ and T^2 are the 4D Minkowski spacetime and the extra-dimensional torus. We denote coordinates on $\mathcal{M}_4$ by x^μ ($\mu = 0, 1, 2, 3$) and the ones on T^2 by x^m ($m = 5, 6$), which are also expressed together as x^M ($M = 0, 1, 2, 3, 5, 6$). To construct T^2, we introduce two shift vectors $(L, 0)$ and $(L\tau_{\rm R}, L\tau_{\rm I})$ ($\tau_{\rm R}, \tau_{\rm I} \in \mathbb{R},\ \tau_{\rm I} > 0$), and impose the identification

$$(x^5, x^6) \sim (x^5, x^6) + n_5(L, 0) + n_6(L\tau_{\rm R}, L\tau_{\rm I}) \quad (n_5, n_6 \in \mathbb{Z}), \tag{5.1}$$

as shown in Fig. 5.1. $\tau_{\rm R}$ and $\tau_{\rm I}$ are the parameters describing the moduli space of the two-dimensional torus, and L parametrizes the size of T^2. Using these parameters, the area of the torus is given by $\mathcal{V}_{T^2} = L^2\tau_I$, and $(\mathcal{V}_{T^2})^{-1/2}$ parametrizes a typical scale of this theory. In the following, we take $L = 1$ for simplicity.

It is sometimes convenient to use complex coordinates defined as

$$z = x^5 + ix^6, \quad \bar{z} = x^5 - ix^6, \tag{5.2}$$

instead of the real coordinates. The differential operators with respect to the coordinates are given by

$$\partial_z = \frac{1}{2}(\partial_5 - i\partial_6), \quad \bar{\partial}_z = \frac{1}{2}(\partial_5 + i\partial_6), \tag{5.3}$$

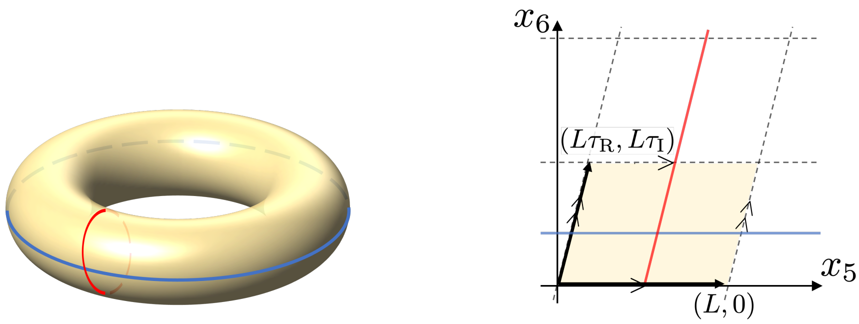

(a) Torus (T^2) **(b)** Identification in Eq. (5.1)

Figure 5.1: Torus assumed as extra-dimensions and identification

and the torus identification is expressed as

$$z \sim z + n_5 + n_6\tau, \tag{5.4}$$

where $\tau = \tau_\mathrm{R} + i\tau_\mathrm{I}$ is a complex moduli parameter. We will often discuss the shift on T^2, so it is also convenient to introduce the translation operators $\mathcal{T}_p$ ($p = 5, 6$) that shift the complex coordinates as

$$\mathcal{T}_5 z = z + 1, \quad \mathcal{T}_6 z = z + \tau. \tag{5.5}$$

The identification (5.4) is rewritten by

$$z \sim \mathcal{T}_6^{n_6}\mathcal{T}_5^{n_5} z. \tag{5.6}$$

We will express boundary conditions by using these operators.

5.3 Pure Yang-Mills Theory and Boundary Condition

In this chapter, we investigate the properties of the 6D pure Yang-Mills theory with a background magnetic field. Let $\boldsymbol{A}_M(x^M) \in su(n)$ be an $SU(n)$ gauge field, where $su(n)$ represents the Lie algebra of the special unitary group $SU(n)$. By the generators t^a ($a = 1, 2, \ldots, n^2 - 1$) of the Lie algebra $su(n)$, the gauge field is expanded as $\boldsymbol{A}_M = A_M^a t_a$. Since we will consider a gauge theory, we also introduce the covariant derivative

$$\boldsymbol{D}_M = \partial_M - ig\boldsymbol{A}_M. \tag{5.7}$$

The action of the pure Yang-Mills theory is

$$\begin{aligned} S &= \int d^6x\ \mathcal{L}_{\mathrm{YM}}, \\ \mathcal{L}_{\mathrm{YM}} &= -\frac{1}{2}\,\mathrm{Tr}(\boldsymbol{F}^{MN}\boldsymbol{F}_{MN}), \end{aligned} \tag{5.8}$$

where $\boldsymbol{F}_{MN}$ is the field strength defined by

$$\boldsymbol{F}_{MN} = \frac{i}{g}[\boldsymbol{D}_M, \boldsymbol{D}_N] = \partial_M \boldsymbol{A}_N - \partial_N \boldsymbol{A}_M - ig[\boldsymbol{A}_M, \boldsymbol{A}_N]. \tag{5.9}$$

The field strength is also an element of $su(n)$ and can be expanded by the generators as $F^a_M t_a$. The gauge transformation

$$\boldsymbol{A}_M \to \boldsymbol{A}_M^{\mathrm{gt}} = \boldsymbol{\Lambda}\boldsymbol{A}_M\boldsymbol{\Lambda}^{-1} + \frac{i}{g}\boldsymbol{\Lambda}\partial_M\boldsymbol{\Lambda}^{-1} \quad (\boldsymbol{\Lambda} = \boldsymbol{\Lambda}(x^M) \in SU(n)), \tag{5.10}$$

keeps the action invariant.

As shown in Chap. 2, a single-valued condition for the 6D pure Yang-Mills Lagrangian yields boundary conditions for the gauge field. Under the shifts (5.5), the gauge field can change up to a gauge transformation as

$$\boldsymbol{A}_M(\mathcal{T}_p z) = T_p(z)\boldsymbol{A}_M(z)T_p^\dagger(z) + \frac{i}{g}T_p(z)\partial_M T_p^\dagger(z), \tag{5.11}$$

where x^μ is suppressed for notational simplicity and $T_p(x^\mu, z) \in SU(n)$ $(p = 5, 6)$ are called twist matrices. $A_M(z+1+\tau)$ can be obtained from $A_M(z)$ by two different ordered shifts, which yields a constraint on the twist matrices. This condition is expressed as

$$\boldsymbol{A}_M(\mathcal{T}_6\mathcal{T}_5 z) = \boldsymbol{A}_M(\mathcal{T}_5\mathcal{T}_6 z), \tag{5.12}$$

from which we obtain the constraint

$$[T_\square(z), \boldsymbol{A}_M(z)] = \frac{i}{g}\partial_M T_\square(z), \qquad T_\square(z) = T_6^\dagger T_5^\dagger(z+\tau)T_6(z+1)T_5(z). \tag{5.13}$$

As shown below, there appear to be additional constraints on T_p when the background flux exists. The twist matrices, which determine the boundary conditions, must be chosen to be consistent with all of these conditions.

5.4 Background Flux

Here, we introduce the background configuration of the gauge field. Let $\boldsymbol{B}_M$ be the background of $\boldsymbol{A}_M$ and $\mathcal{F}_{mn}$ be the background field strength

$$\mathcal{F}_{MN} = \partial_M \boldsymbol{B}_N - \partial_N \boldsymbol{B}_M - ig[\boldsymbol{B}_M, \boldsymbol{B}_N]. \tag{5.14}$$

In what follows, $\boldsymbol{A}_M$ represents the fluctuation from $\boldsymbol{B}_M$. For $\boldsymbol{B}_M$ to be the background configuration, it has to satisfy the classical EoM

$$\mathcal{D}^M \mathcal{F}_{MN} = (\partial^M - ig\mathbf{ad}(\boldsymbol{B}^M))\mathcal{F}_{mn} = 0, \tag{5.15}$$

where $\mathcal{D}^M$ is the background part of the covariant derivative. Here, to keep the 4D Lorentz invariance, we impose

$$\boldsymbol{B}_\mu = 0, \quad \partial_\mu \boldsymbol{B}_M = 0, \tag{5.16}$$

which means that $\mathcal{F}_{\mu\nu} = \mathcal{F}_{\mu N} = 0$ and the classical EoM is reduced to

$$\mathcal{D}^m \mathcal{F}_{mn} = (\partial^m - ig\mathbf{ad}(\boldsymbol{B}^m))\mathcal{F}_{mn} = 0. \tag{5.17}$$

A background configuration that preserves the 4D Lorentz invariance must satisfy Eqs. (5.16) and (5.17).

The configuration

$$\begin{gathered} \boldsymbol{B}_5(z) = \boldsymbol{v}_5 - \frac{1}{2}(1+\gamma)\boldsymbol{f}x^6, \quad \boldsymbol{B}_6(z) = \boldsymbol{v}_6 + \frac{1}{2}(1-\gamma)\boldsymbol{f}x^5, \\ [\boldsymbol{v}_5, \boldsymbol{v}_6] = [\boldsymbol{v}_m, \boldsymbol{f}] = 0, \quad \boldsymbol{v}_m, \boldsymbol{f} \in su(n), \quad \gamma \in \mathbb{R}, \end{gathered} \tag{5.18}$$

is one of the solutions of the EoM (5.17). The constant $\boldsymbol{v}_m$, which we call the continuous Wilson line (phase), corresponds to the background $\langle A_y^{(0)} \rangle$ in the 5D case discussed in Chap. 2. This constant does not contribute to the background field strength of the gauge field. On the other hand, the remaining terms in $\boldsymbol{B}_5$ and $\boldsymbol{B}_6$ give a nonzero constant contribution to the field strength as,

$$\mathcal{F}_{mn} = \epsilon_{mn}\boldsymbol{f} \quad (\epsilon_{56} = -\epsilon_{65} = 1, \ \epsilon_{55} = \epsilon_{66} = 0), \tag{5.19}$$

regardless of the choice of the gauge parameter γ. The background field strength $\boldsymbol{f}$ is referred to as the constant magnetic flux and is quantized as discussed later. In the literature, γ is often chosen to be $\gamma = 0$ and $\gamma = \pm 1$, which correspond to the symmetric and the Landau gauge, respectively. We make these choices to simplify the discussions and calculations, since the physics does not depend on the choice of gauge. However, to keep the generality and applicability as much as possible, we here leave γ arbitrary. We investigate the features of the theory with this flux background, especially the mass spectra of the 4D effective theory.

As mentioned above, the background gives another constraint on the twist matrices. To see this, let us divide the boundary condition into one for the background and one for the fluctuation as

$$\boldsymbol{B}_M(\mathcal{T}_p z) = T_p(z)\boldsymbol{B}_M(z)T_p^\dagger(z) + \frac{i}{g}T_p(z)\partial_M T_p^\dagger(z), \tag{5.20}$$

$$\boldsymbol{A}_M(\mathcal{T}_p z) = T_p(z)\boldsymbol{A}_M(z)T_p^\dagger(z). \tag{5.21}$$

Their summation $\boldsymbol{B}_M + \boldsymbol{A}_M$ follows the original boundary condition (5.11). Substituting the background solutions (5.16) and (5.18) into Eq. (5.20) yields the following differential equations for the twist matrices:

$$\partial_\mu T_p = 0, \tag{5.22}$$

$$\partial_5 T_5 = ig[\boldsymbol{B}_5, T_5], \tag{5.23}$$

$$\partial_6 T_6 = ig[\boldsymbol{B}_6, T_5] + \frac{1}{2} ig(1-\gamma)\boldsymbol{f} T_5, \tag{5.24}$$

$$\partial_5 T_6 = ig[\boldsymbol{B}_5, T_6] - \frac{1}{2} ig(1+\gamma)\tau_{\mathrm{I}}\boldsymbol{f} T_6, \tag{5.25}$$

$$\partial_6 T_6 = ig[\boldsymbol{B}_6, T_6] + \frac{1}{2} ig(1-\gamma)\tau_{\mathrm{R}}\boldsymbol{f} T_6. \tag{5.26}$$

In this setup, the twist matrices must satisfy these equations in addition to Eq. (5.13).

One can easily find that

$$T_5(z) = e^{i\frac{1}{2}g(1-\gamma)\boldsymbol{f}x^6}\tilde{T}_5, \quad T_6(z) = e^{i\frac{1}{2}g\boldsymbol{f}\left\{-(1+\gamma)\tau_{\mathrm{I}}x^5 + (1-\gamma)\tau_{\mathrm{R}}x^6\right\}}\tilde{T}_6, \tag{5.27}$$

satisfy the equations when $\tilde{T}_5$ and $\tilde{T}_6$ are constant matirices and satisfy

$$[\boldsymbol{f}, \tilde{T}_p] = [\boldsymbol{v}_m, \tilde{T}_p] = 0. \tag{5.28}$$

For the solutions (5.27) to be a consistent background, they have to satisfy Eq. (5.13). Now, $T_\square$ is

$$T_\square = e^{-ig\mathcal{V}_{T^2}\boldsymbol{f}}\tilde{T}_6^\dagger \tilde{T}_5^\dagger \tilde{T}_6 \tilde{T}_5, \tag{5.29}$$

and the condition becomes

$$[e^{-ig\mathcal{V}_{T^2}\boldsymbol{f}}\tilde{T}_6^\dagger \tilde{T}_5^\dagger \tilde{T}_6 \tilde{T}_5, \boldsymbol{A}_M] = 0. \tag{5.30}$$

Considering the fact that it must be satisfied for arbitrary $\boldsymbol{A}_M$ including the fluctuation, this condition means that $T_\square$ has to be an element of the center subgroup of $SU(n)$. The center of $SU(n)$ is Z_n, so we obtain

$$e^{-ig\mathcal{V}_{T^2}\boldsymbol{f}}\tilde{T}_6^\dagger \tilde{T}_5^\dagger \tilde{T}_6 \tilde{T}_5 = e^{2\pi i\frac{\tilde{n}}{n}}\boldsymbol{I}, \quad \tilde{n} \in \mathbb{Z}. \tag{5.31}$$

The integer $\tilde{n}$ is referred to as the 't Hooft flux [144] and is known to cause nontrivial symmetry breaking [145]. However, to concentrate only on the effect of the magnetic flux $\boldsymbol{f}$, we assume $\tilde{n} = 0$ and $\tilde{T}_p = \boldsymbol{I}$. Then, the condition (5.31) is reduced to

$$e^{-ig\boldsymbol{f}\mathcal{V}_{T^2}} = \boldsymbol{I}, \tag{5.32}$$

which yields a quantization condition for $\boldsymbol{f}$ in the next section.

As discussed in Chap. 2, the gauge transformation changes the boundary condition and the background while keeping the description of the theory, which means that $\boldsymbol{B}_m$ and T_p have gauge dependence. Using this feature, $\boldsymbol{v}_m$ can be eliminated from the background (5.18) and transferred to the twist matrices T_p. This can be achieved by the gauge transformation function $\boldsymbol{\Lambda} = e^{-ig(\boldsymbol{v}_5 x^5 + \boldsymbol{v}_6 x^6)}$, and the transformed background field and twist matrices are

$$\boldsymbol{B}_5(z) = -\frac{1}{2}(1+\gamma)\boldsymbol{f}x^6, \qquad \boldsymbol{B}_6(z) = \frac{1}{2}(1-\gamma)\boldsymbol{f}x^5, \tag{5.33}$$

$$\begin{gathered} T_5(z) = e^{-ig\boldsymbol{v}_5} e^{i\frac{1}{2}g(1-\gamma)\boldsymbol{f}x^6}, \\ T_6(z) = e^{-ig(\tau_{\mathrm{R}}\boldsymbol{v}_5 + \tau_{\mathrm{I}}\boldsymbol{v}_6)} e^{i\frac{1}{2}g\boldsymbol{f}\{-(1+\gamma)\tau_{\mathrm{I}}x^5 + (1-\gamma)\tau_{\mathrm{R}}x^6\}}. \end{gathered} \tag{5.34}$$

We choose this gauge in the following discussions.

5.5 Parametrization of the Background

The background flux and continuous Wilson lines, which satisfy the commutation relations in Eq. (5.18), can be diagonalized without loss of generality. If $\boldsymbol{f}$ has nonzero off-diagonal elements, we can diagonalize it by a constant gauge transformation $\boldsymbol{\Lambda}$, which transforms $\boldsymbol{f}$ to $\boldsymbol{\Lambda}\boldsymbol{f}\boldsymbol{\Lambda}^{-1}$. Since the commutation relation $[\boldsymbol{v}_m, \boldsymbol{f}] = 0$ means that $\boldsymbol{v}_m$ and $\boldsymbol{f}$ are simultaneously diagonalizable, there must be another constant gauge transformation that diagonalizes $\boldsymbol{v}_m$ while keeping $\boldsymbol{f}$ diagonal. Therefore, we can express $\boldsymbol{f}$ and $\boldsymbol{v}_m$ as

$$\boldsymbol{f} = f^k H_k, \quad \boldsymbol{v}_m = v_m^k H_k, \tag{5.35}$$

where H_k $(k = 1, \ldots, n-1)$ are the Cartan generators of $su(n)$ which satisfy

$$[H_k, H_\ell] = 0. \tag{5.36}$$

In the following, we choose the fundamental representation where H_k are represented by $n \times n$ matrices as

$$\begin{aligned} &\hat{H}_1 = \mathrm{diag}(1, -1, 0, \ldots, 0), \quad \hat{H}_2 = \mathrm{diag}(0, 1, -1, 0, \ldots, 0), \ \ldots, \\ &\hat{H}_{n-2} = \mathrm{diag}(0, \ldots, 0, 1, -1, 0), \quad \hat{H}_{n-1} = \mathrm{diag}(0, \ldots, 0, 1, -1). \end{aligned} \tag{5.37}$$

In what follows, we expand $su(n)$ operators by these matrices.

As mentioned above, the background flux $\boldsymbol{f}$ is quantized in this setup. Now, the background flux is diagonalized as in Eq. (5.35), so f^k has to be

$$f^k = \hat{f}N^k, \qquad \hat{f} = \frac{2\pi}{g\mathcal{V}_{T^2}} = \frac{2\pi}{g\tau_I L^2}, \qquad N^k \in \mathbb{Z} \tag{5.38}$$

for the condition (5.32) to be satisfied. One finds that $\boldsymbol{f}$ is quantized in units of $\hat{f}$, and in the fundamental representation, the flux is expressed as

$$\boldsymbol{f} = \hat{f} N^k \hat{H}_k = \hat{f}\mathrm{diag}(N^1, N^2 - N^1, N^3 - N^2, \ldots, N^{n-1} - N^{n-2}, -N^{n-1}). \quad (5.39)$$

The background flux is specified by giving the values of N^k.

We have covered everything regarding the background magnetic field; however, for the sake of further discussion, let us introduce the step operators in the fundamental representation. To represent the $n(n-1)$ step operators of $su(n)$, we first introduce the basis matrices $\hat{e}_{ij}$ where the (i,j) component is 1, and all other components are zero. Namely, the (i', j') component of $\hat{e}_{ij}$ is expressed as

$$(\hat{e}_{ij})_{i'j'} = \delta_{ii'}\delta_{jj'}. \quad (5.40)$$

By using the basis matrices, the step operators are given by

$$E_{ij}^{(+)} = \hat{e}_{ij}, \quad E_{ij}^{(-)} = \hat{e}_{ji}, \qquad 1 \le i < j \le n, \quad (5.41)$$

and satisfy $E_{ij}^{(-)} = E_{ij}^{(+)\dagger} = E_{ij}^{(+)T}$. We can also express the Cartan generators by $\hat{e}_{ij}$ as

$$\hat{H}_k = \hat{e}_{kk} - \hat{e}_{k+1\,k+1}. \quad (5.42)$$

From these expressions of the Cartan and step operators, we can easily show that the traces are

$$\begin{aligned} \mathrm{Tr}[\hat{H}_k \hat{H}_\ell] = (M^{su(n)})_{k\ell}, \qquad \mathrm{Tr}[E_{ij}^{(+)} E_{i'j'}^{(-)}] = \delta_{ii'}\delta_{jj'}, \\ \mathrm{Tr}[\hat{H}_k E_{ij}^{(\pm)}] = \mathrm{Tr}[E_{ij}^{(+)} E_{i'j'}^{(+)}] = \mathrm{Tr}[E_{ij}^{(-)} E_{i'j'}^{(-)}] = 0, \end{aligned} \quad (5.43)$$

where $(M^{su(n)})_{k\ell}$ is the (k,ℓ) component of the Cartan matrix

$$M^{su(n)} = \begin{pmatrix} 2 & -1 & 0 & \cdots & & & 0 \\ -1 & 2 & -1 & 0 & \cdots & & 0 \\ 0 & -1 & 2 & -1 & 0 & \cdots & 0 \\ & & & \ddots & & & \\ 0 & \cdots & 0 & -1 & 2 & -1 & 0 \\ 0 & & \cdots & 0 & -1 & 2 & -1 \\ 0 & & & \cdots & 0 & -1 & 2 \end{pmatrix}. \quad (5.44)$$

The commutation relations between these matrices are given by

$$\begin{aligned} [\hat{H}_k, \hat{H}_\ell] = 0, \quad [\hat{H}_k, E_{ij}^{(\pm)}] &= \pm(\delta_{ik} - \delta_{jk} - \delta_{i\,k+1} + \delta_{j\,k+1}) E_{ij}^{(\pm)}, \\ [E_{ij}^{(+)}, E_{ij}^{(-)}] &= \sum_{k=i}^{j-1} H_k, \\ [E_{ij}^{(\pm)}, E_{i'j'}^{(\pm)}] &= \pm\delta_{ji'} E_{ij'}^{(\pm)} \quad (i < j'), \\ [E_{ij}^{(\pm)}, E_{i'j'}^{(\mp)}] &= \mp\delta_{ii'} E_{jj'}^{(\mp)} \quad (j < j'). \end{aligned} \quad (5.45)$$

The generators $\hat{H}_k$ and $E_{ij}^{(\pm)}$ form the Lie algebra $su(n)$, and the fields in the fundamental representation can be expanded by them. For instance, the expansion of $\boldsymbol{A}_M$ is given by

$$\boldsymbol{A}_M = A_M^k \hat{H}_k + A_M^{ij} E_{ij}^{(+)} + \bar{A}_M^{ij} E_{ij}^{(-)} = \begin{pmatrix} A_M^1 & A_M^{12} & \cdots & A_M^{1n} \\ \bar{A}_M^{12} & A_M^2 - A_M^1 & & \vdots \\ \vdots & & \ddots & \\ \bar{A}_M^{1n} & \cdots & & -A_M^{n-1} \end{pmatrix}, \tag{5.46}$$

where A_M^k, A_M^{ij}, and $\bar{A}_M^{ij}$ are component fields. The ghost introduced later is also an adjoint field and is expanded similarly.

In the pure Yang-Mills theory, the interaction between the background $\boldsymbol{B}_m$ and $\boldsymbol{A}_M$ arises from the commutator $[\boldsymbol{B}_m, \boldsymbol{A}_M]$. Thus, for later discussion, let us examine this commutator. Since our background is proportional to the Cartan generators, the fields A_M^k do not couple either to the magnetic flux or the WL. On the other hand, the remaining components can interact with the background. The commutation relations of the step operators with the flux and the WL are expressed as

$$[\boldsymbol{f}, E_{ij}^{(\pm)}] = \pm \hat{f} \tilde{N}^{ij} E_{ij}^{(\pm)}, \tag{5.47}$$

$$[\boldsymbol{v}_m, E_{ij}^{(\pm)}] = \pm \tilde{v}_m^{ij} E_{ij}^{(\pm)}, \tag{5.48}$$

where

$$\tilde{N}^{ij} = N^k(\delta_{ik} - \delta_{jk} - \delta_{i\,k+1} + \delta_{j\,k+1}) = N^i - N^{i-1} - N^j + N^{j-1}, \tag{5.49}$$

$$\tilde{v}_m^{ij} = v_m^k(\delta_{ik} - \delta_{jk} - \delta_{i\,k+1} + \delta_{j\,k+1}) = v_m^i - v_m^{i-1} - v_m^j + v_m^{j-1}. \tag{5.50}$$

When $\tilde{N}^{ij} \neq 0$ or $\tilde{v}_m^{ij} \neq 0$, the component field associated with the generator $E_{ij}^{(\pm)}$ interacts with the flux and/or the WL, respectively. We will classify the mass spectra of the fields by these parameters.

5.6 Expansion around the Background

The purpose of this study is to examine the 4D effective theory that is obtained from the 6D pure Yang-Mills action (5.8) with a background and describes the physics below the compactification scale $\sim L^{-1}$. Since the main aim is to obtain the tree-level mass spectrum of the effective theory, we expand the Lagrangian around the background and mainly focus on the quadratic terms of the fluctuation.

In this section, we perform the expansion around the background. Replacing $\boldsymbol{A}_M$ by $\boldsymbol{B}_M + \boldsymbol{A}_M$ and using $D^M = \mathcal{D}^M - ig\boldsymbol{A}_M$ in Eq (5.9) yields the following expansion of the field strength

$$\boldsymbol{F}_{MN} = \mathcal{F}_{MN} + \mathcal{D}_M\boldsymbol{A}_N - \mathcal{D}_N\boldsymbol{A}_M - ig[\boldsymbol{A}_M, \boldsymbol{A}_N]. \tag{5.51}$$

Substituting it into the Lagrangian (5.8), we can obtain the Lagrangian for the fluctuation $\boldsymbol{A}_M$. As mentioned, we mainly focus on the quadratic terms

$$\mathcal{L}_1^{(2)} = \mathrm{Tr}[\boldsymbol{A}^\mu(\eta_{\mu\nu}\Box - \partial_\mu\partial_\nu + \eta_{\mu\nu}\mathcal{D}_m\mathcal{D}^m)\boldsymbol{A}^\nu], \tag{5.52}$$

$$\mathcal{L}_2^{(2)} = \mathrm{Tr}[\boldsymbol{A}^m(\delta_{mn}\Box + \delta_{mn}\mathcal{D}_{m'}\mathcal{D}^{m'} - \mathcal{D}_m\mathcal{D}_m - ig\epsilon_{nm}\mathbf{ad}(\boldsymbol{f}))\boldsymbol{A}^n], \tag{5.53}$$

$$\mathcal{L}_3^{(2)} = 2\mathrm{Tr}[(\partial_\mu\boldsymbol{A}^\mu)(\mathcal{D}_m\boldsymbol{A}^m)], \tag{5.54}$$

where $\Box = \partial_\mu\partial^\mu$ is the 4D d'Alembertian and we have performed integration by parts. The surface terms that arise from the integration by parts vanish as shown in Appx. C.1. $\mathcal{L}_1^{(2)}$ and $\mathcal{L}_2^{(2)}$ are quadratic terms for $\boldsymbol{A}_\mu$ and $\boldsymbol{A}_m$, respectively. $\mathcal{L}_3^{(2)}$ is a mixing term between them which is removed by gauge fixing terms introduced later.

5.7 R_ξ Gauge Fixing and Ghosts

To quantize a theory with gauge symmetry, we have to eliminate the gauge degrees of freedom by gauge fixing. This paper only examines the tree-level mass spectrum obtained from the 6D pure Yang-Mills theory. However, we will derive the effective potential for the WLs calculating quantum corrections in future work. Therefore, we carry out the standard gauge fixing procedure known as the Faddeev-Popov method. The gauge fixing also helps us to discuss physical modes in the 4D effective theory.

To fix the gauge, we add the gauge fixing term

$$\begin{aligned}\mathcal{L}_{\mathrm{GF}} =& -\frac{1}{\xi}\mathrm{Tr}[(\partial_\mu\boldsymbol{A}^\mu + \xi\mathcal{D}_m\boldsymbol{A}^m)^2]\\ =&\frac{1}{\xi}\mathrm{Tr}[\boldsymbol{A}^\mu\partial_\mu\partial_\nu\boldsymbol{A}^\nu] - 2\mathrm{Tr}[(\partial_\mu\boldsymbol{A}^\mu)(\mathcal{D}_m\boldsymbol{A}^m)] + \xi\mathrm{Tr}[\boldsymbol{A}^m\mathcal{D}_m\mathcal{D}_n\boldsymbol{A}^n],\end{aligned} \tag{5.55}$$

and the ghost term

$$\mathcal{L}_c = -2\mathrm{Tr}[\bar{\boldsymbol{c}}\{\partial^\mu(\partial_\mu - ig\mathbf{ad}(\boldsymbol{A}_\mu)) + \xi\mathcal{D}^m(\mathcal{D}_m - ig\mathbf{ad}(\boldsymbol{A}_m))\}\boldsymbol{c}], \tag{5.56}$$

and consider the gauge fixed theory

$$\mathcal{L}_{\mathrm{YM}}^{\mathrm{gf}} = \mathcal{L}_{\mathrm{YM}} + \mathcal{L}_{\mathrm{GF}} + \mathcal{L}_c. \tag{5.57}$$

Here, $\boldsymbol{c}$ is a Grassmann field that is called the Faddeev-Popov ghost, and $\xi \in \mathbb{R}$ is referred to as the gauge fixing parameter. Note that $\boldsymbol{A}_M$ in $\mathcal{L}_{\mathrm{GF}}$ and $\mathcal{L}_c$ is already a fluctuation from $\boldsymbol{B}_M$.

5.8 Quadratic Terms

Since we are interested in the tree-level mass spectrum, we focus on the quadratic terms of the fluctuations $\boldsymbol{A}_M$ and $\boldsymbol{c}$

$$\mathcal{L}_{\mathrm{YM}}^{\mathrm{gf}} \ni \mathcal{L}_{A_\mu}^{(2)} + \mathcal{L}_{A_m}^{(2)} + \mathcal{L}_{c}^{(2)} \tag{5.58}$$

$$\mathcal{L}_{A_\mu}^{(2)}, = \mathrm{Tr}[\boldsymbol{A}^\mu(\eta_{\mu\nu}\Box + \eta_{\mu\nu}\mathcal{D}_m\mathcal{D}^m - (1-\xi^{-1})\partial_\mu\partial_\nu)\boldsymbol{A}^\nu], \tag{5.59}$$

$$\mathcal{L}_{A_m}^{(2)} = \mathrm{Tr}[\boldsymbol{A}^m(\delta_{mn}\Box + \delta_{mn}\mathcal{D}_{m'}\mathcal{D}^{m'} - (1-\xi)\mathcal{D}_m\mathcal{D}_n - 2ig\epsilon_{mn}\mathbf{ad}(\boldsymbol{f}))\boldsymbol{A}^n], \tag{5.60}$$

$$\mathcal{L}_{c}^{(2)} = -2\mathrm{Tr}[\bar{\boldsymbol{c}}(\Box + \xi\mathcal{D}_m\mathcal{D}^m)\boldsymbol{c}]. \tag{5.61}$$

To obtain Eq. (5.60), we have rewritten the third term in Eq. (5.53) by using the relation

$$\mathcal{D}_n\mathcal{D}_m = [\mathcal{D}_n, \mathcal{D}_m] + \mathcal{D}_m\mathcal{D}_n = ig\epsilon_{mn}\mathbf{ad}(\boldsymbol{f}) + \mathcal{D}_m\mathcal{D}_n. \tag{5.62}$$

The last term proportional to $\mathbf{ad}(\boldsymbol{f})$ in Eq. (5.60) arises from the nontrivial helicity of $\boldsymbol{A}_m$ in the extra-dimensional directions.

Let us expand $\boldsymbol{A}_M$ by the $su(n)$ generators as in Eq. (5.46). The derivative $\mathcal{D}_m\boldsymbol{A}_M$ can also be expanded as

$$\mathcal{D}_m\boldsymbol{A}_M = (\partial_m A_M^k)\hat{H}_k + (D_m^{(ij)}A_M^{ij})E_{ij}^{(+)} + (\bar{D}_m^{(ij)}\bar{A}_M^{ij})E_{ij}^{(-)}, \tag{5.63}$$

where we defined the covariant derivatives for the component fields

$$\begin{aligned} D_5^{ij} &= \partial_5 + \frac{1}{2}ig\hat{f}\tilde{N}^{ij}(1+\gamma)x^6, \quad & D_6^{ij} &= \partial_6 - \frac{1}{2}ig\hat{f}\tilde{N}^{ij}(1-\gamma)x^5, \\ \bar{D}_5^{ij} &= \partial_5 - \frac{1}{2}ig\hat{f}\tilde{N}^{ij}(1+\gamma)x^6, \quad & \bar{D}_6^{ij} &= \partial_6 + \frac{1}{2}ig\hat{f}\tilde{N}^{ij}(1-\gamma)x^5. \end{aligned} \tag{5.64}$$

The operator in the first term is the ordinary partial derivative since the Cartan-valued field A_M^k does not couple with the background. Using Eqs. (5.46) and (5.63), the quadratic term (5.59) can be expressed in terms of the component fields as

$$\mathcal{L}_{A_\mu}^{(2)} = \mathcal{L}_{A_\mu}^{\mathrm{Cartan}} + \sum_{1\le i<j\le n}\mathcal{L}_{A_\mu}^{(ij)}, \tag{5.65}$$

$$\mathcal{L}_{A_\mu}^{\mathrm{Cartan}} = (M^{su(n)})_{k\ell}A_\mu^k[\eta^{\mu\nu}\Box - (1-\xi^{-1})\partial^\mu\partial^\nu + \eta^{\mu\nu}\partial_m\partial^m]A_\nu^\ell, \tag{5.66}$$

$$\mathcal{L}_{A_\mu}^{(ij)} = 2\bar{A}_\mu^{ij}[\eta^{\mu\nu}\Box - (1-\xi^{-1})\partial^\mu\partial^\nu + \eta^{\mu\nu}(D_m'^{(ij)})^2]A_\nu^{ij}, \tag{5.67}$$

where we have performed integration by parts to obtain the expressions (5.67) and ignored the surface term based on the discussion in Appx. C.1. In the same way, from Eq. (5.60), we obtain

$$\mathcal{L}^{(2)}_{A_m} = \mathcal{L}^{\rm Cartan}_{A_m} + \sum_{1\le i<j\le n} \mathcal{L}^{(ij)}_{A_m}, \tag{5.68}$$

$$\mathcal{L}^{\rm Cartan}_{A_m} = (M^{su(n)})_{k\ell} A^k_m \left[\eta^{mn}\Box + \eta^{mn}\partial_{m'}\partial^{m'} - (1-\xi)\partial^m\partial^n\right] A^\ell_n, \tag{5.69}$$

$$\mathcal{L}^{(ij)}_{A_m} = 2\bar{A}^{ij}_m[\delta^{mn}\Box + \delta^{mn}(D^{(ij)}_{m'})^2 - (1-\xi)D^{m(ij)}D^{n(ij)} - 2ig\hat{f}\tilde{N}^{ij}\epsilon^{mn}]A^{ij}_n, \tag{5.70}$$

In these expressions, $\mathcal{L}^{\rm Cartan}_{A_\mu}$ and $\mathcal{L}^{\rm Cartan}_{A_m}$ represent the quadratic Lagrangians for the Cartan component fields A^k_M, while $\mathcal{L}^{(ij)}_{A_\mu}$ and $\mathcal{L}^{(ij)}_{A_m}$ correspond to the ones for A^{ij}_M.

The quadratic Lagrangians (5.66) and (5.69) are not diagonalized in this basis where the representation of H_k is given by Eq. (5.37) and the trace between generators is given by Eq. (5.43). However, in the basis where the representation is given by

$$\hat{H}'_k = \frac{1}{\sqrt{2k(k+1)}}\mathrm{diag}(\underbrace{1,\dots,1}_{k\ \text{components}}, -k, 0, \dots, 0), \tag{5.71}$$

the Cartan generators satisfy $\mathrm{Tr}[\hat{H}'_k\hat{H}'_\ell] = \frac{1}{2}\delta_{k\ell}$. This fact means that there exist linear combinations of A^k_M that diagonalize the quadratic terms for the Cartan component fields. The linear combination leaves the terms inside the square brakets unchanged, ultimately resulting in the replacement $(M^{su(n)})_{k\ell} \to \frac{1}{2}\delta_{k\ell}$. On the other hand, the Lagrangians for A^{ij}_M are completely separated for each (ij), requiring no diagonalization.

Let us discuss the boundary conditions for the component fields. Using the twist matrices in Eq. (5.33), Eq. (5.21) yields the boundary conditions

$$\boldsymbol{A}_M(\mathcal{T}_5 z) = e^{-ig\mathbf{ad}(\boldsymbol{v}_5)} e^{i\frac{1}{2}g(1-\gamma)x^6\mathbf{ad}(\boldsymbol{f})}\boldsymbol{A}_M(z), \tag{5.72}$$

$$\boldsymbol{A}_M(\mathcal{T}_6 z) = e^{-ig(\tau_{\rm R}\mathbf{ad}(\boldsymbol{v}_5+\tau_{\rm I}\mathbf{ad}(\boldsymbol{v}_6)))} e^{i\frac{1}{2}g\{-(1+\gamma)\tau_{\rm I}x^5+(1-\gamma)\tau_{\rm R}x^6\}\mathbf{ad}(\boldsymbol{f})}\boldsymbol{A}_M(z). \tag{5.73}$$

We have used the Campbell-Baker-Hausdorff formula $e^XYe^{-X} = e^{\mathbf{ad}(X)}Y$ in order to obtain these expressions. Substituting the generator expansion (5.46) allows us to obtain the boundary conditions for the component fields. For the Cartan component fields, which do not interact with the background, we obtain the periodic boundary condition

$$A^k_M(\mathcal{T}_5 z) = A^k_M(\mathcal{T}_6 z) = A^k_M(z). \tag{5.74}$$

On the other hand, the boundary conditions for A^{ij}_M take the following nontrivial forms:

$$A^{ij}_M(\mathcal{T}_5 z) = e^{-ig\tilde{v}^{ij}_5} e^{i\frac{1}{2}g\hat{f}\tilde{N}^{ij}(1-\gamma)x^6} A^{ij}_M(z), \tag{5.75}$$

$$A^{ij}_M(\mathcal{T}_6 z) = e^{-ig(\tau_{\rm R}\tilde{v}^{ij}_5+\tau_{\rm I}\tilde{v}^{ij}_6)} e^{i\frac{1}{2}g\hat{f}\tilde{N}^{ij}\{-(1+\gamma)\tau_{\rm I}x^5+(1-\gamma)\tau_{\rm R}x^6\}} A^{ij}_M(z). \tag{5.76}$$

The boundary conditions for $\bar{A}_M^{ij}$ are obtained by taking the Hermitian conjugates of Eqs. (5.75) and (5.76).

From the boundary condition (5.74) and the quadratic terms (5.66) and (5.69), we find that A_M^k are completely decoupled from the continuous Wilson lines and the flux. Therefore, as seen in the next section, the mass spectra for these fields are obtained independently of these backgrounds. On the other hand, A_M^{ij} couples to the background flux and Wilson line when $\tilde{N}^{ij} \neq 0$ and $\tilde{v}_m^{ij} \neq 0$. When $N^{ij} \neq 0$ and $\tilde{v}_m^{ij} \neq 0$, A_M^{ij} couples to the flux and Wilson lines, respectively. In particular, when $\tilde{N}^{ij} \neq 0$, the boundary conditions (5.75) and (5.76) depend on x^m. In the next section, we will see that there is a significant difference in the mass spectrum of A_M^{ij} between the cases with $\tilde{N}^{ij} = 0$ and $\tilde{N}^{ij} \neq 0$.

5.9 Mass Spectrum around Flux Background

5.9.1 Mass Spectrum for KK Modes of A_μ^k

We first discuss the tree-level mass spectrum for A_μ^k. Since this field satisfies the periodic boundary conditions (5.74) under the shifts by $\mathcal{T}_5$ and $\mathcal{T}_6$, we can introduce the KK expansion

$$\begin{aligned} A_\mu^k(x,z) &= \sum_{\hat{n},\hat{m}\in\mathbb{Z}} A^k_{\mu(\hat{n},\hat{m})}(x)\xi^{A_\mu^k}_{\hat{n},\hat{m}}(z), \\ \xi^{A_\mu^k}_{\hat{n},\hat{m}}(z) &= C^{(\hat{n},\hat{m})} e^{2\pi i \hat{n} x^5} e^{2\pi i \tau_{\mathrm{I}}^{-1}(\hat{m}-\hat{n}\tau_{\mathrm{R}})x^6}, \end{aligned} \tag{5.77}$$

where $C^{(\hat{n},\hat{m})}$ is a normalization constant, and each KK mode $A^k_{\mu(\hat{n},\hat{m})}(x^\mu)$ $(\hat{n},\hat{m} \in \mathbb{Z})$ is a 4D field. This is simply a six-dimensional extension of the KK expansion (2.13) by the plane wave (2.14) introduced in Sec. 2.2.

The masses of A_μ^k are derived from the last term in Eq. (5.66). The mass $M^2(A^k_{\mu(\hat{n},\hat{m})})$ is obtained as the eigenvalue of the operator $-\partial_m\partial^m$ acting on $\xi^{A_\mu^k}_{\hat{n},\hat{m}}$ and given by

$$M^2(A^k_{\mu(\hat{n},\hat{m})}) = \left(\frac{2\pi}{L}\right)^2 \left[\hat{n}^2 + \tau_{\mathrm{I}}^{-2}(\hat{m}-\hat{n}\tau_{\mathrm{R}})^2\right], \tag{5.78}$$

where we have temporarily written L explicitly. This mass spectrum is the six-dimensional version of Eq. (2.24). The mass (5.78) is zero for $(\hat{n},\hat{m}) = (0,0)$. Namely, the 4D effective Lagrangian obtained from Eq. (5.66) contains the massless gauge fields $A_\mu^{k(0,0)}$. Therefore, the related symmetry remains in the effective theory.

5.9.2 Mass Spectrum for KK Modes of A_m^k

Let us next derive the mass spectrum for A_m^k. Since the boundary conditions for A_m^k are also periodic like those for A_μ^{ij}, the KK expansion of A_m^k has the same form as that of A_μ^k given in Eq. (5.77). We denote the KK mode of A_m^k as $A_{m(\hat{n},\hat{m})}^k$ and the mode function as $\xi_{\hat{n},\hat{m}}^{A_m^k}$. The mode function $\xi_{\hat{n},\hat{m}}^{A_m^k}$ is equivalent to that of A_μ^k, *i.e.*, $\xi_{\hat{n},\hat{m}}^{A_m^k} = \xi_{\hat{n},\hat{m}}^{A_\mu^k}$.

The KK mass $M^2(A_{m(\hat{n},\hat{m})}^k)$ of $A_{m(\hat{n},\hat{m})}^k$ is determined by the operator $-\eta^{mn}\partial_{m'}\partial^{m'} + (1-\xi)\partial^m\partial^n$ in the quadratic Lagrangian (5.69). We obtain the mass matrix for $(A_{5(\hat{n},\hat{m})}^k \; A_{6(\hat{n},\hat{m})}^k)$ and it is given by

$$\begin{aligned}\mathcal{M}^2(A_{m(\hat{n},\hat{m})}^k) = \left(\frac{2\pi}{L}\right)^2 \Bigg[& \left[\hat{n}^2 + \tau_{\mathrm{I}}^{-2}(\hat{m} - \hat{n}\tau_{\mathrm{R}})^2\right] \begin{pmatrix} 1 & 0 \\ 0 & 1 \end{pmatrix} \\ & - (1-\xi) \begin{pmatrix} \hat{n}^2 & \hat{n}\tau_{\mathrm{I}}^{-1}(\hat{m} - \hat{n}\tau_{\mathrm{R}}) \\ \hat{n}\tau_{\mathrm{I}}^{-1}(\hat{m} - \hat{n}\tau_{\mathrm{R}}) & \tau_{\mathrm{I}}^{-2}(\hat{m} - \hat{n}\tau_{\mathrm{R}})^2 \end{pmatrix} \Bigg]. \end{aligned} \tag{5.79}$$

The off-diagonal second term is obtained from the term $(1-\xi)\partial^m\partial^n$. The mass matrix is diagonalizable, and its mass eigenvalues are

$$M_{\mathrm{ph}}^2(A_{m(\hat{n},\hat{m})}^k) = \left(\frac{2\pi}{L}\right)^2 \left[\hat{n}^2 + \tau_{\mathrm{I}}^{-2}(\hat{m} - \hat{n}\tau_{\mathrm{R}})^2\right], \tag{5.80}$$

$$M_{\xi}^2(A_{m(\hat{n},\hat{m})}^k) = \xi \left(\frac{2\pi}{L}\right)^2 \left[\hat{n}^2 + \tau_{\mathrm{I}}^{-2}(\hat{m} - \hat{n}\tau_{\mathrm{R}})^2\right], \tag{5.81}$$

from which one finds that the part depending on ξ is separated from the independent part.

The zero modes $A_{m(0,0)}^k$ are massless scalars, and their masses do not dependent on the gauge parameter ξ. Except for the NG modes associated with the broken translational symmetry on T^2 discussed later, some of these zero modes may acquire nonzero masses through quantum corrections, which will be briefly discussed in section 5.9.6. The modes with $(\hat{n},\hat{m}) \neq (0,0)$ correspond to massive scalar modes. The massive modes with the ξ-dependent masses $M_\xi^2(A_{m(\hat{n},\hat{m})}^k)$ are would-be Goldstone modes and provide physical degrees of freedom to longitudinal modes of massive vector fields $A_{\mu(\hat{n},\hat{m})}^k$.

5.9.3 Mass Spectrum for KK Modes of A_μ^{ij} and A_m^{ij} with $\tilde{N}^{ij} = 0$

We discuss the mass spectrum for A_μ^{ij} and A_m^{ij} in the $\tilde{N}^{ij} = 0$ case. In this case, the Lagrangians (5.67) and (5.70) can be reduced to

$$\mathcal{L}_{A_\mu}^{(ij)} \to 2\bar{A}_\mu^{ij}[\eta^{\mu\nu}\Box - (1-\xi^{-1})\partial^\mu\partial^\nu + \eta^{\mu\nu}\partial_{m'}\partial^{m'}]A_\nu^{ij}, \tag{5.82}$$
$$\mathcal{L}_{A_m}^{(ij)} \to 2\bar{A}_m^{ij}[\delta^{mn}\Box + \delta^{mn}\partial_{m'}\partial^{m'} - (1-\xi)\partial^m\partial^n]A_n^{ij}, \tag{5.83}$$

which are equivalent to the quadratic Lagrangians for the Cartan components (5.66) and (5.65). Therefore, the differential operators whose eigenvalues give the mass are the same as those for A_μ^k and A_m^k. On the other hand, the boundary conditions for A_M^{ij} are different from those for A_M^k. For $\tilde{N}^{ij} = 0$, the boundary conditions (5.75) and (5.76) become

$$A_M^{ij}(\mathcal{T}_5 z) = e^{-ig\tilde{v}_5^{ij}}A_M^{ij}(z), \quad A_M^{ij}(\mathcal{T}_6 z) = e^{-ig(\tau_R\tilde{v}_5^{ij}+\tau_I\tilde{v}_6^{ij})}A_M^{ij}(z), \tag{5.84}$$

respectively. Since the exponents are constant, these boundary conditions are equivalent to the boundary condition with $\eta_\psi \neq 0$ for the matter field (2.10) discussed in Chap. (2). As shown in Sec. 2.3, the nontrivial phase η_ψ in the boundary condition simply yields the shift $n \to n + \frac{\eta_\psi}{2\pi}$ from the mass spectrum with the periodic boundary condition. In the present case, the integers $\hat{n}$ and $\hat{m}$ are replaced by $\hat{n} - g\tilde{v}_5^{ij}/2\pi$ and $\hat{m} - g\tilde{v}_6^{ij}/2\pi$, respectively. Thus, the KK masses for A_μ^{ij} and A_m^{ij} are given by

$$\begin{aligned} M^2(A_{\mu(\hat{n},\hat{m})}^{ij}) &= M_{\text{ph}}^2(A_{m(\hat{n},\hat{m})}^{ij}) \\ &= \left(\frac{2\pi}{L}\right)^2\left[(\hat{n}-\tilde{a}_5^{ij})^2 + \tau_{\text{I}}^{-2}((\hat{m}-\tilde{a}_6^{ij}) - (\hat{n}-\tilde{a}_5^{ij})\tau_{\text{R}})^2\right], \end{aligned} \tag{5.85}$$
$$M_\xi^2(A_{m(\hat{n},\hat{m})}^{ij}) = \xi\left(\frac{2\pi}{L}\right)^2\left[(\hat{n}-\tilde{a}_5^{ij})^2 + \tau_{\text{I}}^{-2}((\hat{m}-\tilde{a}_6^{ij}) - (\hat{n}-\tilde{a}_5^{ij})\tau_{\text{R}})^2\right], \tag{5.86}$$

where we have introduced $\tilde{a}_m^{ij} = g\tilde{v}_m^{ij}/2\pi$. This continuous quantity $\tilde{a}_m^{ij}$ corresponds to θ_5 in Chap. 2, and the above mass spectra are invariant under integer shifts of $\tilde{a}_m^{ij}$.

Except for the case with $\tilde{a}_m^{ij} = 0$ mod 1, these spectra have no massless modes. In other words, the fields A_M^{ij} that couples only with the continuous Wilson lines have no dynamical modes in the low-energy effective theory. The gauge symmetries related to these fields are broken in the effective theory. As for A_M^k, half of the scalar KK modes have ξ-dependent masses $M_\xi^2(A_{m(\hat{n},\hat{m})}^{ij})$ and are would-be Goldstone modes giving longitudinal modes to the massive gauge fields.

5.9.4 Mass Spectrum for KK modes of A_μ^{ij} with $\tilde{N}^{ij} \neq 0$

Next, we calculate the mass spectrum for A_μ^{ij} in the $\tilde{N}^{ij} \neq 0$ case. The field A_μ^{ij} with $\tilde{N}^{ij} \neq 0$ couples to the background flux, and the Lagrangian and boundary conditions largely change due to the existence of this interaction. The mass spectrum is obtained as the eigenvalues of the operator

$$\begin{aligned} -(D_m^{(ij)})^2 = \left(-i\partial_5 + \frac{1}{2} g\hat{f}\tilde{N}^{ij}(1+\gamma)x^6\right)^2 \\ + \left(-i\partial_6 - \frac{1}{2} g\hat{f}\tilde{N}^{ij}(1-\gamma)x^5/2\right)^2, \end{aligned} \tag{5.87}$$

and the mode function is given as the eigenfunction of this operator. The mode function must be consistent with the boundary conditions (5.75) and (5.76).

This operator is equivalent to the Hamiltonian (2.74) for the two-dimensional quantum mechanical system with a constant magnetic field. Therefore, the discussion in Sec. (2.8) is helpful to derive the mass spectrum. The quantum mechanical momentum operator defined by $p_m = -i\partial_m$ satisfies $[x^m, p_n] = i\delta_n^m$. We define the operators

$$-iD_5^{(ij)} = p_5 + \frac{1}{2} g\hat{f}\tilde{N}^{ij}(1+\gamma)x^6, \quad -iD_6^{(ij)} = p_6 - \frac{1}{2} g\hat{f}\tilde{N}^{ij}(1-\gamma)x^5, \tag{5.88}$$

satisfying the commutation relation $[-iD_5^{(ij)}, -iD_6^{(ij)}] = ig\hat{f}\tilde{N}^{ij}$ independently to the background gauge parameter γ. These operators correspond to $\hat{\Pi}_x$ and $\hat{\Pi}_y$ in Sec. (2.8), and we can define creation and annihilation operators from them. As done in Eq. (2.87), we further define the operators

$$\Pi_z^{(ij)} = -i\sqrt{\frac{2}{g\hat{f}|\tilde{N}^{ij}|}} \frac{D_5^{(ij)} - iD_6^{(ij)}}{2} = \sqrt{\frac{2}{g\hat{f}|\tilde{N}^{ij}|}} \left[p_z + i\frac{g\hat{f}\tilde{N}^{ij}}{4}(\bar{z} - \gamma z)\right], \tag{5.89}$$

$$\bar{\Pi}_z^{(ij)} = -i\sqrt{\frac{2}{g\hat{f}|\tilde{N}^{ij}|}} \frac{D_5^{(ij)} + iD_6^{(ij)}}{2} = \sqrt{\frac{2}{g\hat{f}|\tilde{N}^{ij}|}} \left[\bar{p}_z - i\frac{g\hat{f}\tilde{N}^{ij}}{4}(z - \gamma \bar{z})\right], \tag{5.90}$$

where we have used $p_z = -i\partial_z$ and $\bar{p}_z = -i\bar{\partial}_z$.

These operators correspond to creation and annihilation operators. They satisfy $[\bar{\Pi}_z^{(ij)}, \Pi_z^{(ij)}] = 1$ for $\tilde{N}^{ij} > 0$ and $[\Pi_z^{(ij)}, \bar{\Pi}_z^{(ij)}] = 1$ for $\tilde{N}^{ij} < 0$. Therefore, we can define the creation and annihilation operators $(\hat{a}, \hat{a}^\dagger) = (\bar{\Pi}_z^{(ij)}, \Pi_z^{(ij)})$ for $\tilde{N}^{ij} > 0$, and $(\hat{a}, \hat{a}^\dagger) = (\Pi_z^{(ij)}, \bar{\Pi}_z^{(ij)})$ for $\tilde{N}^{ij} < 0$ to express Eq. (5.87) as

$$-(D_m^{(ij)})^2 = 2g\hat{f}|\tilde{N}^{ij}| \left(\hat{a}^\dagger \hat{a} + 1/2\right). \tag{5.91}$$

The eigenvalues of these operators are equivalent to the energy eigenvalues (2.86). Namely, we obtain a Landau-level like spectrum, where the eigenvalue of the $\hat{\ell}$–th exited state is proportional to $(\hat{\ell}+\frac{1}{2})$ $(\hat{\ell}=1,2,\ldots)$ and each state labeled by $\hat{\ell}$ has $|\tilde{N}^{ij}|$ degenerated states.

We can also derive the mode functions that are the eigenfunctions of the operator (5.91). Let $\zeta^{ij}_{0,d}(z)$ $(d=0,1,\ldots,|\tilde{N}^{ij}|-1)$ be the mode function for the degenerated ground state. The ground state is defined by

$$\hat{a}\zeta^{ij}_{0,d}(z)=0. \tag{5.92}$$

The mode functions for excited states $\zeta^{ij}_{\hat{\ell},d}(z)$ can be obtained from $\zeta^{ij}_{0,d}$ as

$$\zeta^{ij}_{\hat{\ell},d}(z)=\frac{1}{\sqrt{\hat{\ell}!}}(\hat{a}^\dagger)^{\hat{\ell}}\zeta^{ij}_{0,d}(z). \tag{5.93}$$

In addition, the mode functions must satisfy the same boundary conditions as those for A^{ij}_M in Eqs. (5.75) and (5.76), *i.e.*,

$$\zeta^{ij}_{\hat{\ell},d}(\mathcal{T}_5 z)=e^{-2\pi i\tilde{a}^{ij}_5}e^{ig(1-\gamma)(x^6/2)\hat{f}\tilde{N}^{ij}}\zeta^{ij}_{\hat{\ell},d}(z), \tag{5.94}$$

$$\zeta^{ij}_{\hat{\ell},d}(\mathcal{T}_6 z)=e^{-2\pi i(\tau_{\mathrm{R}}\tilde{a}^{ij}_5+\tau_{\mathrm{I}}\tilde{a}^{ij}_6)}e^{ig\{-(1+\gamma)\tau_{\mathrm{I}}x^5/2+(1-\gamma)\tau_{\mathrm{R}}x^6/2\}\hat{f}\tilde{N}^{ij}}\zeta^{ij}_{\hat{\ell},d}(z). \tag{5.95}$$

As shown in Appx. C.2, we can obtain the explicit form of the mode function

$$\begin{aligned}\zeta^{ij}_{\hat{\ell},d}(z)=&\left(\frac{2\pi\tilde{N}^{ij}}{\tau_{\mathrm{I}}}\right)^{1/4}\frac{1}{2^{\hat{\ell}}\sqrt{\hat{\ell}!}}e^{\frac{\pi\tilde{N}^{ij}}{2\tau_{\mathrm{I}}}[z(z-\bar{z})-\frac{\gamma}{2}(z+\bar{z})(z-\bar{z})]}\\ &\times\sum_{n=-\infty}^{+\infty}H_{\hat{\ell}}(w_{n,d}(z))e^{i\pi\tilde{N}^{ij}\tau(n-(\tilde{a}^{ij}_5-d)/\tilde{N}^{ij})^2}\\ &\qquad\times e^{2\pi i(n-(\tilde{a}^{ij}_5-d)/\tilde{N}^{ij})(\tilde{N}^{ij}z+\tau_{\mathrm{R}}\tilde{a}^{ij}_5+\tau_{\mathrm{I}}\tilde{a}^{ij}_6-\gamma\tilde{N}^{ij}\tau_{\mathrm{R}}/2)},\end{aligned} \tag{5.96}$$

for $\tilde{N}^{ij}>0$, where $H_{\hat{\ell}}(x)$ are the Hermite polynomials, and we have used

$$w_{n,d}(z)=\sqrt{\frac{2\pi N^{ij}}{\tau_{\mathrm{I}}}}\left[\frac{z-\bar{z}}{2i}+\tau_{\mathrm{I}}\left(n-\frac{\tilde{a}^{ij}_5-d}{\tilde{N}^{ij}}\right)\right]. \tag{5.97}$$

The overall normalization $(2\pi\tilde{N}^{ij}/\tau_{\mathrm{I}})$ has been determined so that the orthogonal relation

$$\int_{\mathcal{V}_{T^2}}dx^5dx^6\ \bar{\zeta}^{ij}_{\hat{\ell},d}\zeta^{ij}_{\hat{\ell}',d'}=\delta_{\hat{\ell}\hat{\ell}'}\delta_{dd'}, \tag{5.98}$$

is satisfied, where $\bar{\zeta}^{ij}_{\hat{\ell},d} = (\zeta^{ij}_{\hat{\ell},d})^\dagger$. The explicit mode function for $\tilde{N}^{ij} < 0$ can be obtained by taking the complex conjugate of Eq. (5.96).

Using the mode functions, we can expand $A^{ij}_\mu(x,z)$ as

$$A^{ij}_\mu(x,z) = \sum_{\hat{\ell}=0}^{\infty} \sum_{d=1}^{|\tilde{N}^{ij}|} A^{ij}_{\mu(\hat{\ell},d)}(x)\zeta^{ij}_{\hat{\ell},d}(z), \tag{5.99}$$

where we call $A^{ij}_{\mu(\hat{\ell},d)}(x)$ the $\hat{\ell}$–th Landau level. The mass for the $\hat{\ell}$–th Landau level $M^2(A^{ij}_{\mu(\hat{\ell},d)})$ is given by the eigenvalue of the operator (5.91) as

$$M^2(A^{ij}_{\mu(\hat{\ell},d)}) = 2g\hat{f}|\tilde{N}^{ij}|(\hat{\ell}+1/2). \tag{5.100}$$

All $A^{ij}_{\mu(\hat{\ell},d)}$ have masses proportional to the compactification scale since $f \propto L^{-2}$. Thus, the gauge symmetry related to A^{ij}_μ ($\tilde{N}^{ij} \neq 0$) is broken by the interaction with the flux. The Wilson line phases do not affect the mass spectrum, which implies that the linear combination of the Wilson lines (5.50) can be the NG boson of the translational symmetry broken by the flux $\propto \tilde{N}^{ij}$.

5.9.5 Masses Spectrum for KK Modes for A^{ij}_m with $\tilde{N}^{ij} \neq 0$

Finally, let us discuss the mass spectrum for A^{ij}_m in the $\tilde{N}^{ij} \neq 0$ case. In this case, the extra-dimensional components of the gauge field couple to the flux. The last three terms in the Lagrangian (5.70) determine the mass spectrum. Let us define the mass operator matrix

$$\begin{aligned}\hat{\mathcal{M}}^2(A^{ij}_m) =& -\mathbf{1}_{2\times 2}(D^{(ij)}_m)^2 \\ &+ (1-\xi)\begin{pmatrix} (D^{(ij)}_5)^2 & D^{(ij)}_5 D^{(ij)}_6 \\ D^{(ij)}_6 D^{(ij)}_5 & (D^{(ij)}_6)^2 \end{pmatrix} + 2ig\hat{f}\tilde{N}^{ij}\begin{pmatrix} 0 & 1 \\ -1 & 0 \end{pmatrix}\end{aligned} \tag{5.101}$$

to express the Lagrangian as

$$\mathcal{L}^{(ij)}_{A_m} = 2(\bar{A}^{ij}_5\ \bar{A}^{ij}_6)(\mathbf{1}_{2\times 2}\Box - \hat{\mathcal{M}}^2(A^{ij}_m))\begin{pmatrix} A^{ij}_5 \\ A^{ij}_6 \end{pmatrix}. \tag{5.102}$$

Here, $\mathbf{1}_{2\times 2}$ is the 2×2 identity matrix. We can rewrite the mass operator by using $\Pi^{(ij)}_z$ and $\bar{\Pi}^{(ij)}_z$ and obtain

$$\begin{aligned}\hat{\mathcal{M}}^2(A^{ij}_m) =& -\frac{1+\xi}{2}\mathbf{1}_{2\times 2}(D^{(ij)}_m)^2 \\ &- \frac{1-\xi}{2}g\hat{f}\tilde{N}^{ij}\begin{pmatrix} (\Pi^{(ij)}_z)^2 + (\bar{\Pi}^{(ij)}_z)^2 & i[(\Pi^{(ij)}_z)^2 - (\bar{\Pi}^{(ij)}_z)^2 + 1] \\ i[(\Pi^{(ij)}_z)^2 - (\bar{\Pi}^{(ij)}_z)^2 - 1] & -(\Pi^{(ij)}_z)^2 - (\bar{\Pi}^{(ij)}_z)^2 \end{pmatrix} \\ &+ 2ig\hat{f}\tilde{N}^{ij}\begin{pmatrix} 0 & 1 \\ -1 & 0 \end{pmatrix}\end{aligned} \tag{5.103}$$

for $\tilde{N}^{ij} > 0$. Here, we used the commutation relation $[\bar{\Pi}_z^{(ij)}, \bar{\Pi}_z^{(ij)}] = 1$. It is convenient to introduce

$$\begin{pmatrix} A_-^{ij} \\ A_+^{ij} \end{pmatrix} = U \begin{pmatrix} A_5^{ij} \\ A_6^{ij} \end{pmatrix}, \qquad U = \frac{1}{\sqrt{2}} \begin{pmatrix} 1 & -i \\ 1 & i \end{pmatrix}. \tag{5.104}$$

The matrix U is an unitary matrix $UU^\dagger = 1$. In terms of these complex fields, the Lagrangian is rewritten as

$$\mathcal{L}_{A_m}^{(ij)} = \left(\bar{A}_-^{ij}\ \bar{A}_+^{ij}\right) \left[\mathbf{1}_{2\times 2}\Box - \hat{\mathcal{M}}^2(A_\pm^{ij})\right] \begin{pmatrix} A_-^{ij} \\ A_+^{ij} \end{pmatrix} \tag{5.105}$$

$$\begin{aligned} \hat{\mathcal{M}}^2(A_\pm^{ij}) &= U\hat{\mathcal{M}}^2(A_m^{ij})U^\dagger \\ &= \begin{pmatrix} g\hat{f}\tilde{N}^{ij}((1+\xi)\hat{a}^\dagger\hat{a} - 1) & -g\hat{f}\tilde{N}^{ij}(1-\xi)\hat{a}^\dagger\hat{a}^\dagger \\ -g\hat{f}\tilde{N}^{ij}(1-\xi)\hat{a}\hat{a} & g\hat{f}\tilde{N}^{ij}((1+\xi)\hat{a}^\dagger\hat{a} + \xi + 2) \end{pmatrix}, \end{aligned} \tag{5.106}$$

where we used the creation and annihilation operator $(\hat{a}, \hat{a}^\dagger) = (\bar{\Pi}_z^{(ij)}, \Pi_z^{(ij)})$. For the $\tilde{N}^{ij} < 0$ case, we also have a similar expression.

The field A_m^{ij} satisfies the same boundary conditions as A_μ^{ij}, so its Kaluza-Klein expansion is also expressed by

$$A_\pm^{ij}(x,z) = \sum_{\hat{\ell}=0}^{\infty} \sum_{d=1}^{\tilde{N}^{ij}} A_{\pm(\hat{\ell},d)}^{ij}(x) \zeta_{\hat{\ell},d}^{ij}(z), \tag{5.107}$$

where $A_{\pm(\hat{\ell},d)}^{ij}$ is the $\hat{\ell}$–th Landau level, and $\zeta_{\hat{\ell},d}^{ij}(z)$ is the same mode function as that for A_μ^{ij}. Substituting the KK expansion into Eq. (5.105) and integrating out the extra dimension yields the following 4D Lagrangian

$$\begin{aligned} \mathcal{L}_{A_m}^{(ij)} = {} & 2\bar{A}_{-(0,d)}^{ij}\left[\Box + g\hat{f}\tilde{N}^{ij}\right] A_{-(0,d)}^{ij} + 2\bar{A}_{-(1,d)}^{ij}\left[\Box - \xi g\hat{f}\tilde{N}^{ij}\right] A_{-(1,d)}^{ij} \\ & + 2\sum_{\hat{\ell}=0}^{\infty} \left(\bar{A}_{+(\hat{\ell},d)}^{ij} \quad \bar{A}_{-(\hat{\ell}+2,d)}^{ij}\right) \left[\mathbf{1}_{2\times 2}\Box - \mathcal{M}^2(A_{\pm(\hat{\ell},d)})\right] \begin{pmatrix} A_{+(\hat{\ell},d)}^{ij} \\ A_{-(\hat{\ell}+2,d)}^{ij} \end{pmatrix}. \end{aligned} \tag{5.108}$$

We have defined the mass matrix $\mathcal{M}^2(A_{\pm(\hat{\ell},d)})$ by

$$\begin{aligned} & \mathcal{M}^2(A_{\pm(\hat{\ell},d)}) \\ & = -g\hat{f}\tilde{N}^{ij} \begin{pmatrix} -[(1+\xi)\hat{\ell} + 2 + \xi] & (1-\xi)\sqrt{(\hat{\ell}+1)(\hat{\ell}+2)} \\ (1-\xi)\sqrt{(\hat{\ell}+1)(\hat{\ell}+2)} & -[(1+\xi)(\hat{\ell}+2) - 1] \end{pmatrix}. \end{aligned} \tag{5.109}$$

To derive it, we have used the relations

$$\hat{a}^\dagger \zeta_{\hat{\ell},d}^{ij}(z) = \sqrt{\ell+1}\,\zeta_{\hat{\ell}+1,d}^{ij}(z), \quad \hat{a}\zeta_{\hat{\ell},d}^{ij}(z) = \sqrt{\ell}\,\zeta_{\hat{\ell}-1,d}^{ij}(z). \tag{5.110}$$

In Eq. (5.108), the index d is also summed over the degenerated states. Taking suitable values of the gauge parameter ξ and $\tilde{N}^{ij}$ for the $SU(2)$ case, the above expression is consistent with similar equations shown in [114]. The last term in the Lagrangian (5.108) can be diagonalized by using the orthogonal matrix

$$O = \frac{1}{\sqrt{2\hat{\ell}+3}} \begin{pmatrix} \sqrt{\hat{\ell}+2} & \sqrt{\hat{\ell}+1} \\ -\sqrt{\hat{\ell}+1} & \sqrt{\hat{\ell}+2} \end{pmatrix}, \tag{5.111}$$

as $O\mathcal{M}^2(A_{\pm(\hat{\ell},d)})O^{-1}$, and we finally obtain the following mass spectrum for $A^{ij}_{\pm(\hat{\ell},d)}$

$$M^2_{\text{ph}}(A^{ij}_{-(0,d)}) = 2g\hat{f}\tilde{N}^{ij}(-1/2), \tag{5.112}$$
$$M^2_{\xi}(A^{ij}_{+(0,d)}) = 2g\hat{f}\tilde{N}^{ij}\xi(1/2), \tag{5.113}$$
$$M^2_{\text{ph}}(A^{ij}_{\pm(\hat{\ell},d)}) = 2g\hat{f}\tilde{N}^{ij}(\hat{\ell}+1/2) \quad (\hat{\ell}\geq 1), \tag{5.114}$$
$$M^2_{\xi}(A^{ij}_{\pm(\hat{\ell},d)}) = 2g\hat{f}\tilde{N}^{ij}\xi(\hat{\ell}+1/2) \quad (\hat{\ell}\geq 1). \tag{5.115}$$

We can also obtain the same mass spectrum for $\tilde{N}^{ij} < 0$ repeating similar calculations. All of the KK modes whose masses are given by Eq. (5.114) are massive and decouple from the low-energy effective theory. There exist the would-be Goldstone modes, whose masses depend on ξ, and whose degrees of freedom will be absorbed by the infinite tower of vector fields. The scalars $A^{ij}_{-(0,d)}$ are tachyonic, which implies the instability of the background configuration (5.18). We will discuss this point in Sec. 5.10.

5.9.6 Vanishing One-loop Potentials for NG Bosons

As mentioned in Chap 1, the flux breaks the translational symmetry on T^2, which yields NG bosons related with the broken symmetry. In our non-abelian setup, the NG bosons are regarded as some combinations of the zero modes $A^k_{m(0,0)}$. More precisely, for a given set of N^k in Eq. (5.38), the NG bosons correspond to the linear combinations of the Wilson lines (5.50) in the nonzero directions of $\tilde{N}^{ij}$ given by Eq. (5.49).

We can understand from the tree-level mass spectrum that one-loop corrections do not induce masses and potentials for the NG bosons, as follows. In general, as shown in Chap. 2 for the 5D $U(1)$ gauge theory, background values of the Wilson line phases are not determined at tree-level but may be fixed by an effective potential dynamically generated through quantum corrections. We can obtain the effective potential for the Wilson line phases in a similar way as discussed in Sec. 2.6, although the tachyonic states exist. The KK modes whose masses depend on the Wilson lines phases contribute to the effective potential. The crucial point is that the Wilson line phases $\tilde{v}_m^{ij}$ in the $\tilde{N}^{ij} \neq 0$ directions do not appear in the mass spectrum. Thus, Wilson line phases along the flux direction $N^k \hat{H}_k$ have completely flat potential even when including one-loop corrections. The other Wilson line phases appear in the mass spectra and have non-vanishing one-loop effective potentials, in general. However, the result may be disturbed by tachyonic states, which are discussed in the next section.

5.9.7 Example: $SU(3)$

The previous discussion was done for the general background configuration of $SU(n)$, but let us provide a specific example in $SU(3)$. In this case, $\hat{H}_k$ $(k = 1, 2)$ are given as

$$\hat{H}_1^{su(3)} = \begin{pmatrix} 1 & 0 & 0 \\ 0 & -1 & 0 \\ 0 & 0 & 0 \end{pmatrix}, \qquad \hat{H}_2^{su(3)} = \begin{pmatrix} 0 & 0 & 0 \\ 0 & 1 & 0 \\ 0 & 0 & -1 \end{pmatrix}. \tag{5.116}$$

We assume the background

$$\boldsymbol{f}^{su(3)} = \hat{f} \begin{pmatrix} 1 & 0 & 0 \\ 0 & 1 & 0 \\ 0 & 0 & -2 \end{pmatrix}, \qquad \boldsymbol{v}_M^{su(3)} = v \begin{pmatrix} 1 & 0 & 0 \\ 0 & -1 & 0 \\ 0 & 0 & 0 \end{pmatrix}, \tag{5.117}$$

which gives $N^1 = 1,\ N^2 = 2,\ v_m^1 = v$ and $v_m^2 = 0$.

In this setup, the $SU(3)$ gauge field is written as

$$\boldsymbol{A}_M^{su(3)} = \begin{pmatrix} A_M^1 & A_M^{12} & A_M^{13} \\ \bar{A}_M^{12} & A_M^2 - A_M^1 & A_M^{23} \\ \bar{A}_M^{13} & \bar{A}_M^{23} & -A_M^2 \end{pmatrix}. \tag{5.118}$$

Since the parameters $\tilde{N}^{ij}$ and $\tilde{v}_m^{ij}$ are

$$\tilde{N}^{12} = 0, \quad \tilde{N}^{13} = 3, \quad \tilde{N}^{23} = 3, \tag{5.119}$$

$$\tilde{v}_m^{12} = 2v, \quad \tilde{v}_m^{13} = v, \quad \tilde{v}_m^{23} = -v, \tag{5.120}$$

for this background configuration, A_M^{12} and $\bar{A}_M^{12}$ couple only to the continuous WL. On the other hand, the fields A_M^{13}, A_M^{23}, and their conjugates interact both with the flux and WL. This can be read off from the background matrices (5.117). The upper-left 2×2 submatrix of $\boldsymbol{f}$ is proportional to an identity matrix and commutes with the first 2×2 part of $\boldsymbol{A}_M$. Therefore, in addition to the Cartan parts, A_M^{12} also does not interact with the flux.

Let us discuss the breaking of the gauge symmetry in this setup. First, we set $v = 0$ and consider the breaking caused by the background flux $\boldsymbol{f}^{su(3)}$. In this case, the mass spectrum for A_μ^{13}, A_μ^{23} and their conjugate are given by Eq. (5.100), and they have no massless modes. On the other hand, for $v = 0$, all the other fields have massless modes, and the related symmetries remain in the 4D effective theory. Therefore, $SU(3)$ is broken to $SU(2) \times U(1)$ by the flux as naively expected from the matrix form of the flux background. The $SU(2)$ corresponds to the upper-left 2×2 components of the gauge field that commutes with the flux, and the $U(1)$ corresponds to the diagonal part.

We consider next the case where there exists a non-vanishing Wilson line ($v \neq 0$) in addition to the flux. In this case, A_μ^{12} and its conjugate, whose mass spectrum is given by Eq. (5.86), do not have massless modes. The remaining $SU(2)$ symmetry in the $v = 0$ case is further broken by the coupling with the Wilson line, and therefore, $SU(3)$ is finally broken to $U(1) \times U(1)$. Only the Cartan components A_M^1 and A_M^2 remain in the 4D effective theory.

In this setup, A_m^{13} and A_m^{23} each contain three tachyonic modes since $\tilde{N}^{12} = \tilde{N}^{13}$. As discussed in the next section, they can condense and induce further symmetry breaking.

5.10 Phenomenological Implications

We have obtained the mass spectra in the low-energy effective theory of a 6D $SU(n)$ gauge theory with non-vanishing flux background. In this section, we discuss the phenomenological implications of this mass spectra.

A crucial feature of this setup is the existence of tachyonic states, which were also obtained in Refs. [105, 113, 114] for their specific setups. We have shown that the tachyonic states appear independently of the gauge parameter ξ in a general $SU(n)$ gauge theory with a general background flux configuration (5.18), which implies that the background configuration is unstable in general. In other words, the background corresponds to a local maximum, not the ground state of the system. Thus, they are expected to acquire nonzero vevs, and further breaking or restoration of gauge symmetries may be induced. The tachyon condensation may be very interesting for discussing phenomenological applications of this theory with magnetic flux background, but we do not further examine it here.

In this study, instead of discussing the condensation of the tachyon, we focus on stabilizing them by considering additional contributions to the masses. One possible way to realize tachyon stabilization is to consider extending the number of extra dimensions to more than two. In the context of flux compactifications in superstring theories, there are usually more than two extra dimensions, and the tachyon stabilization by Wilson line phases is often adopted [142]. For instance, let us consider an 8D gauge theory and assume a flat 4D torus as the compact extra dimensions. In this setup, a gauge field has four extra-dimensional components

$\boldsymbol{A}_5$, $\boldsymbol{A}_6$, $\boldsymbol{A}_7$, and $\boldsymbol{A}_8$. We assume that the backgrounds $\boldsymbol{B}_5$ and $\boldsymbol{B}_6$ of $\boldsymbol{A}_5$ and $\boldsymbol{A}_6$ give the background flux. As shown above, the flux background breaks the gauge symmetry G to its subgroup H. In addition, we consider constant Wilson line phases in the other extra-dimensional components $\boldsymbol{A}_7$ and $\boldsymbol{A}_8$ and represent them by $\boldsymbol{B}_7$ and $\boldsymbol{B}_8$. Since the broken translational symmetry in the x^5- and x^6-directions is irrelevant to $\boldsymbol{B}_7$ and $\boldsymbol{B}_8$, all of the tachyonic states appearing in the Landau level excitations receive additional contributions from the Wilson line phases in the x^7- and x^8-directions if the flux background and the Wilson line phases are in the same direction in the representation space of G. Then, if the contribution from the Wilson line phases is larger than that of the flux, the tachyonic states no longer have negative masses and can be eliminated from the tree-level mass spectrum.

Let us make the above discussion a little more concrete. In the eight-dimensional setup, the tree-level mass spectrum is determined by the eigenvalues of the differential operator $-(D^{(ij)}_{m'})^2$, with $m' = 5, 6, 7, 8$. For simplicity, we denote the tree-level mass squared for physical excitations of A^{ij}_μ and (A^{ij}_7, A^{ij}_8) by M^2_+ and those of (A^{ij}_5, A^{ij}_6) by M^2_-. In this setup, the masses of the fields coupling to the flux background can be parametrized as

$$M^2_\pm = 2g\hat{f}|\tilde{N}|(\hat{\ell} \pm 1/2) + (2\pi\rho)^2 \left[(\hat{n} - \tilde{a}_7)^2 + (\hat{m} - \tilde{a}_8)^2\right], \tag{5.121}$$

where $\hat{f}$ is a flux unit, $\tilde{N}$ is an integer, and ρ parametrizes the relative size of the compact extra dimensions. When the extra dimensions in the x^7- and x^8-directions are compactified to be smaller than the other two, the parameter ρ has a large value, and the contribution from the second term gets large.

The real parameters $\tilde{a}_7$ and $\tilde{a}_8$ in the second term correspond to the Wilson phases. In this 8D setup, each KK mode of the flux charged fields is labeled by four integers $\hat{\ell}, d, n$, and m. The non-negative integer $\hat{\ell}$ labels the Landau level excitations, $d(= 0, \ldots, |\tilde{N}|-1)$ labels the degeneracy of each Landau level, and the integers $\hat{n}$ and $\hat{m}$ label KK modes. In the case with vanishing Wilson line phases $\tilde{a}_7 = \tilde{a}_8 = 0$ (mod 1), negative mass squared appears in M^2_- for $\hat{\ell} = \hat{n} = \hat{m} = 0$ as in the 6D setup. On the other hand, when the non-vanishing Wilson line phases exists, the second term in Eq. (5.121) gives an additional contribution to the mass spectrum. In this case, the mass of the mode with $\hat{\ell} = \hat{n} = \hat{m} = 0$ is

$$M^2_- \to -g\hat{f}|\tilde{N}| + (2\pi\rho)^2(\tilde{a}_7^2 + \tilde{a}_8^2), \tag{5.122}$$

and the $\tilde{N}$ degenerated tachyonic modes are removed when the second term exceeds the first term.

As repeatedly mentioned, the values of a_7 and a_8 are not determined at tree-level. Therefore, at tree-level, we can freely set their values so that the tachyonic modes are eliminated from the mass spectrum (5.121). However, quantum corrections can yield an effective potential for a_7 and a_8. It is nontrivial whether the configuration of the Wilson line phases that eliminates the tachyonic mode is stabilized under quantum corrections. To justify the above stabilization, we must calculate the effective potential and find at least a local minimum of the potential in the region

$$\tilde{a}_7^2 + \tilde{a}_8^2 \geq \frac{g\hat{f}|\tilde{N}|}{(2\pi\rho)^2}. \tag{5.123}$$

The discussion on this matter is left for future studies.

Finally, we briefly mention matter fields under the flux background. It is well known that we can realize a chiral theory as a low energy effective theory of a 6D theory with bulk fermions on a magnetized torus. The bulk fermions have nontrivial helicity in the extra-dimensions, and the helicity of 4D left- and right-handed Weyl fermions are different. As a result, they couple differently to the flux, and only one of them can have a massless mode. In addition, the integer $\tilde{N}^{ij}$ in Eq. (5.49) expresses the coupling of the fermion to the flux and determines the generation number of the chiral fermions at a low-energy regime. These properties help to construct realistic GUT models.

5.11 Summary

In this chapter, we have investigated an $SU(n)$ gauge theory in a 6D spacetime with a constant magnetic flux in the two-dimensional torus. First, we analyzed the classical equations of motion for the gauge field and clarified the conditions that the background, including the Wilson line phases and magnetic flux, satisfies. Then, assuming a Cartan direction background consistent with the equations of motion, we have derived the boundary conditions for fields associated with the discrete translations on the torus. We have performed the standard R_ξ gauge fixing procedure to clarify the physical degrees of freedom in the low energy effective theory.

The complete mass spectrum is newly obtained for a general $SU(n)$ case with an arbitrary gauge parameter and background configurations. Our analysis confirmed the existence of tachyonic modes, which appear independently of the gauge fixing parameter ξ or the background configuration of Wilson line phases with flux. We have confirmed that some tachyonic modes exist in the 4D complex scalar field originating from the extra components of the gauge field. In addition, they were shown to be independent of the choice of the gauge parameters and the direction of the background gauge field. Some of the remaining scalar fields coupled to the flux were found to be massive, while others that showed dependence on ξ were identified as would-be Goldstone modes. As expected, only the non-Cartan components that do not couple to the flux receive contributions from the Wilson line phases.

From the mass spectrum, we have also discussed vanishing one-loop potentials for NG bosons related to the broken translational symmetry on the extra-dimensional torus. The Wilson lines, which are in the same direction as the flux in the representation space, correspond to NG bosons and do not appear in the mass spectrum. As a result, the one-loop effective potential is not generated in those directions.

Based on our findings, we have discussed the phenomenological implications associated with the stabilization of tachyonic modes. We have provided a concrete example of an 8D pure Yang-Mills theory where tachyonic modes can be eliminated from the tree-level mass spectrum. This elimination can be realized by the Wilson line phases introduced in a different direction from the flux in the extra dimensions. To justify the stabilization, we have to derive the effective potential for the newly introduced Wilson line phase, which is left for future research.

Chapter 6

Conclusion

In this thesis, we presented two different studies based on the framework of higher-dimensional gauge theory. One was an application to a cosmological scenario, and the other was the analysis of a non-abelian gauge theory with a background magnetic flux. Here, we briefly summarize the content of this thesis.

In Chap. 2, we reviewed the fundamental aspects of higher-dimensional gauge theory mainly using the 5D QED defined on $\mathcal{M}_4 \times S^1$ spacetime as a concrete example. In the first few sections, we introduced the basic concepts such as compact extra-dimension, boundary condition, and Kaluza-Klein expansion, and derived the 4D effective theory from the 5D QED Lagrangian. After discussing gauge transformation in the following few chapters, the dynamically generated effective potential was introduced. We also introduced S^1/Z_2 orbifold as another geometry of the extra dimension and reviewed the quantum mechanics of a charged particle in a constant magnetic field.

Chap. 3 was also a review and treated Early Dark Energy, which is a promising solution to the Hubble tension in cosmology. In the first section, we explained why the existence of EDE can make the value of the Hubble constant obtained from the CMB data larger. In the next section, using the extended PNGB potential as an example, we examined how the scalar potential must be for the energy density of the scalar field to behave as EDE.

In Chap. 4, we proposed a model of an EDE based on the 5D $U(1)$ gauge theory with matter fields defined on $\mathcal{M}_4 \times S^1$ spacetime. We identified the zero-mode of the extra component of the gauge field as the EDE scalar, whose energy density accounts for a few percent of the total energy density of the universe at a particular time before the recombination and then decreases faster than that of matter. We examined the possibility that the effective potential for the scalar field generated by quantum effects has suitable features for realizing the EDE behavior. The analysis clarified the conditions that the parameters such as gauge coupling, bulk mass, charge, and degrees of freedom must satisfy. We presented two examples that satisfied the conditions and checked the behavior of the system numerically. Finally, we discussed the parameter dependence of the behavior of the system, as well as the effect of the higher-order corrections. The results showed that the 5D $U(1)$ gauge theory can explain EDE without unnatural assumptions and fine-tuning.

In Chap. 5, we investigated the mass spectrum of an $SU(n)$ gauge theory with background magnetic flux defined on a $\mathcal{M}_4 \times T^2$ spacetime aiming to future apply it to GHU and GUT model buildings. The mass spectrum was obtained while keeping as much generality as possible in the choice of background and gauge parameter in the R_ξ gauge fixing. Our result showed that tachyonic modes exist in the sector of the scalar field arising from the extra components of the gauge field. In this thesis, instead of discussing tachyon condensation, which requires a complete understanding of the vacuum structure, we discussed the possibility of removing the tachyonic modes by Wilson line phases in a 8D model. To justify the stabilization, we have to calculate the effective potential for the Wilson line phases, which was left for our future study.

The two studies in this thesis show the further possibility of higher dimensional gauge theory. In the first study, we applied a 5D $U(1)$ gauge theory to the cosmological scenario, EDE. In our model, the scalar potential was not assumed and was derived from the Lagrangian of a higher-dimensional gauge theory. As a result, the effective potential was expressed in terms of the parameters in the 5D gauge theory. Therefore, we may be able to obtain some physical implications in higher dimensions from future observations in cosmology. In addition, our model is the simplest one with a single extra dimension and abelian gauge symmetry which can be extended to models with higher extra dimensions or with other gauge symmetries. Such extensions may yield nontrivial behavior that is not realized in our simple model. The scalar field arising from higher-dimensional gauge theories can also be regarded as another cosmological scalar, as has already been done. Therefore, higher-dimensional gauge theories may be able to naturally explain some cosmological scenarios. The second study can be helpful for GUT and GHU model buildings after investigating the tachyon condensation and stabilization in future study. Higher-dimensional gauge theory is one of the promising theoretical approaches for the construction of BSMs.

Appendix A

Appendix for Chapter 2

A.1 Gauge Transformation of the KK Modes (2.52)

In Sec. 2.5, we presented the transformations of the KK modes $A_M^{(n)}$ and $\psi^{(n)}$ under the gauge transformation by the function (2.53). Here, we provide the proof.

As mentioned, the gauge transformation does not change the boundary conditions for ψ and A_M. This means that ψ^{gt} and A_M^{gt} can be expanded by the same mode function as in Eq. (2.14). Therefore, the KK expansions of the gauge transformed fields are given by

$$\psi^{\text{gt}}(x,y) = \frac{1}{\sqrt{2\pi R}} \sum_{n=-\infty}^{+\infty} \psi^{\text{gt}(n)}(x)\xi_n^{\psi}(y), \tag{A.1}$$

$$A_M^{\text{gt}}(x,y) = \frac{1}{\sqrt{2\pi R}} \sum_{n=-\infty}^{+\infty} A_M^{\text{gt}(n)}(x)\xi_n^{A_M}(y). \tag{A.2}$$

The KK expansions before the transformation are Eqs. (2.12) and (2.13).

Let us first discuss the transformation of the gauge field (2.54). Substituting the KK expansions of A_M^{gt} and A_M yields

$$\sum_{n=-\infty}^{+\infty} A_\mu^{\text{gt}(n)}(x)\xi_n^{A_M}(y) = \sum_{n=-\infty}^{+\infty} A_\mu^{(n)}(x)\xi_n^{A_M}(y) + \frac{1}{\tilde{g}_4}\partial_\mu\tilde{\Lambda}(x)\xi_0^{A_M}(y), \tag{A.3}$$

$$\sum_{n=-\infty}^{+\infty} A_y^{\text{gt}(n)}(x)\xi_n^{A_M}(y) = \sum_{n=-\infty}^{+\infty} A_y^{(n)}(x)\xi_n^{A_M}(y) + \frac{m}{\tilde{g}_4 R}\xi_0^{A_M}(y), \tag{A.4}$$

where we explicitly write $1 = \xi_0^{A_M}(y)$ for the y-independent terms. Multiplying both sides of these equations by $\xi_m^{(n)}(y)$ and performing the y-integration, we obtain the first two lines in Eq. (2.52).

Next, we derive the transformation of the fermion KK modes. By substituting the KK expansions (2.12) and (A.1) into Eq. (2.55), we get

$$\sum_{n=-\infty}^{+\infty} \psi^{\mathrm{gt}(n)}(x)\xi_n^{\psi} = \sum_{n=-\infty}^{+\infty} e^{i\tilde{\Lambda}(x)}\psi^{(n)}(x)\xi_{n-m}^{\psi}. \tag{A.5}$$

Multiplying by the mode function $\xi_{\psi}^{n'}$ and performing integration using the orthogonality condition again, it becomes

$$\psi^{\mathrm{gt}(n')}(x) = \sum_{n=-\infty}^{+\infty} e^{i\tilde{\Lambda}(x)}\psi^{(n)}(x)\delta_{n'\,n-m} = e^{i\tilde{\Lambda}(x)}\psi^{(n'+m)}(x), \tag{A.6}$$

which is the third line in Eq. (2.52).

A.2 Derivation of the Effective Potential

We perform the momentum integral in Eq. (2.60) to obtain the expression (2.61). Here, we set $q_\varphi = 1$ and $\eta_\varphi = 0$ and express the contribution from φ as

$$\Delta V_\varphi = \frac{n_\varphi}{2} i \sum_{n=-\infty}^{\infty} \int \frac{d^4p}{(2\pi)^4} \log\left[-p^2 + m_n^2\right] , \tag{A.7}$$

$$m_n^2 = M_\varphi^2 + \left(\frac{n}{R} + \tilde{g}_4 \langle A_y^{(0)} \rangle\right)^2. \tag{A.8}$$

It is convenient to perform the Wick rotation and rewrite it as

$$\Delta V_\varphi = -\frac{n_\varphi}{2} \sum_{n=-\infty}^{\infty} \int \frac{d^4p_E}{(2\pi)^4} \log\left[p_E^2 + m_n^2\right]. \tag{A.9}$$

Now, we calculate the Euclidean momentum integral.

First, we use the mathematical formula

$$\ln x = \text{constant} - \int_0^\infty \frac{e^{-xt}}{t} dt, \tag{A.10}$$

to remove part of the constant divergence that the effective potential contains. One can check this identity by differentiating both sides of it. Applying Eq. (A.10) to Eq. (A.9) and ignoring the constant term, we obtain

$$\begin{aligned}\Delta V_\varphi &= \frac{n_\varphi}{2} \sum_{n=-\infty}^{\infty} \int_0^\infty dt \int \frac{d^4p_E}{(2\pi)^4} \frac{e^{-(p_E^2+m_n^2)t}}{t} \\ &= \frac{n_\varphi}{2} \sum_{n=-\infty}^{\infty} \int_0^\infty dt \, \frac{e^{-m_n^2 t}}{t} \int \frac{d^4p_E}{(2\pi)^4} e^{-p_E^2 t}.\end{aligned} \tag{A.11}$$

The p_E integral can be evaluated in the 4D polar coordinates as

$$\begin{aligned}
\int \frac{d^4 p_E}{(2\pi)^4} e^{-p_E^2 t} &= \frac{1}{8\pi^2}\int_0^\infty dk^2\ k^2 e^{-tk^2} \\
&= \frac{-1}{8\pi^2}\frac{\partial}{\partial t}\int_0^\infty dk^2\ e^{-tk^2} \\
&= \frac{-1}{8\pi^2}\frac{\partial}{\partial t}\frac{1}{t} \\
&= \frac{1}{8\pi^2}\frac{1}{t^2} \qquad \text{(A.12)}
\end{aligned}$$

Therefore, the potential is rewritten as

$$\Delta V_\varphi = \frac{n_\varphi}{16\pi^2}\sum_{n=-\infty}^{\infty}\int_0^\infty dt\ \frac{e^{-m_n^2 t}}{t^3} = \frac{n_\varphi}{16\pi^2}\int_0^\infty dt\ \frac{e^{-M_\varphi^2 t}}{t^3}\sum_{n=-\infty}^{\infty} e^{-(\frac{n}{R}+\tilde{g}_4\langle A_y^{(0)}\rangle)^2 t}. \qquad \text{(A.13)}$$

Next, we use the Poisson resummation formula

$$\sum_{n=-\infty}^{\infty} f\left(\frac{n}{R}\right) = 2\pi R\sum_{\ell=-\infty}^{\infty} F(2\pi R\ell), \qquad \text{(A.14)}$$

where $F(x)$ is the Fourier transformed function of f, *i.e.*,

$$F(x) = \int_{-\infty}^{\infty}\frac{dk}{2\pi}e^{-ikx}f(k). \qquad \text{(A.15)}$$

We derive the Poisson resummation formula in Sec. A.3. After using this formula, the sum over n becomes

$$\sum_{n=-\infty}^{\infty} e^{-(\frac{n}{R}+\tilde{g}_4\langle A_y^{(0)}\rangle)^2 t} = 2\pi R\sum_{\ell=-\infty}^{\infty}\int_{-\infty}^{\infty}\frac{dk}{2\pi}e^{-ik\cdot 2\pi R\ell}e^{-(k+\tilde{g}_4\langle A_y^{(0)}\rangle)^2 t}. \qquad \text{(A.16)}$$

By shifting the integration variable $s = k + \tilde{g}_4\langle A_y^{(0)}\rangle$, we get

$$\sum_{n=-\infty}^{\infty} e^{-(\frac{n}{R}+\tilde{g}_4\langle A_y^{(0)}\rangle)^2 t} = R\sum_{\ell=-\infty}^{\infty} e^{i\ell 2\pi R\tilde{g}_4\langle A_y^{(0)}\rangle}e^{-\frac{(\pi R\ell)^2}{t}}\int_{-\infty}^{\infty} ds\ e^{-t(s+i\frac{\pi R\ell}{t})^2}. \qquad \text{(A.17)}$$

The integral over s is just a complex Gaussian integral:

$$\int_{-\infty}^{\infty} ds\ e^{-t(s+i\frac{\pi R\ell}{t})^2} = \sqrt{\frac{\pi}{t}}. \qquad \text{(A.18)}$$

Thus, we can calculate the summation over n as follows

$$\begin{aligned}\sum_{n=-\infty}^{\infty} e^{-(\frac{n}{R}+\tilde{g}_4\langle A_y^{(0)}\rangle)^2 t} &= R\sqrt{\frac{\pi}{t}}\sum_{\ell=-\infty}^{\infty} e^{i\ell 2\pi R\tilde{g}_4\langle A_y^{(0)}\rangle} e^{-\frac{(\pi R\ell)^2}{t}} \\ &= R\left[1+\sum_{\ell\neq 0} e^{i\ell 2\pi R\tilde{g}_4\langle A_y^{(0)}\rangle} e^{-\frac{(\pi R\ell)^2}{t}}\right] \\ &= R\left[1+\sum_{\ell=1}^{\infty} e^{-\frac{(\pi R\ell)^2}{t}}\left(e^{i\ell 2\pi R\tilde{g}_4\langle A_y^{(0)}\rangle}+e^{-i\ell 2\pi R\tilde{g}_4\langle A_y^{(0)}\rangle}\right)\right] \\ &= R\left[1+2\sum_{\ell=1}^{\infty} e^{-\frac{(\pi R\ell)^2}{t}}\cos(\ell 2\pi R\tilde{g}_4\langle A_y^{(0)}\rangle)\right]. \end{aligned} \tag{A.19}$$

The first term can be ignored because it gives only a constant contribution to the potential.

Substituting Eq. (A.19) into Eq. (A.13), we obtain

$$\Delta V_\varphi = \frac{n_\varphi R}{8\pi^{3/2}}\sum_{\ell=1}^{\infty}\cos(\ell 2\pi R\tilde{g}_4\langle A_y^{(0)}\rangle)\int_0^\infty dt\; t^{-7/2} e^{-M_\varphi^2 t} e^{-\frac{(\pi R\ell)^2}{t}}. \tag{A.20}$$

We can rewrite this using the integral form of the Modified Bessel functions of the second kind

$$K_\nu(z) = \frac{1}{2}\left(\frac{z}{2}\right)^{-\nu}\int_0^\infty dt\; t^{\nu-1}\exp\left(-t-\frac{z^2}{4t}\right). \tag{A.21}$$

and the variable transformation $Mt^2 = x$. It results

$$\begin{aligned}\int_0^\infty dt\; t^{-7/2} e^{-M_\varphi^2 t} e^{-\frac{(\pi R\ell)^2}{t}} &= M_\varphi^5\int_0^\infty dx\; x^{-7/2}\exp\left(-x-\frac{(\ell\cdot 2\pi R M_\varphi)^2}{x}\right) \\ &= 2M_\varphi^5(\ell\cdot\pi R M_\varphi)^{5/2} K_{\frac{5}{2}}(\ell 2\pi R M_\varphi). \end{aligned} \tag{A.22}$$

Using another expression of $K_{\frac{5}{2}}(z)$

$$K_{\frac{5}{2}}(z) = \sqrt{\frac{\pi}{2z}}e^{-z}\left(1+3\frac{1}{z}+3\frac{1}{z^2}\right) = \frac{3}{z^2}\sqrt{\frac{\pi}{2z}}e^{-z}\left(1+z+\frac{z^2}{3}\right), \tag{A.23}$$

yields

$$\Delta V_\varphi(\theta_5) = \frac{3n_\varphi M_c^4}{4\pi^2}\sum_{\ell=1}^{\infty} e^{-\ell M_\varphi/M_c}\left[\frac{1}{\ell^5}+\frac{1}{\ell^4}\frac{M_\varphi}{M_c}+\frac{1}{3\ell^3}\frac{M_\varphi^2}{M_c^2}\right]\cos(\ell\theta_5), \tag{A.24}$$

where we used $\theta_5 = 2\pi R\tilde{g}_4\langle A_y^{(0)}\rangle$ and $M_c = (2\pi R)^{-1}$. We can perform the same calculation for the $\eta_\varphi \neq 0$ case. Here, instead, we simply shift $\theta_5 \to \theta_5 - \eta_\varphi$, which corresponds to the inverse of the gauge transformation (2.44) that shifted the $\eta_\varphi \neq 0$ gauge to the $\eta_\varphi = 0$ gauge. We can also recover the $U(1)$ charge of φ by the replacement $\theta_5 \to q_\varphi\theta_5$.

A.3 Poisson Resummation

We derive the Poisson resummation formula (A.14), here. To show it, we use another identity:

$$\frac{1}{2\pi R}\sum_{n=-\infty}^{+\infty} e^{i\frac{n}{R}x} = \sum_{\ell=-\infty}^{+\infty} \delta(x - 2\pi R\ell). \tag{A.25}$$

Proof. The right-hand side

$$Ш(x) = \sum_{\ell=-\infty}^{+\infty} \delta(x - 2\pi R w) \tag{A.26}$$

is called the *Dirac comb* and a periodic function with periodicity $2\pi R$. To show the formula (A.25), we expand the Dirac comb in a Fourier series as

$$Ш(x) = \sum_{n=-\infty}^{+\infty} c_n e^{i\frac{n}{R}x}. \tag{A.27}$$

The coefficient c_n is determined as

$$c_m = \frac{1}{2\pi R}\int_{-\pi R}^{+\pi R} dx \;\, Ш(x) e^{-i\frac{m}{R}x} \tag{A.28}$$

$$= \frac{1}{2\pi R}\int_{-\pi R}^{+\pi R} dx \;\delta(x) e^{-i\frac{m}{R}x} \tag{A.29}$$

$$= \frac{1}{2\pi R}, \tag{A.30}$$

where we used the fact that only $\ell = 0$ Dirac delta in Eq. (A.26) is nonzero in the integral region. Thus, the Fourier series expansion of the Dirac comb is finally given by

$$Ш(x) = \frac{1}{2\pi R}\sum_{n=-\infty}^{+\infty} e^{i\frac{n}{R}x}, \tag{A.31}$$

and this is the left-handed side in Eq. (A.26). $\square$

By using this formula, we can easily show the Poisson resummation. The left-handed side of Eq. (A.14) can be calculated as follows.

$$\sum_{n=-\infty}^{+\infty} f\left(\frac{n}{R}\right) = \sum_{n=-\infty}^{+\infty} \int_{-\infty}^{+\infty} dx\ e^{i\frac{n}{R}x} F(x) \tag{A.32}$$

$$= 2\pi R \int_{-\infty}^{+\infty} dx\ F(x) \sum_{\ell=-\infty}^{+\infty} \delta(x - 2\pi R\ell) \tag{A.33}$$

$$= 2\pi R \sum_{\ell=-\infty}^{+\infty} F(2\pi R\ell) \tag{A.34}$$

The last line is the right-handed side of the Poisson resummation. Here, we used the inverse of Eq. (A.15) in the first equality and Eq. (A.25) in the second equality.

Appendix B

Appendix for Chapter 4

B.1 Derivation of the Solution of Eq. (4.13)

In this appendix, we show that the solution of Eq. (4.13) is given by Eq. (4.15).Let us suppose that there are N kinds of bulk matter fields with different charges in the 5D $U(1)$ gauge theory as studied in Sec. 4.3. The effective potential for θ_5 can be written as

$$V_{\text{eff}}(\theta_5) = -V_0 \sum_{i=1}^{N} d_i[1 - \cos(q_i\theta_5)], \tag{B.1}$$

where d_i and q_i represent the degrees of freedom and the $U(1)$ charge of a field φ_i. We define $|q_i| \neq |q_j|$ for $i \neq j$ and $q_i \neq 0$. Here, we distinguish fields only based on the absolute values of their $U(1)$ charge. Namely, if multiple fields have the same $U(1)$ charge squared, they are labeled by the same index i.The overall scale V_0 given by Eq. (4.8) is irrelevant for the following discussion.

The potential (B.1) takes an extreme value at $\theta_5 = 0$ and is expanded around this point as

$$V_{\text{eff}}(\theta_5) = V_0 \left[\frac{1}{2!}\left(-\sum_{i=1}^{N} d_i q_i^2\right)\theta_5^2 + \frac{1}{4!}\left(\sum_{i=1}^{N} d_i q_i^4\right)\theta_5^4 + \cdots\right]. \tag{B.2}$$

To obtain a potential dominated by the θ_5^{2n} $(n \geq 2)$ term for $\theta_5 \simeq 0$, the following $n-1$ algebraic equations must be satisfied:

$$\sum_{i=1}^{N} d_i q_i^{2k} = 0, \qquad k = 1, \ldots, n-1. \tag{B.3}$$

They can be interpreted as $n-1$ simultaneous equations for d_i. We do not consider the trivial solution $d_i = 0$ because the potential becomes completely flat in this case. If the above condition is satisfied, the effective potential is written as

$$V_{\text{eff}}(\theta_5) = V_0 \frac{(-1)^n}{(2n)!} \left(\sum_{i=1}^{N} d_i q_i^{2n} \right) \theta_5^{2n} + \mathcal{O}(\theta_5^{2n+2}). \tag{B.4}$$

Here, we show that the simultaneous equations (B.3) can be solved for d_i for a given set of q_i. First, Eq. (B.3) is not affected by a simultaneous rescaling of d_i as $d_i \to c d_i$ with an arbitrary parameter c, which means that the set of parameters $\{d_1, d_2, \ldots, d_N\}$ has $N-1$ degrees of freedom that are relevant to solve Eq. (B.3). Therefore, to obtain a nontrivial solution of the $n-1$ conditions in Eq. (B.3), the condition $N-1 \geq n-1$ should be satisfied.

In the following, we focus on the minimal case with $N = n$. It is convenient to normalize q_i and d_i by using those of the n-th field and define

$$\tilde{Q}_i \equiv \frac{q_i^2}{q_n^2}, \qquad \tilde{d}_i \equiv \frac{d_i}{d_n}, \tag{B.5}$$

for $i = 1, \cdots, n-1$. Then, the conditions (B.3) can be expressed as

$$1 + \sum_{j=1}^{n-1} \tilde{d}_j \tilde{Q}_j^k = 0, \qquad k = 1, \ldots, n-1. \tag{B.6}$$

To solve these equations for $\tilde{d}_i$, let us introduce

$$\begin{aligned} V &= \begin{pmatrix} \tilde{Q}_1 & \tilde{Q}_2 & \cdots & \tilde{Q}_{n-1} \\ \tilde{Q}_1^2 & \tilde{Q}_2^2 & \cdots & \tilde{Q}_{n-1}^2 \\ \vdots & \vdots & \ddots & \vdots \\ \tilde{Q}_1^{n-1} & \tilde{Q}_2^{n-1} & \cdots & \tilde{Q}_{n-1}^{n-1} \end{pmatrix} \\ &= \begin{pmatrix} 1 & 1 & \cdots & 1 \\ \tilde{Q}_1 & \tilde{Q}_2 & \cdots & \tilde{Q}_{n-1} \\ \vdots & \vdots & \ddots & \vdots \\ \tilde{Q}_1^{n-2} & \tilde{Q}_2^{n-2} & \cdots & \tilde{Q}_{n-1}^{n-2} \end{pmatrix} \begin{pmatrix} \tilde{Q}_1 & 0 & \cdots & 0 \\ 0 & \tilde{Q}_2 & \cdots & 0 \\ \vdots & \vdots & \ddots & \vdots \\ 0 & 0 & \cdots & \tilde{Q}_{n-1} \end{pmatrix}, \end{aligned} \tag{B.7}$$

where the first matrix on the right-hand side is known as the Vandermonde matrix. From the definition (B.7), one finds that the (i, j) component of V can be expressed as

$$(V)_{ij} = (\tilde{Q}_j)^i. \tag{B.8}$$

By using V, Eq. (B.6) is rewritten as

$$V \begin{pmatrix} \tilde{d}_1 \\ \vdots \\ \tilde{d}_{n-1} \end{pmatrix} = - \begin{pmatrix} 1 \\ \vdots \\ 1 \end{pmatrix}. \tag{B.9}$$

One sees that the determinant of V is given by

$$\det V = \left(\prod_{\substack{i,j=1\\ j>i}}^{n-1} (\tilde{Q}_j - \tilde{Q}_i) \right) \left(\prod_{m=1}^{n-1} \tilde{Q}_m \right), \tag{B.10}$$

where the inside the first bracket is the determinant of the Vandermonde matrix and known as the Vandermonde's determinant. Since $\tilde{Q}_j \neq \tilde{Q}_i$ for $i \neq j$ and $\tilde{Q}_i \neq 0$ in the present case, the determinant has a nonzero value, and there is an inverse of V, denoted by V^{-1}. From the definition of the inverse matrix, it follows that

$$\delta_{ij} = \sum_{k=1}^{n-1} (V^{-1})_{ik} (V)_{kj} = \sum_{k=1}^{n-1} (V^{-1})_{ik} (\tilde{Q}_j)^i, \tag{B.11}$$

where we used Eq. (B.8) in the last equality. The solution of Eq. (B.9) is given by

$$\tilde{d}_i = -\sum_{k=1}^{n-1} (V^{-1})_{ik}, \tag{B.12}$$

where $(V^{-1})_{ik}$ is the (i, k) element of V^{-1}.

To obtain an explicit expression for $\tilde{d}_i$, let us introduce the function

$$R_i(\tilde{Q}) = \frac{\tilde{Q}}{\tilde{Q}_i} \prod_{\substack{k=1\\ k\neq i}}^{n-1} \frac{\tilde{Q} - \tilde{Q}_k}{\tilde{Q}_i - \tilde{Q}_k}, \tag{B.13}$$

which satisfies

$$R_i(\tilde{Q}_j) = \delta_{ij}, \tag{B.14}$$

by definition. Combining Eq. (B.14) and Eq. (B.11) yields

$$R_i(\tilde{Q}_j) = \sum_{k=1}^{n-1} (V^{-1})_{ik} \tilde{Q}_j^k. \tag{B.15}$$

Comparing it with Eq. (B.12), we find that $\tilde{d}_i$ can be expressed by using the function $R_i(\tilde{Q})$ as

$$\tilde{d}_i = -R_i(1) = -\frac{1}{\tilde{Q}_i} \prod_{\substack{k=1\\ k\neq i}}^{n-1} \frac{1 - \tilde{Q}_k}{\tilde{Q}_i - \tilde{Q}_k}. \tag{B.16}$$

Substituting Eq. B.5 into Eq. (B.16), we finally obtain the solution of Eq. (B.3) as

$$\frac{d_i}{d_j} = -\frac{q_j^2}{q_i^2}\prod_{\substack{k=1\\k\neq i,j}}^{n}\frac{q_j^2-q_k^2}{q_i^2-q_k^2}, \tag{B.17}$$

which holds for any $i, j \in \{1, \ldots, n\}$ and $i \neq j$. The charges must be consistent with the fact that d_i represents the degrees of freedom.

Using the solution above, we can rewrite the leading term of the effective potential in Eq. (B.4). By using $\tilde{d}_i$ and $\tilde{Q}_i$, the coefficient of the θ^{2n}-proportional term appearing in Eq. (B.4) is expressed as

$$\frac{(-1)^n}{(2n)!}\sum_{i=1}^{n} d_i q_i^{2n} = \frac{(-1)^n}{(2n)!} d_n q_n^{2n}\left(1+\sum_{i=1}^{n-1}\tilde{d}_i\tilde{Q}_i^n\right). \tag{B.18}$$

Substituting Eq. (B.16) into Eq. (B.18) yields

$$\begin{aligned}1+\sum_{i=1}^{n-1}\tilde{d}_i\tilde{Q}_i^n &= 1-\sum_{i=1}^{n-1}\tilde{Q}_i^{n-1}\left[\prod_{\substack{k=1\\k\neq i}}^{n-1}\frac{1-\tilde{Q}_k}{\tilde{Q}_i-\tilde{Q}_k}\right]\\ &= 1-\tilde{Q}_1^{n-1}\prod_{\substack{k=1\\k\neq 1}}^{n-1}\frac{1-\tilde{Q}_k}{\tilde{Q}_1-\tilde{Q}_k}\\ &\quad -\tilde{Q}_2^{n-1}\prod_{\substack{k=1\\k\neq 2}}^{n-1}\frac{1-\tilde{Q}_k}{\tilde{Q}_2-\tilde{Q}_k}\\ &\quad -\cdots-\tilde{Q}_{n-1}^{n-1}\prod_{\substack{k=1\\k\neq n-1}}^{n-1}\frac{1-\tilde{Q}_k}{\tilde{Q}_{n-1}-\tilde{Q}_k}.\end{aligned} \tag{B.19}$$

Since the quantity above vanishes for $\tilde{Q}_i = 1$ with an arbitrary i and is linear for any $\tilde{Q}_i$, we can also write

$$1+\sum_{i=1}^{n-1}\tilde{d}_i\tilde{Q}_i^n = C(1-\tilde{Q}_1)(1-\tilde{Q}_2)\cdots(1-\tilde{Q}_{n-1}), \tag{B.20}$$

where C is a constant. One sees that $C = 1$ should be satisfied by taking a specific value of $\tilde{Q}_i$, *e.g.*, $\tilde{Q}_i = 1 - i$. Thus, we finally obtain

$$\begin{aligned}
\frac{(-1)^n}{(2n)!}\sum_{i=1}^{n} d_i q_i^{2n} &= \frac{(-1)^n}{(2n)!} d_n q_n^{2n}(1-\tilde{Q}_1)\cdots(1-\tilde{Q}_{n-1}) \\
&= \frac{-1}{(2n)!} d_n q_n^2 \left(q_1^2 - q_n^2\right)\cdots\left(q_{n-1}^2 - q_n^2\right) \\
&= \frac{-1}{(2n)!} d_j q_j^2 \left(\prod_{\substack{k=1 \\ k\neq j}}^{n} (q_k^2 - q_j^2)\right), \qquad \text{(B.21)}
\end{aligned}$$

where we have used Eq. (B.17) in the last equality. Note that the last expression in Eq. (B.21) holds for any $j \in \{1, \ldots, n\}$. We used this result in Eq. (4.16).

Appendix C

Appendix for Chapter. 5

C.1 Surface Terms

In Chap. 5, we often performed integration by parts for the background covariant derivative defined in Eq. (5.15) and ignored surface terms when calculating the quadratic Lagrangians. In this appendix, we examine the surface terms and verify that they are zero.

Let us first examine the extra-dimensional components of the background covariant derivative $\mathcal{D}_m(z)$ defined in Eq. (5.15). We have denoted the argument z since the derivative depends on the torus coordinates through the background gauge field (5.18). The background covariant derivative follows the boundary condition

$$\mathcal{D}_m(\mathcal{T}_p z) = T_p(z)\mathcal{D}_m(z)T_p^\dagger(z), \tag{C.1}$$

where the twist matrices are given in Eqs. (5.33) and (5.34).

Let $\boldsymbol{\phi}(z), \boldsymbol{\phi}'(z) \in su(n)$ be general fields in the adjoint representation that obey the following relations:

$$\mathcal{D}_m\boldsymbol{\phi} = (\partial_m - ig\,\mathbf{ad}(\boldsymbol{B}_m))\boldsymbol{\phi}, \qquad \boldsymbol{\phi}(\mathcal{T}_p z) = T_p(z)\boldsymbol{\phi}(z)T_p^\dagger(z). \tag{C.2}$$

The other field $\boldsymbol{\phi}'(z)$ satisfies the same relations. The trace of the product $(\mathcal{D}_m\boldsymbol{\phi})(\mathcal{D}_n\boldsymbol{\phi}')$ can be calculated as follows.

$$\begin{aligned}
\mathrm{Tr}[(\mathcal{D}_m\boldsymbol{\phi})(\mathcal{D}_n\boldsymbol{\phi}')] &= \mathrm{Tr}\,[(\partial_m\boldsymbol{\phi})(\mathcal{D}_n\boldsymbol{\phi}')] - ig\mathrm{Tr}\,[[\boldsymbol{B}_m, \boldsymbol{\phi}](\mathcal{D}_n\boldsymbol{\phi}')] \\
&= \partial_m\mathrm{Tr}\,[\boldsymbol{\phi}(\mathcal{D}_n\boldsymbol{\phi}')] - \mathrm{Tr}\,[\boldsymbol{\phi}\partial_m\mathcal{D}_n\boldsymbol{\phi}'] \\
&\quad - ig\mathrm{Tr}\,[\boldsymbol{B}_m\boldsymbol{\phi}(\mathcal{D}_n\boldsymbol{\phi}')] + ig\mathrm{Tr}\,[\boldsymbol{\phi}\boldsymbol{B}_m(\mathcal{D}_n\boldsymbol{\phi}')] \\
&= \partial_m\mathrm{Tr}\,[\boldsymbol{\phi}(\mathcal{D}_n\boldsymbol{\phi}')] - \mathrm{Tr}\,[\boldsymbol{\phi}\partial_m\mathcal{D}_n\boldsymbol{\phi}'] \\
&\quad - ig\mathrm{Tr}\,[\boldsymbol{\phi}(\mathcal{D}_n\boldsymbol{\phi}')\boldsymbol{B}_m] + ig\mathrm{Tr}\,[\boldsymbol{\phi}\boldsymbol{B}_m(\mathcal{D}_n\boldsymbol{\phi}')] \\
&= \partial_m\mathrm{Tr}\,[\boldsymbol{\phi}(\mathcal{D}_n\boldsymbol{\phi}')] - \mathrm{Tr}\,[\boldsymbol{\phi}\partial_m\mathcal{D}_n\boldsymbol{\phi}'] + ig\mathrm{Tr}\,[\boldsymbol{\phi}[\boldsymbol{B}_m, (\mathcal{D}_n\boldsymbol{\phi}')]] \\
&= -\mathrm{Tr}[\boldsymbol{\phi}(\mathcal{D}_m\mathcal{D}_n\boldsymbol{\phi}')] + \partial_m\mathrm{Tr}[\boldsymbol{\phi}(\mathcal{D}_n\boldsymbol{\phi}')].
\end{aligned} \tag{C.3}$$

Here, we used the cyclic property of the trace in the third term of the third equality. In the action, the last term gives a vanishing contribution as

$$\int_{\mathcal{M}^4} d^4x \int_{T^2} d^2x\ \partial_m \mathrm{Tr}[\boldsymbol{\phi}(\mathcal{D}_n\boldsymbol{\phi}')] \propto \left[\mathrm{Tr}[\boldsymbol{\phi}(\mathcal{D}_n\boldsymbol{\phi}')]\right]_z^{\mathcal{T}_p z} = 0. \tag{C.4}$$

Here, we have used the boundary conditions in Eqs. (C.1) and (C.2) and the cyclic property of traces. Therefore, the surface term can be neglected, and the relation

$$\int_{\mathcal{M}^4} d^4x \int_{T^2} d^2x\ \mathrm{Tr}[(\mathcal{D}_m\boldsymbol{\phi})(\mathcal{D}_m\boldsymbol{\phi}')] = -\int_{\mathcal{M}^4} d^4x \int_{T^2} d^2x\ \mathrm{Tr}[\boldsymbol{\phi}(\mathcal{D}_m\mathcal{D}_n\boldsymbol{\phi}')] \tag{C.5}$$

holds in the action. Using similar discussions, we obtain Eqs. (5.52)–(5.54), (5.55), (5.67), and (5.70) without contributions from surface terms.

C.2 Mode Functions

In section 5.9.4, we showed the explicit form of the mode functions (5.96) without derivation. Here, we offer its derivation.

C.2.1 Zero-mode Functions

First, let us derive the zero-mode function $\zeta_{0,d}$ appearing in Eq. (5.92). For the case with $N^{ij} > 0$, the annihilation operator is given by $\bar{\Pi}_z^{(ij)}$ in Eq. (5.90), and Eq. (5.92) becomes the differential equation

$$\left(\bar{\partial}_z + \frac{g\hat{f}\tilde{N}}{4}(z - \gamma\bar{z})\right)\zeta_{0,d}(z) = 0, \tag{C.6}$$

for the zero-mode function. Here, we omit the upper script ij for notational simplicity. The zero-mode function must also satisfy the boundary conditions in Eqs. (5.94) and (5.95). The differential equation (C.6) can be solved, and a solution is given by

$$\zeta_{0,d}(z) = Ce^{-\frac{g\hat{f}\tilde{N}}{4}(z\bar{z}-\frac{1}{2}\gamma\bar{z}^2)}\tilde{\zeta}_{0,d}(z), \tag{C.7}$$

where C is a constant. The function $\tilde{\zeta}_{0,d}(z)$ depends only on z and is determined by the boundary conditions (5.94) and (5.95). It is convenient to introduce a new function $\chi_{0,d}$ by

$$\tilde{\zeta}_{0,d}(z) = e^{\frac{g\hat{f}\tilde{N}}{4}(1-\frac{\gamma}{2})z^2}\chi_{0,d}(z), \tag{C.8}$$

to express the solution as

$$\zeta_{0,d}(z) = Ce^{-\frac{g\hat{f}\tilde{N}}{4}(z\bar{z}-z^2+\frac{\gamma}{2}(z^2-\bar{z}^2))}\chi_{0,d}(z). \tag{C.9}$$

The boundary conditions (5.94) and (5.95) yields the boundary conditions for $\chi_{0,d}(z)$ as

$$\chi_{0,d}(z+1) = e^{-2\pi i\tilde{a}_5}\chi_{0,d}(z), \tag{C.10}$$

$$\chi_{0,d}(z+\tau) = e^{-2\pi i(\tau_{\mathrm{R}}\tilde{a}_5+\tau_{\mathrm{I}}\tilde{a}_6)}e^{-\pi i\tilde{N}\tau}e^{\gamma\pi i\tilde{N}\tau_{\mathrm{R}}}e^{-2\pi i\tilde{N}z}\chi_{0,d}(z), \tag{C.11}$$

where we have used $\hat{f} = 2\pi/(g\mathcal{V}_{T^2}) = 2\pi/(g\tau_{\mathrm{I}})$ to obtain the second relation. The function $\chi_{0,d}$ satisfying these boundary conditions can be expressed by the Jacobi theta function [105]. The Jacobi theta function $\vartheta\begin{bmatrix}a\\b\end{bmatrix}(z'|\tau')$ is defined by

$$\vartheta\begin{bmatrix}a\\b\end{bmatrix}(z'|\tau') = \sum_{n\in\mathbb{Z}} e^{i\pi\tau'(n+a)^2}e^{2\pi i(n+a)(z'+b)} \qquad (a,b\in\mathbb{R},\quad z',\tau'\in\mathbb{C}), \tag{C.12}$$

which satisfies

$$\vartheta\begin{bmatrix}a\\b\end{bmatrix}(z'+k|\tau') = e^{2\pi ika}\vartheta\begin{bmatrix}a\\b\end{bmatrix}(z'|\tau') \qquad (k\in\mathbb{Z}), \tag{C.13}$$

$$\vartheta\begin{bmatrix}a\\b\end{bmatrix}(z'+\tau'|\tau') = e^{-i\pi\tau'}e^{-2\pi i(z'+b)}\vartheta\begin{bmatrix}a\\b\end{bmatrix}(z'|\tau')\,. \tag{C.14}$$

Using the Jacobi theta function, the function $\chi_{0,d}$, which satisfies the boundary conditions (C.10) and (C.11), is expressed as

$$\chi_{0,d}(z) = \vartheta\begin{bmatrix}-(\tilde{a}_5+d)/\tilde{N}\\ \tau_{\mathrm{R}}\tilde{a}_5+\tau_{\mathrm{I}}\tilde{a}_6-\gamma\tau_{\mathrm{R}}\tilde{N}/2\end{bmatrix}(\tilde{N}z|\tilde{N}\tau). \tag{C.15}$$

Finally, the zero-mode function is expressed as

$$\zeta_{0,d}(z) = Ce^{-\frac{\pi\tilde{N}}{2\tau_{\mathrm{I}}}(z\bar{z}-zz+\frac{\gamma}{2}(zz-\bar{z}\bar{z}))}\vartheta\begin{bmatrix}-(\tilde{a}_5+d)/\tilde{N}\\ \tau_{\mathrm{R}}\tilde{a}_5+\tau_{\mathrm{I}}\tilde{a}_6-\gamma\tau_{\mathrm{R}}\tilde{N}/2\end{bmatrix}(\tilde{N}z|\tilde{N}\tau). \tag{C.16}$$

Imposing the normalization condition

$$\int_{\mathcal{V}_{T^2}} dx^5dx^6\;\bar{\zeta}_{0,d}(z)\zeta_{0,d'}(z) = \delta_{d,d'}, \tag{C.17}$$

determines the constant C as

$$C = \left(\frac{2\pi\tilde{N}}{\tau_{\mathrm{I}}}\right)^{1/4}. \tag{C.18}$$

C.2.2 Excited Mode Functions

The excited mode functions are obtained from the zero-mode function by using

$$\zeta_{\hat{\ell},d}(z) = \frac{1}{\sqrt{\hat{\ell}!}}(\hat{a}^\dagger)^{\hat{\ell}}\zeta_{0,d}(z), \tag{C.19}$$

where the creation operator $\hat{a}^\dagger$ is given by

$$\hat{a}^\dagger = \Pi_z = -i\sqrt{\frac{\tau_{\mathrm{I}}}{2\pi\tilde{N}}}\left[\partial_z - \frac{\pi\tilde{N}}{2\tau_{\mathrm{I}}}(\bar{z}-\gamma z)\right], \tag{C.20}$$

for $\tilde{N}^{ij} > 0$. We show that the excited mode functions are given by

$$\begin{aligned}\zeta_{\hat{\ell},d}(z) = \frac{C}{2^{\hat{\ell}}\sqrt{\hat{\ell}!}}\sum_{n=-\infty}^{+\infty} Z_{\hat{\ell}}(w_{n,d}(z))e^{-\frac{\pi\tilde{N}}{2\tau_{\mathrm{I}}}(z\bar{z}-zz+\frac{\gamma}{2}(zz-\bar{z}\bar{z}))}e^{i\pi\tilde{N}\tau(n-(\tilde{a}_5+d)/\tilde{N})^2} \\ \times e^{2\pi i\tilde{N}(n-(\tilde{a}_5+d)/\tilde{N})(z+(\tau_{\mathrm{R}}\tilde{a}_5+\tau_{\mathrm{I}}\tilde{a}_6)/\tilde{N}-\gamma\tau_{\mathrm{R}}/2)}.\end{aligned} \tag{C.21}$$

where the function $w_{n,d}(z)$ and $Z_{\hat{\ell}}$ are defined by

$$w_{n,d}(z) = \sqrt{\frac{2\pi\tilde{N}}{\tau_{\mathrm{I}}}}\left[\frac{z-\bar{z}}{2i} + \tau_{\mathrm{I}}\left(n - \frac{\tilde{a}_5+d}{\tilde{N}}\right)\right], \tag{C.22}$$

$$Z_0(w_{n,d}) = 1, \qquad Z_{\hat{\ell}+1}(w_{n,d}) = 2w_n Z_{\hat{\ell}}(w_{n,d}) - \frac{dZ_{\hat{\ell}}(w_{n,d})}{dw_{n,d}}, \tag{C.23}$$

respectively.

To derive the excited mode functions, let us define

$$\begin{aligned}F_{n,d}(z) \equiv & e^{-\frac{\pi\tilde{N}}{2\tau_{\mathrm{I}}}(z\bar{z}-zz+\frac{\gamma}{2}(zz-\bar{z}\bar{z}))}e^{i\pi\tilde{N}\tau(n-(\tilde{a}_5+d)/\tilde{N})^2} \\ & \times e^{2\pi i(n-(\tilde{a}_5+d)/\tilde{N})(\tilde{N}z+\tau_{\mathrm{R}}\tilde{a}_5+\tau_{\mathrm{I}}\tilde{a}_6-\gamma\tau_{\mathrm{R}}\tilde{N}/2)},\end{aligned} \tag{C.24}$$

to express the zero-mode function in Eq. (C.16) as

$$\zeta_{0,d}(z) = C\sum_{n=-\infty}^{+\infty} Z_0(w_{n,d})F_{n,d}(z), . \tag{C.25}$$

The first-excited function is obtained from the zero-mode function as

$$\zeta_{1,d}(z) = \frac{1}{\sqrt{1!}}\hat{a}^\dagger\zeta_{0,d}(z) = -i\sqrt{\frac{\tau_{\mathrm{I}}}{2\pi\tilde{N}}}\left[\partial_z - \frac{\pi\tilde{N}}{2\tau_{\mathrm{I}}}(\bar{z}-\gamma z)\right]\zeta_{0,d}(z), \tag{C.26}$$

and substituting Eq. (C.25) yields

$$\zeta_{1,d}(z) = -iC\sqrt{\frac{\tau_{\rm I}}{2\pi\tilde{N}}}\sum_n \Bigg[(\partial_z Z_0)F_{n,d} + Z_0(\partial_z F_{n,d}) - \frac{\pi\tilde{N}}{2\tau_{\rm I}}(\bar{z}-\gamma z)Z_0 F_{n,d}\Bigg]. \tag{C.27}$$

We can rewrite the first term as

$$(\partial_z Z_0)F_{n,d} = \frac{\partial w_{n,d}}{\partial z}\frac{dZ_0}{dw_{n,d}}F_{n,d} = \frac{1}{2i}\sqrt{\frac{2\pi\tilde{N}}{\tau_{\rm I}}}\frac{dZ_0}{dw_{n,d}}F_{n,d}, \tag{C.28}$$

and rearrange the last two terms as

$$\begin{aligned} &Z_0(\partial_z F_{n,d}) - \frac{\pi\tilde{N}}{2\tau_{\rm I}}(\bar{z}-\gamma z)Z_0 F_{n,d} \\ &= \frac{2\pi\tilde{N}}{\tau_{\rm I}}i\left(\frac{z-\bar{z}}{2i} + \tau_{\rm I}\left(n - \frac{g\tilde{v}_5}{2\pi\tilde{N}} - \frac{d}{\tilde{N}}\right)\right)Z_0 F_{n,d} = i\sqrt{\frac{2\pi\tilde{N}}{\tau_{\rm I}}}w_{n,d}Z_0 F_{n,d}. \end{aligned} \tag{C.29}$$

By using these results, the first-excited function (C.27) becomes

$$\zeta_{1,d}(z) = \frac{C}{2}\sum_{n=-\infty}^{+\infty}\left(2w_{n,d}(z)Z_0(w_{n,d}) - \frac{dZ_0(w_{n,d})}{dw_{n,d}}\right)F_{n,d}(z). \tag{C.30}$$

Identifying the square bracket with Z_1, *i.e.*,

$$Z_1 = 2w_{n,d}Z_0 - \frac{dZ_0}{dw_{n,d}}, \tag{C.31}$$

the first-excited mode can be written as

$$\zeta_{1,d}(z) = \frac{C}{2}\sum_{n=-\infty}^{+\infty} Z_1(w_{n,d}(z))F_{n,d}(z). \tag{C.32}$$

Therefore, Eq. (C.21) is correct for $\hat{\ell} = 1$.

Let us assume that Eq. (C.21) holds for $\hat{\ell} = k$ and show that it also holds for $\hat{\ell} = k+1$. Using the relation

$$\zeta_{k+1,d}(z) = \frac{1}{\sqrt{k+1}}a^\dagger \zeta_{k,d}(z), \tag{C.33}$$

and repeating the same calculation we did for $\hat{\ell} = 0$, we obtain

$$\zeta_{k+1,d}(z) = \frac{C}{2^{k+1}\sqrt{(k+1)!}} \sum_{n=-\infty}^{+\infty} \left(2w_{n,d} Z_k - \frac{dZ_k}{dw_{n,d}} \right) F_{n,d}(z). \tag{C.34}$$

Hence, Eq. (C.21) is also satisfied for $\hat{\ell} = k+1$. Therefore, this assumption holds for any $\hat{\ell}$.

The function $Z_{\hat{\ell}}(w_n)$, which satisfies the differential equation in Eq. (C.23), can be expressed by Hermite polynomials $H_{\hat{\ell}}(x)$. Therefore, we obtain the expression in Eq. (C.21) for $\tilde{N}^{ij} > 0$. The mode function for $\tilde{N}^{ij} < 0$ can be derived in the same way, and we obtain

$$\begin{aligned} \zeta_{\hat{\ell},d}(z) = \frac{C}{2^{\hat{\ell}}\sqrt{\hat{\ell}!}} \sum_{n=-\infty}^{+\infty} H_{\hat{\ell}}(w_{n,d}(z)) e^{-\frac{\pi \tilde{N}}{2\tau_{\mathrm{I}}}(\bar{z}z - \bar{z}\bar{z} + \frac{\gamma}{2}(\bar{z}\bar{z} - zz))} e^{-i\pi \tilde{N}\bar{\tau}(n-(\tilde{a}_5+d)/\tilde{N})^2} \\ \times e^{-i2\pi \tilde{N}(n-(\tilde{a}_5+d)/\tilde{N})(\bar{z}+(\tau_{\mathrm{R}}\tilde{a}_5+\tau_{\mathrm{I}}\tilde{a}_6)/\tilde{N}-\gamma\tau_{\mathrm{R}}/2)}. \end{aligned} \tag{C.35}$$

This function satisfies the boundary conditions (5.94) and (5.95) and the orthogonal relation (5.98).

Acknowledgements

Firstly, I would like to express my utmost gratitude to my supervisor and collaborator, Prof. Kentaro Kojima, for his academic supervision and personal support. He has consistently provided considerate guidance and offered encouragement. Without his support, I would not have been able to complete the research in this thesis. I wish to give a special thank you to another collaborator, Ms. Carolina Sayuri Takeda for the collaboration of related researches in this thesis. She also gave a lot of advice on the draft of this thesis.

I am also grateful to Prof. Kazuhiro Yamamoto and Prof. Yutaka Ookouchi for their valuable comments in the preliminary examination. Prof. Ookouchi has also provided guidance as a member of our laboratory, and his enthusiasm for physics has always been encouraging to me.

I would like to extend my thanks to other members of the Theory of Subatomic Physics and Astrophysics laboratory in Kyushu University. In particular, Prof. Koji Harada, Prof. Ken'ichiro Nakazato, and Prof. Tokuro Fukui offered valuable advice from a variety of perspectives. My colleagues, Mr. Sohei Tsukahara, Mr. Yin Qiang, Mr. Ryota Sato, Mr. Yuki Yamamoto, and Mr. Ryuta Sugiyama, have been a pleasure to engage in discussions and learn physics with. I am also grateful to the former members of the laboratory, including Prof. Shuichiro Tao, Dr. Issei Koga, Mr. Shunsuke Taniwaki, and Mr. Yusuke Enomoto. I sincerely think that joining this lab was one of the best decisions of my life.

I appreciate the support from the Kyushu University Leading Human Resources Development Fellowship Program. Thanks to their support, I have been able to concentrate on my research without worrying about finances and I have had many opportunities to participate in various conferences and workshops. In addition, the interaction with other fellows from different backgrounds helped me to broaden my perspective.

Finally, my sincere thanks go to my family and my partner, Maya, for their encouragement and support.

Bibliography

[1] Georges Aad et al. Measurement of the Higgs boson mass in the $H \to ZZ^* \to 4\ell$ decay channel using 139 fb^{-1} of $\sqrt{s} = 13$ TeV pp collisions recorded by the ATLAS detector at the LHC. *Phys. Lett. B*, 843:137880, 2023.

[2] J. Wess and J. Bagger. *Supersymmetry and supergravity.* Princeton University Press, Princeton, NJ, USA, 1992.

[3] Stephen P. Martin. A Supersymmetry primer. *Adv. Ser. Direct. High Energy Phys.*, 18:1–98, 1998.

[4] H. Georgi and S. L. Glashow. Unity of All Elementary Particle Forces. *Phys. Rev. Lett.*, 32:438–441, 1974.

[5] Djuna Croon, Tomás E. Gonzalo, Lukas Graf, Nejc Košnik, and Graham White. GUT Physics in the era of the LHC. *Front. in Phys.*, 7:76, 2019.

[6] Yoshiharu Kawamura. Gauge symmetry breaking from extra space S**1 / Z(2). *Prog. Theor. Phys.*, 103:613–619, 2000.

[7] Lawrence J. Hall and Yasunori Nomura. Grand unification in higher dimensions. *Annals Phys.*, 306:132–156, 2003.

[8] Yoshiharu Kawamura. Triplet doublet splitting, proton stability and extra dimension. *Prog. Theor. Phys.*, 105:999–1006, 2001.

[9] N. S. Manton. A New Six-Dimensional Approach to the Weinberg-Salam Model. *Nucl. Phys. B*, 158:141–153, 1979.

[10] D. B. Fairlie. Higgs' Fields and the Determination of the Weinberg Angle. *Phys. Lett. B*, 82:97–100, 1979.

[11] Yutaka Hosotani. Dynamical Mass Generation by Compact Extra Dimensions. *Phys. Lett. B*, 126:309–313, 1983.

[12] Yutaka Hosotani. Dynamics of Nonintegrable Phases and Gauge Symmetry Breaking. *Annals Phys.*, 190:233, 1989.

[13] Hisaki Hatanaka, Takeo Inami, and C. S. Lim. The Gauge hierarchy problem and higher dimensional gauge theories. *Mod. Phys. Lett. A*, 13:2601–2612, 1998.

[14] Lawrence J. Hall, Yasunori Nomura, and David Tucker-Smith. Gauge Higgs unification in higher dimensions. *Nucl. Phys. B*, 639:307–330, 2002.

[15] Ignatios Antoniadis, K. Benakli, and M. Quiros. Finite Higgs mass without supersymmetry. *New J. Phys.*, 3:20, 2001.

[16] Masahiro Kubo, C. S. Lim, and Hiroyuki Yamashita. The Hosotani mechanism in bulk gauge theories with an orbifold extra space S**1 / Z(2). *Mod. Phys. Lett. A*, 17:2249–2264, 2002.

[17] Csaba Csaki, Christophe Grojean, and Hitoshi Murayama. Standard model Higgs from higher dimensional gauge fields. *Phys. Rev. D*, 67:085012, 2003.

[18] Gustavo Burdman and Yasunori Nomura. Unification of Higgs and Gauge Fields in Five Dimensions. *Nucl. Phys. B*, 656:3–22, 2003.

[19] Ilia Gogoladze, Yukihiro Mimura, and S. Nandi. Gauge Higgs unification on the left right model. *Phys. Lett. B*, 560:204–213, 2003.

[20] Claudio A. Scrucca, Marco Serone, and Luca Silvestrini. Electroweak symmetry breaking and fermion masses from extra dimensions. *Nucl. Phys. B*, 669:128–158, 2003.

[21] Naoyuki Haba, Yutaka Hosotani, Yoshiharu Kawamura, and Toshifumi Yamashita. Dynamical symmetry breaking in gauge Higgs unification on orbifold. *Phys. Rev. D*, 70:015010, 2004.

[22] Naoyuki Haba and Toshifumi Yamashita. Dynamical symmetry breaking in gauge Higgs unification of 5-D N=1 SUSY theory. *JHEP*, 04:016, 2004.

[23] Yutaka Hosotani, Shusaku Noda, and Kazunori Takenaga. Dynamical gauge symmetry breaking and mass generation on the orbifold T**2 / Z(2). *Phys. Rev. D*, 69:125014, 2004.

[24] Yutaka Hosotani, Shusaku Noda, and Kazunori Takenaga. Dynamical gauge-Higgs unification in the electroweak theory. *Phys. Lett. B*, 607:276–285, 2005.

[25] Naoyuki Haba, Kazunori Takenaga, and Toshifumi Yamashita. Higgs mass in the gauge-Higgs unification. *Phys. Lett. B*, 615:247–256, 2005.

[26] C. S. Lim and Nobuhito Maru. Towards a realistic grand gauge-Higgs unification. *Phys. Lett. B*, 653:320–324, 2007.

[27] Kentaro Kojima, Kazunori Takenaga, and Toshifumi Yamashita. Grand Gauge-Higgs Unification. *Phys. Rev. D*, 84:051701, 2011.

[28] Toshifumi Yamashita. Doublet-Triplet Splitting in an SU(5) Grand Unification. *Phys. Rev. D*, 84:115016, 2011.

[29] Yutaka Hosotani and Naoki Yamatsu. Gauge–Higgs grand unification. *PTEP*, 2015:111B01, 2015.

[30] Naoki Yamatsu. Gauge coupling unification in gauge–Higgs grand unification. *PTEP*, 2016(4):043B02, 2016.

[31] Atsushi Furui, Yutaka Hosotani, and Naoki Yamatsu. Toward Realistic Gauge-Higgs Grand Unification. *PTEP*, 2016(9):093B01, 2016.

[32] Kentaro Kojima, Kazunori Takenaga, and Toshifumi Yamashita. Gauge symmetry breaking patterns in an SU(5) grand gauge-Higgs unification model. *Phys. Rev. D*, 95(1):015021, 2017.

[33] Kentaro Kojima, Kazunori Takenaga, and Toshifumi Yamashita. The Standard Model Gauge Symmetry from Higher-Rank Unified Groups in Grand Gauge-Higgs Unification Models. *JHEP*, 06:018, 2017.

[34] Yutaka Hosotani and Naoki Yamatsu. Electroweak symmetry breaking and mass spectra in six-dimensional gauge–Higgs grand unification. *PTEP*, 2018(2):023B05, 2018.

[35] Nobuhito Maru and Yoshiki Yatagai. Fermion Mass Hierarchy in Grand Gauge-Higgs Unification. *PTEP*, 2019(8):083B03, 2019.

[36] Christoph Englert, David J. Miller, and Dumitru Dan Smaranda. Phenomenology of GUT-inspired gauge-Higgs unification. 11 2019.

[37] Andrei Angelescu, Andreas Bally, Simone Blasi, and Florian Goertz. Minimal SU(6) gauge-Higgs grand unification. *Phys. Rev. D*, 105(3):035026, 2022.

[38] Hiroaki Nakano, Masamichi Sato, Osamu Seto, and Toshifumi Yamashita. Dirac gaugino from grand gauge-Higgs unification. *PTEP*, 2022(3):033B06, 2022.

[39] Kentaro Kojima, Kazunori Takenaga, and Toshifumi Yamashita. Grand gauge-Higgs unification on T2/Z3 via the diagonal embedding method. *Phys. Rev. D*, 108(3):035031, 2023.

[40] Adam G. Riess, Stefano Casertano, Wenlong Yuan, Lucas M. Macri, and Dan Scolnic. Large Magellanic Cloud Cepheid Standards Provide a 1% Foundation for the Determination of the Hubble Constant and Stronger Evidence for Physics beyond ΛCDM. *Astrophys. J.*, 876(1):85, 2019.

[41] N. Aghanim et al. Planck 2018 results. VI. Cosmological parameters. *Astron. Astrophys.*, 641:A6, 2020. [Erratum: Astron.Astrophys. 652, C4 (2021)].

[42] Adam G. Riess et al. "A Comprehensive Measurement of the Local Value of the Hubble Constant with 1 km s^{-1} Mpc^{-1} Uncertainty from the Hubble Space Telescope and the SH0ES Team". *Astrophys. J. Lett.*, 934(1):L7, 2022.

[43] Eleonora Di Valentino, Olga Mena, Supriya Pan, Luca Visinelli, Weiqiang Yang, Alessandro Melchiorri, David F. Mota, Adam G. Riess, and Joseph Silk. In the realm of the Hubble tension—a review of solutions. *Class. Quant. Grav.*, 38(15):153001, 2021.

[44] Nils Schöneberg, Guillermo Franco Abellán, Andrea Pérez Sánchez, Samuel J. Witte, Vivian Poulin, and Julien Lesgourgues. The H0 Olympics: A fair ranking of proposed models. *Phys. Rept.*, 984:1–55, 2022.

[45] Jian-Ping Hu and Fa-Yin Wang. Hubble Tension: The Evidence of New Physics. *Universe*, 9(2):94, 2023.

[46] Luis A. Anchordoqui, Vernon Barger, Haim Goldberg, Xing Huang, Danny Marfatia, Luiz H. M. da Silva, and Thomas J. Weiler. IceCube neutrinos, decaying dark matter, and the Hubble constant. *Phys. Rev. D*, 92(6):061301, 2015. [Erratum: Phys.Rev.D 94, 069901 (2016)].

[47] S. Carneiro, P. C. de Holanda, C. Pigozzo, and F. Sobreira. Is the H_0 tension suggesting a fourth neutrino generation? *Phys. Rev. D*, 100(2):023505, 2019.

[48] Manuel A. Buen-Abad, Razieh Emami, and Martin Schmaltz. Cannibal Dark Matter and Large Scale Structure. *Phys. Rev. D*, 98(8):083517, 2018.

[49] Andrzej Hryczuk and Krzysztof Jodłowski. Self-interacting dark matter from late decays and the H_0 tension. *Phys. Rev. D*, 102(4):043024, 2020.

[50] Kyriakos Vattis, Savvas M. Koushiappas, and Abraham Loeb. Dark matter decaying in the late Universe can relieve the H0 tension. *Phys. Rev. D*, 99(12):121302, 2019.

[51] Kanhaiya L. Pandey, Tanvi Karwal, and Subinoy Das. Alleviating the H_0 and σ_8 anomalies with a decaying dark matter model. *JCAP*, 07:026, 2020.

[52] P. Ko, Natsumi Nagata, and Yong Tang. Hidden Charged Dark Matter and Chiral Dark Radiation. *Phys. Lett. B*, 773:513–520, 2017.

[53] Suresh Kumar and Rafael C. Nunes. Probing the interaction between dark matter and dark energy in the presence of massive neutrinos. *Phys. Rev. D*, 94(12):123511, 2016.

[54] Suresh Kumar, Rafael C. Nunes, and Santosh Kumar Yadav. Dark sector interaction: a remedy of the tensions between CMB and LSS data. *Eur. Phys. J. C*, 79(7):576, 2019.

[55] Eleonora Di Valentino, Alessandro Melchiorri, and Olga Mena. Can interacting dark energy solve the H_0 tension? *Phys. Rev. D*, 96(4):043503, 2017.

[56] J. F. Jesus, A. A. Escobal, D. Benndorf, and S. H. Pereira. Can dark matter–dark energy interaction alleviate the cosmic coincidence problem? *Eur. Phys. J. C*, 82(3):273, 2022.

[57] Nima Khosravi, Shant Baghram, Niayesh Afshordi, and Natacha Altamirano. H_0 tension as a hint for a transition in gravitational theory. *Phys. Rev. D*, 99(10):103526, 2019.

[58] Sergei D. Odintsov, Diego Sáez-Chillón Gómez, and German S. Sharov. Analyzing the H_0 tension in $F(R)$ gravity models. *Nucl. Phys. B*, 966:115377, 2021.

[59] Sheng-Feng Yan, Pierre Zhang, Jie-Wen Chen, Xin-Zhe Zhang, Yi-Fu Cai, and Emmanuel N. Saridakis. Interpreting cosmological tensions from the effective field theory of torsional gravity. *Phys. Rev. D*, 101(12):121301, 2020.

[60] Janina Renk, Miguel Zumalacárregui, Francesco Montanari, and Alexandre Barreira. Galileon gravity in light of ISW, CMB, BAO and H_0 data. *JCAP*, 10:020, 2017.

[61] Maria Giovanna Dainotti, Biagio De Simone, Tiziano Schiavone, Giovanni Montani, Enrico Rinaldi, Gaetano Lambiase, Malgorzata Bogdan, and Sahil Ugale. On the Evolution of the Hubble Constant with the SNe Ia Pantheon Sample and Baryon Acoustic Oscillations: A Feasibility Study for GRB-Cosmology in 2030. *Galaxies*, 10(1):24, 2022.

[62] Eleonora Di Valentino, Alessandro Melchiorri, and Joseph Silk. Reconciling Planck with the local value of H_0 in extended parameter space. *Phys. Lett. B*, 761:242–246, 2016.

[63] Eleonora Di Valentino, Alessandro Melchiorri, Eric V. Linder, and Joseph Silk. Constraining Dark Energy Dynamics in Extended Parameter Space. *Phys. Rev. D*, 96(2):023523, 2017.

[64] Sunny Vagnozzi, Suhail Dhawan, Martina Gerbino, Katherine Freese, Ariel Goobar, and Olga Mena. Constraints on the sum of the neutrino masses in dynamical dark energy models with $w(z) \geq -1$ are tighter than those obtained in ΛCDM. *Phys. Rev. D*, 98(8):083501, 2018.

[65] Weiqiang Yang, Supriya Pan, Eleonora Di Valentino, Emmanuel N. Saridakis, and Subenoy Chakraborty. Observational constraints on one-parameter dynamical dark-energy parametrizations and the H_0 tension. *Phys. Rev. D*, 99(4):043543, 2019.

[66] Eleonora Di Valentino, Alessandro Melchiorri, Olga Mena, and Sunny Vagnozzi. Nonminimal dark sector physics and cosmological tensions. *Phys. Rev. D*, 101(6):063502, 2020.

[67] Sunny Vagnozzi. New physics in light of the H_0 tension: An alternative view. *Phys. Rev. D*, 102(2):023518, 2020.

[68] G. Alestas, L. Kazantzidis, and L. Perivolaropoulos. H_0 tension, phantom dark energy, and cosmological parameter degeneracies. *Phys. Rev. D*, 101(12):123516, 2020.

[69] Eleonora Di Valentino, Ankan Mukherjee, and Anjan A. Sen. Dark Energy with Phantom Crossing and the H_0 Tension. *Entropy*, 23(4):404, 2021.

[70] Maria Giovanna Dainotti, Biagio De Simone, Tiziano Schiavone, Giovanni Montani, Enrico Rinaldi, and Gaetano Lambiase. On the Hubble constant tension in the SNe Ia Pantheon sample. *Astrophys. J.*, 912(2):150, 2021.

[71] Tanvi Karwal and Marc Kamionkowski. Dark energy at early times, the Hubble parameter, and the string axiverse. *Phys. Rev. D*, 94(10):103523, 2016.

[72] Edvard Mörtsell and Suhail Dhawan. Does the Hubble constant tension call for new physics? *JCAP*, 09:025, 2018.

[73] Vivian Poulin, Tristan L. Smith, Tanvi Karwal, and Marc Kamionkowski. Early Dark Energy Can Resolve The Hubble Tension. *Phys. Rev. Lett.*, 122(22):221301, 2019.

[74] Tristan L. Smith, Vivian Poulin, and Mustafa A. Amin. Oscillating scalar fields and the Hubble tension: a resolution with novel signatures. *Phys. Rev. D*, 101(6):063523, 2020.

[75] Tristan L. Smith, Vivian Poulin, José Luis Bernal, Kimberly K. Boddy, Marc Kamionkowski, and Riccardo Murgia. Early dark energy is not excluded by current large-scale structure data. *Phys. Rev. D*, 103(12):123542, 2021.

[76] Marc Kamionkowski and Adam G. Riess. The Hubble Tension and Early Dark Energy. *Ann. Rev. Nucl. Part. Sci.*, 73:153–180, 2023.

[77] Vivian Poulin, Tristan L. Smith, and Tanvi Karwal. The Ups and Downs of Early Dark Energy solutions to the Hubble tension: A review of models, hints and constraints circa 2023. *Phys. Dark Univ.*, 42:101348, 2023.

[78] Marc Kamionkowski, Josef Pradler, and Devin G. E. Walker. Dark energy from the string axiverse. *Phys. Rev. Lett.*, 113(25):251302, 2014.

[79] Vivian Poulin, Tristan L. Smith, Daniel Grin, Tanvi Karwal, and Marc Kamionkowski. Cosmological implications of ultralight axionlike fields. *Phys. Rev. D*, 98(8):083525, 2018.

[80] Prateek Agrawal, Francis-Yan Cyr-Racine, David Pinner, and Lisa Randall. Rock 'n' roll solutions to the Hubble tension. *Phys. Dark Univ.*, 42:101347, 2023.

[81] Stephon Alexander and Evan McDonough. Axion-Dilaton Destabilization and the Hubble Tension. *Phys. Lett. B*, 797:134830, 2019.

[82] Florian Niedermann and Martin S. Sloth. New early dark energy. *Phys. Rev. D*, 103(4):L041303, 2021.

[83] Kim V. Berghaus and Tanvi Karwal. Thermal Friction as a Solution to the Hubble Tension. *Phys. Rev. D*, 101(8):083537, 2020.

[84] Jeremy Sakstein and Mark Trodden. Early Dark Energy from Massive Neutrinos as a Natural Resolution of the Hubble Tension. *Phys. Rev. Lett.*, 124(16):161301, 2020.

[85] Gen Ye and Yun-Song Piao. Is the Hubble tension a hint of AdS phase around recombination? *Phys. Rev. D*, 101(8):083507, 2020.

[86] Anton Chudaykin, Dmitry Gorbunov, and Nikita Nedelko. Combined analysis of Planck and SPTPol data favors the early dark energy models. *JCAP*, 08:013, 2020.

[87] S. X. Tian and Zong-Hong Zhu. Early dark energy in k-essence. *Phys. Rev. D*, 103(4):043518, 2021.

[88] Balakrishna S. Haridasu, Matteo Viel, and Nicola Vittorio. Sources of H_0-tension in dark energy scenarios. *Phys. Rev. D*, 103(6):063539, 2021.

[89] Kim V. Berghaus and Tanvi Karwal. Thermal friction as a solution to the Hubble and large-scale structure tensions. *Phys. Rev. D*, 107(10):103515, 2023.

[90] Nima Arkani-Hamed, Hsin-Chia Cheng, Paolo Creminelli, and Lisa Randall. Extra natural inflation. *Phys. Rev. Lett.*, 90:221302, 2003.

[91] L. Pilo, D. A. J. Rayner, and A. Riotto. Gauge quintessence. *Phys. Rev. D*, 68:043503, 2003.

[92] Ralph Blumenhagen, Boris Kors, Dieter Lust, and Stephan Stieberger. Four-dimensional String Compactifications with D-Branes, Orientifolds and Fluxes. *Phys. Rept.*, 445:1–193, 2007.

[93] Michael R. Douglas and Shamit Kachru. Flux compactification. *Rev. Mod. Phys.*, 79:733–796, 2007.

[94] Mariana Grana. Flux compactifications in string theory: A Comprehensive review. *Phys. Rept.*, 423:91–158, 2006.

[95] Frederik Denef, Michael R. Douglas, and Shamit Kachru. Physics of String Flux Compactifications. *Ann. Rev. Nucl. Part. Sci.*, 57:119–144, 2007.

[96] Edward Witten. Some Properties of O(32) Superstrings. *Phys. Lett. B*, 149:351–356, 1984.

[97] Hiroyuki Abe, Kang-Sin Choi, Tatsuo Kobayashi, and Hiroshi Ohki. Three generation magnetized orbifold models. *Nucl. Phys. B*, 814:265–292, 2009.

[98] Tatsuo Kobayashi, Ryosuke Maruyama, Masaki Murata, Hiroshi Ohki, and Manabu Sakai. Three-generation Models from E_8 Magnetized Extra Dimensional Theory. *JHEP*, 05:050, 2010.

[99] Tomo-hiro Abe, Yukihiro Fujimoto, Tatsuo Kobayashi, Takashi Miura, Kenji Nishiwaki, Makoto Sakamoto, and Yoshiyuki Tatsuta. Classification of three-generation models on magnetized orbifolds. *Nucl. Phys. B*, 894:374–406, 2015.

[100] Hiroyuki Abe, Tatsuo Kobayashi, Hajime Otsuka, and Yasufumi Takano. Realistic three-generation models from SO(32) heterotic string theory. *JHEP*, 09:056, 2015.

[101] Makoto Sakamoto, Maki Takeuchi, and Yoshiyuki Tatsuta. Zero-mode counting formula and zeros in orbifold compactifications. *Phys. Rev. D*, 102(2):025008, 2020.

[102] Makoto Sakamoto, Maki Takeuchi, and Yoshiyuki Tatsuta. Index theorem on $T^2/\mathbb{Z}_N$ orbifolds. *Phys. Rev. D*, 103(2):025009, 2021.

[103] Tatsuo Kobayashi, Hajime Otsuka, Makoto Sakamoto, Maki Takeuchi, Yoshiyuki Tatsuta, and Hikaru Uchida. Index theorem on magnetized blow-up manifold of T2/ZN. *Phys. Rev. D*, 107(7):075032, 2023.

[104] Hiroki Imai, Makoto Sakamoto, Maki Takeuchi, and Yoshiyuki Tatsuta. Index and winding numbers on T2/ZN orbifolds with magnetic flux. *Nucl. Phys. B*, 990:116189, 2023.

[105] D. Cremades, L. E. Ibanez, and F. Marchesano. Computing Yukawa couplings from magnetized extra dimensions. *JHEP*, 05:079, 2004.

[106] Hiroyuki Abe, Tatsuo Kobayashi, Keigo Sumita, and Yoshiyuki Tatsuta. Gaussian Froggatt-Nielsen mechanism on magnetized orbifolds. *Phys. Rev. D*, 90(10):105006, 2014.

[107] Yukihiro Fujimoto, Tatsuo Kobayashi, Kenji Nishiwaki, Makoto Sakamoto, and Yoshiyuki Tatsuta. Comprehensive analysis of Yukawa hierarchies on T^2/Z_N with magnetic fluxes. *Phys. Rev. D*, 94(3):035031, 2016.

[108] Hiroyuki Abe, Tatsuo Kobayashi, Hajime Otsuka, Yasufumi Takano, and Takuya H. Tatsuishi. Flavor structure in $SO(32)$ heterotic string theory. *Phys. Rev. D*, 94(12):126020, 2016.

[109] Tatsuo Kobayashi, Kenji Nishiwaki, and Yoshiyuki Tatsuta. CP-violating phase on magnetized toroidal orbifolds. *JHEP*, 04:080, 2017.

[110] Wilfried Buchmuller and Ketan M. Patel. Flavor physics without flavor symmetries. *Phys. Rev. D*, 97(7):075019, 2018.

[111] Wilfried Buchmuller and Julian Schweizer. Flavor mixings in flux compactifications. *Phys. Rev. D*, 95(7):075024, 2017.

[112] Makoto Ishida, Kenji Nishiwaki, and Yoshiyuki Tatsuta. Seesaw mechanism in magnetic compactifications. *JHEP*, 07:125, 2018.

[113] C. Bachas. A Way to break supersymmetry. 3 1995.

[114] Wilfried Buchmuller, Markus Dierigl, Emilian Dudas, and Julian Schweizer. Effective field theory for magnetic compactifications. *JHEP*, 04:052, 2017.

[115] Wilfried Buchmuller, Markus Dierigl, and Emilian Dudas. Flux compactifications and naturalness. *JHEP*, 08:151, 2018.

[116] Takuya Hirose and Nobuhito Maru. Cancellation of One-loop Corrections to Scalar Masses in Yang-Mills Theory with Flux Compactification. *JHEP*, 08:054, 2019.

[117] Masaki Honda and Toshihide Shibasaki. Wilson-line Scalar as a Nambu-Goldstone Boson in Flux Compactifications and Higher-loop Corrections. *JHEP*, 03:031, 2020.

[118] Takuya Hirose and Nobuhito Maru. Cancellation of One-loop Corrections to Scalar Masses in Flux Compactification with Higher Dimensional Operators. *J. Phys. G*, 48(5):055005, 2021.

[119] Takuya Hirose and Nobuhito Maru. Nonvanishing finite scalar mass in flux compactification. *JHEP*, 06:159, 2021.

[120] Takuya Hirose and Nobuhito Maru. Extranatural flux inflation. *JHEP*, 09:124, 2021.

[121] Arthur Hebecker and John March-Russell. The structure of GUT breaking by orbifolding. *Nucl. Phys. B*, 625:128–150, 2002.

[122] Y. Aharonov and D. Bohm. Significance of electromagnetic potentials in the quantum theory. *Phys. Rev.*, 115:485–491, 1959.

[123] A. Delgado, A. Pomarol, and M. Quiros. Supersymmetry and electroweak breaking from extra dimensions at the TeV scale. *Phys. Rev. D*, 60:095008, 1999.

[124] Nobuhito Maru and Kazunori Takenaga. Effects of bulk mass in gauge-Higgs unification. *Phys. Lett. B*, 637:287–294, 2006.

[125] Naoyuki Haba, Yoshiharu Kawamura, and Kin-ya Oda. Dynamical Rearrangement of Theta Parameter in Presence of Mixed Chern-Simons Term. *Phys. Rev. D*, 78:085021, 2008.

[126] Yoshiharu Kawamura and Takashi Miura. μ Parameter from Dynamical Rearrangement of U(1) and θ Parameter. *Int. J. Mod. Phys. A*, 27:1250023, 2012.

[127] Yugo Abe, Yuhei Goto, Yoshiharu Kawamura, and Yasunari Nishikawa. Conjugate boundary condition, hidden particles, and gauge-Higgs inflation. *Mod. Phys. Lett. A*, 31(35):1650208, 2016.

[128] David Tong. Lectures on the Quantum Hall Effect. 6 2016.

[129] John C. Mather, D. J. Fixsen, R. A. Shafer, C. Mosier, and D. T. Wilkinson. Calibrator design for the COBE far infrared absolute spectrophotometer (FIRAS). *Astrophys. J.*, 512:511–520, 1999.

[130] Julien Lesgourgues and Sergio Pastor. Massive neutrinos and cosmology. *Phys. Rept.*, 429:307–379, 2006.

[131] Kensuke Akita and Masahide Yamaguchi. A precision calculation of relic neutrino decoupling. *JCAP*, 08:012, 2020.

[132] David J. E. Marsh. Axion Cosmology. *Phys. Rept.*, 643:1–79, 2016.

[133] S. Dimopoulos, S. Kachru, J. McGreevy, and Jay G. Wacker. N-flation. *JCAP*, 08:003, 2008.

[134] Michael S. Turner. Coherent Scalar Field Oscillations in an Expanding Universe. *Phys. Rev. D*, 28:1243, 1983.

[135] Adam G. Riess et al. A 2.4% Determination of the Local Value of the Hubble Constant. *Astrophys. J.*, 826(1):56, 2016.

[136] Christina D. Kreisch, Francis-Yan Cyr-Racine, and Olivier Doré. Neutrino puzzle: Anomalies, interactions, and cosmological tensions. *Phys. Rev. D*, 101(12):123505, 2020.

[137] Francesco D'Eramo, Ricardo Z. Ferreira, Alessio Notari, and José Luis Bernal. Hot Axions and the H_0 tension. *JCAP*, 11:014, 2018.

[138] Marco Fabbrichesi, Emidio Gabrielli, and Gaia Lanfranchi. The Dark Photon. 5 2020.

[139] Kento Akamatsu, Takuya Hirose, and Nobuhito Maru. Gauge symmetry breaking in flux compactification with a Wilson-line scalar condensate. *Phys. Rev. D*, 106(3):035035, 2022.

[140] Victor Franken. Tachyons and (non)vanishing scalar masses in six-dimensional gauge theories with flux compactification. 3 2022.

[141] N. K. Nielsen and P. Olesen. An Unstable Yang-Mills Field Mode. *Nucl. Phys. B*, 144:376–396, 1978.

[142] Wilfried Buchmuller, Emilian Dudas, and Yoshiyuki Tatsuta. Quantum corrections for D-brane models with broken supersymmetry. *JHEP*, 12:022, 2019.

[143] Wilfried Buchmuller, Emilian Dudas, and Yoshiyuki Tatsuta. Tachyon condensation in magnetic compactifications. *JHEP*, 03:070, 2021.

[144] Gerard 't Hooft. A Property of Electric and Magnetic Flux in Nonabelian Gauge Theories. *Nucl. Phys. B*, 153:141–160, 1979.

[145] J. Alfaro, A. Broncano, M. B. Gavela, S. Rigolin, and M. Salvatori. Phenomenology of symmetry breaking from extra dimensions. *JHEP*, 01:005, 2007.